A Tale of Two Prefrontal Cortices:

Connections of the Orbitofrontal Cortex in the Rat

By

Monika Jill Magram Murphy

Dissertation

Submitted to the Faculty of the

Graduate School of Vanderbilt University

in partial fulfillment of the requirements

for the degree of

DOCTOR OF PHILOSOPHY

in

Neuroscience

May 11, 2018

Nashville, Tennessee

Committee:

Roger Colbran, Ph.D.

Stephan Heckers, M.D.

Danny Winder, Ph.D.

Richard Caprioli, Ph.D.

Ariel Deutch, Ph.D.

To my parents, Jeanne and Drew, for their infinite support and

for instilling in me a love and appreciation for science

And

To my husband, Rob, for his support, endless patience and encouragement,

and for making me laugh after every bad day

ACKNOWLEDGEMENTS

Nashville. A special thank you to two of the women who really got me through graduate school: Michelle Williams and Leslie Roteta, you are the best I wouldn't be here without friends like you keeping me sane. And to my friends across the country, Alyssa Ogonek especially, you have supported me in this crazy endeavor and have been the best support system.

Thank you to my family. My parents, scientists themselves, have taught me what it means to be a good scientist and a good person. My sister has always provided a listening ear when I just need to vent and has shown me how to be a better person. My extended family has been so supportive, provided many fun times and delicious meals, and has also inspired me to continue my journey in neuroscience.

Last but not least, I could not have gotten to this point without my husband, Rob. You have been the best support that I could have ever asked for – putting every bad day and failed experiment in perspective and keeping me laughing along the way. Nashville will always have a piece of my heart because this is where I met and married you. Without your support, I would have gone crazy long ago. The words thank you aren't enough for all that you've done over these past three years, I love you.

TABLE OF CONTENTS

CHAPTER

LIST OF TABLES

LIST OF FIGURES

LIST OF ABBREVIATIONS

5-HT	serotonin
A10dc	dorsocaudal extent of the A10 cell group
A10vr	ventrorostral extent of the A10 cell group
ac	anterior commissure
ACC	anterior cingulate cortex
AI	agranular insular cortex
AId	dorsal agranular insular cortex
AId$_1$	dorsal agranular insular cortex, dorsal part
AId$_2$	dorsal agranular insular cortex, ventral part
AIv	ventral agranular insular cortex
alv	alveus of the hippocampus
AST	amygdalostriatal transition zone
BA	Brodmann's area
BDA	lysine fixable, biotinylated dextran amine
BLA	basolateral amygdala
BMA	basomedial amygdala
CaMKIIα	calcium-calmodulin-dependent kinase II alpha
cPFC	contralateral prefrontal cortex
CL	central lateral nucleus of the thalamus
CM	central medial nucleus of the thalamus
cp	caudatoputamen

CTB	cholera toxin subunit B
DA	dopamine
DAB	diaminobenzidine tetrahydrochloride
DBB	diagonal band of Broca
DHA	2,5-dihydroxyacetophenone
DI	dysgranular insular cortex
DLO	dorsolateral orbitofrontal cortex
DLO_1	dorsolateral orbitofrontal cortex, dorsal part
DLO_2	dorsolateral orbitofrontal cortex, ventral part
DOPAC	3,4-dihydroxyphenylacetic acid
ENT	Entorhinal cortex
FG	fluoro-gold
FISH	fluorescent *in situ* hybridization
fMRI	functional magnetic resonance imaging
fr	fasciculus retroflexus
GAD2	glutamate decarboxylase 2
GFAP	glial fibrillary acidic protein
GI	granular insular cortex
GP	globus pallidus
HPLC	high-performance liquid chromatography
HVA	homovanillic acid
IAM	interanteromedial nucleus of the thalamus
IL	infralimbic cortex

IMD	intermediodorsal nucleus of the thalamus
IMS	imaging mass spectrometry
L1	cortical layer 1
L2/3	cortical layer 2/3
L5	cortical layer 5
L6	cortical layer 6
Lat	lateral nucleus of the amygdala
LCM	laser capture microdissection
LH	lateral hypothalamus
LO	lateral orbitofrontal cortex
MALDI-TOF	matrix-assisted laser desorption/ionization time-of-flight mass spectrometry
MD	mediodorsal nucleus of the thalamus
MO	medial orbitofrontal cortex
mPFC	medial prefrontal cortex
MRI	magnetic resonance imaging
MuDPIT	multi-dimensional protein identification technology
NAS	nucleus accumbens
NE	norepinephrine
OCD	obsessive compulsive disorder
OFC	orbitofrontal cortex
OMPFC	orbital and medial prefrontal cortex
PBS	phosphate-buffered saline
PC	paracentral nucleus of the thalamus

PCs	pyramidal cells
PET	positron emission tomography
PF	parafascicular nucleus of the thalamus
PFC	prefrontal cortex
PHA-L	Phytohemagglutinin-L from *Phaseolus vulgaris*
PL	prelimbic cortex
PVT	paraventricular nucleus of the thalamus
qPCR	quantitative polymerase chain reaction
rs	rhinal sulcus
SI	substantia innominata
SMI-32	non-phosphorylated neurofilament H
Sub	subiculum
TBS	tris-buffered saline
TH	tyrosine hydroxylase
TH-ir	tyrosine hydroxylase immunoreactive
VLO	ventrolateral orbitofrontal cortex
VLO$_p$	posterior ventrolateral orbitofrontal cortex
VO	ventral orbitofrontal cortex
VM	ventromedial nucleus of the thalamus
VMS	ventromedial striatum
VPM	ventral posteromedial nucleus of the thalamus
VTA	ventral tegmental area

CHAPTER 1

INTRODUCTION

The Frontal Lobe

The brain has been a subject of interest dating back to Hippocrates in the 5th century BC, who first suggested that the brain, not the heart, was the source of thought and intelligence (see Filley, 2010). It wasn't until the 17th century that Thomas Willis ascribed higher thought processes to the convolutions of the cerebral cortex. In the 18th century, Francois Chuassier divided the brain into the four lobes that we know today: the frontal, temporal, parietal and occipital lobes (see Filley, 2010). Around the same time, the Swedish scientist Emmanuel Swedenborg (1688-1772) attributed higher-order functions such as imagination and thought to the frontal lobe. However, his work was largely ignored at the time because he was not associated with any university and was heavily involved in theology and mysticism (see Filley, 2010; Schiller, 1985). Franz Joseph Gall (1758-1828) and Johann Kaspar Spurzheim (1776-1832) found that the frontal lobes occupied a much larger territory in humans, compared with other species and therefore attributed higher-order functions to these anterior areas. However, their advocacy of phrenology overshadowed their neuroanatomical findings (Filley, 2010; Schiller, 1985).

The frontal lobes became of great interest following reports of an accident involving the railroad foreman, Phineas Gage in 1848. An accidental explosion sent a metal tamping rod through Gage's skull and brain. Shockingly, Gage survived the injury, but not without significant damage to his frontal lobe. Gage's physician, J.M. Harlow (1868), described substantial personality and behavioral changes caused by the injury 12 years later, shortly following Gage's

1

death. In 1878, after learning of Harlow's report, David Ferrier suggested that the behavioral changes that Gage exhibited following his injury were attributable to the brain areas that were damaged, which avoided frontal motor and speech areas and instead localized to frontal areas involving more complex behavioral control including attention (Filley, 2010; García-Molina, 2012). In his own studies of monkeys, Ferrier had found that frontal cortical lesions in monkeys led to apathy and impulsiveness, and attributed these changes to a problem with attentional state, which he compared with the case of Phineas Gage (see Filley, 2010). However, neither Ferrier nor other scientists of the time had access to Gage's brain, so his suspicions could not be confirmed by analyzing the lesion. Since this time, Phineas Gage's body has been exhumed and recently, H. Damasio and colleagues (1994) used 3-D reconstructions and analyses of Gage's skull to determine the areas within the brain that were likely lesioned. They suggested the presence of significant damage bilaterally in anterior portions of the orbitofrontal cortex (Brodmann's areas 11 and 12), the polar and medial frontal cortices (BA 8, 9, 10, and 32), and the most anterior regions of the anterior cingulate gyrus (BA 24). The majority of the supplementary motor area, Broca's area, and the dorsolateral prefrontal cortex were likely spared.

Interest in the frontal cortices spiked in response to the Phineas Gage case. In 1884, Moses Allen Starr performed a comprehensive review of previous case reports on frontal cortex damage secondary to abscesses, tumors, or lesions. He noted tremendous variability in the nature of the behavioral changes, concluding that disruptions of the frontal lobe can lead to wide variety of syndromes. However, Starr also concluded that the frontal lobe is critical for higher-order functions and is a distinguishing feature of humans (see Filley, 2010 and Starr, 1891). Around the same time, Fristch and Hitzig were performing important electrical stimulation studies in

dogs. They found that stimulation of certain cortical areas leads to muscle contraction, but no

motor changes were detected when the frontal lobes were stimulated. However, the frontal lobe

stimulation did elicit behavioral changes (Filley, 2010; García-Molina, 2012). In the early 20th

century, following the studies of Fritsch and Hitzig, Bianchi performed frontal cortical lesions in

both monkeys and dogs; his results echoed those previously reported: the frontal lobe seemed to

be critical for planning, inhibition of action, and likely personality (see Filley, 2010).

Despite the accumulation of data in both humans and other species, the precise function

of the frontal cortices remained elusive for much of the 20th century. Clinicopathological

correlations are very useful, but the often imprecise delineation of pathological involvement in

various frontal lobe cases, coupled with fact that clinical lesions don't conform to

cytoarchitectonic boundaries, did not advance the field much beyond Starr's (1891) conclusion

that frontal cortical lesions lead to a variety of behavioral changes, ranging from attentional

problems to disinhibition to fundamental changes in personality.

The Prefrontal Cortex

The frontal lobe, as discussed, is positioned at the front of the brain above the temporal

lobe (lateral sulcus) and anterior to the parietal lobe (central sulcus). I have alluded to the

heterogeneity within the frontal lobe, highlighting the various behavioral changes that occur

following lesions affecting different components of this broad area. It is evident from both

functional and neuroanatomical data that the frontal lobe is not a singular structure, but in fact

consists of a large number of distinct cortical areas. In order to meaningfully resolve the

components of the frontal lobe, however, it is important to establish criteria that may be used to

define any cortical area. To define homologous cortical regions across species, three criteria are

used: cytoarchitectonics (cell packing), hodology (connections with other brain areas), and function.

Within the frontal lobe, one area has emerged from functional analyses as a critical region for executive function: the prefrontal cortex (PFC). The PFC is now known to be involved in the pathophysiology of many neuropsychiatric illnesses ranging from schizophrenia to addiction (Goldman-Rakic and Selemon, 1997; Goldstein and Volkow, 2011). In order to better understand, model, and examine these disorders, it is critical to determine homologous areas in other species. To this end, research groups have assessed and compared the function, cytoarchitectonics, and connectivity of the PFC, and compared these criteria across species.

Function.

The frontal lobe, and the PFC in particular has been examined for over a century. In recent years, many new methodologies have been developed, which have allowed neuroscientists interrogate the function of the PFC. In particular, magnetic resonance imaging (MRI) has provided new insights into the anatomy of the human PFC, and functional MRI (fMRI) has allowed for the real-time analysis of brain function while performing tasks, which has helped elucidate the role of the PFC in both typical and disease states. Using positron emission tomography (PET) imaging (Swartz et al. 1994; Weinberger et al., 1986), and subsequently using fMRI, multiple groups have found that aspects of the PFC are critically involved in working memory processes (Braver et al., 1997; Cohen et al., 1994; D'Esposito et al., 1995).

Pathophysiology of the PFC is involved in various neuropsychiatric illnesses. In patients diagnosed with schizophrenia, for example, there are a number of cognitive deficits that have been attributed to PFC dysfunction (Barch and Ceaser, 2012). Notably, there is a working

4

memory deficit in patients diagnosed with schizophrenia, and the extent of this impairment is predictive of patient's outcome (see Barch and Smith, 2008), emphasizing the role of the PFC in the pathophysiology of schizophrenia. The PFC, however, occupies a large territory in the human, and is made up of multiple areas which subserve various functions (Wilson et al., 2010). In order to subdivide the PFC, it is critical to understand the microstructure and connections of these areas, as well as their function.

Cytoarchitectonics.

The frontal lobe is made of numerous distinct areas with different cytoarchitectonic characteristics; in other words, the cell packing, orientation of cells, and presence or absence of certain lamina varies across the frontal lobe. Brodmann (1909/2006) defined 44 distinct cytoarchitectonic areas in the human brain. Of these 44 areas, eight are located in the frontal lobe. However, Brodmann (1909/2006) was hesitant in the boundaries within these frontal areas, which exhibit varying degrees of structural heterogeneity. Nearly twenty years after the publication of Brodmann's parcellation scheme, Economo and Koskinas published their own atlas in 1925 and provided a more detailed analysis of the frontal cortices. In their atlas, von Economo and Koskinas divided the frontal lobe into 13 areas. These areas were then further subdivided into structural cortical types, and described by variations, or modifications, of these cortical types (Triarhou, 2007; Zilles and Amunts, 2010). The terminology of the atlas departed from the simplistic numbering scheme of Brodmann and instead relied on confusing combinations of roman characters with calligraphic capitals and Greek lettering to denote specific brain areas, which is likely one reason that the nomenclature was never widely adopted, despite the atlas's intricate detail.

In 1940, Walker generated a parcellation scheme for the non-human primate brain and, like Brodmann, noted heterogeneity and poorly defined borders of areas within the frontal lobe (Walker, 1940). Both Walker and Brodmann described both granular and agranular regions within the frontal lobe. In the rodent, however, the prefrontal cortices are largely agranular, a key cytoarchitectonic difference between the species (Leonard, 1969).

Hodology.

In two papers published in 1948, Rose and Woolsey used retrograde degeneration methods to define a region of the frontal lobe as the projection area of the mediodorsal thalamic nucleus (MD). This area is now known as the prefrontal cortex (PFC). Two decades later, the development of an anterograde tract tracing method, the Fink-Heimer method, allowed Leonard (1969) to visualize degenerating axons in the frontal lobe after MD lesions in the rat. She observed two frontal territories that receive MD projections: one in the medial wall of the hemisphere, and the second in an area dorsal to the rhinal sulcus, which Leonard designated the sulcal cortex. Importantly, Leonard's data suggested that not only primates but also rodents have a prefrontal cortex. This opened the door for future studies of the prefrontal cortex in rodents.

Using the MD innervation to define the PFC highlights the ability to define brain areas on the basis of connectivity. However, it soon became clear that contrary to the idea of Rose and Woolsey (1948a,b), the frontal region innervated by the MD also received other thalamic inputs, including the paraventricular, parataenial, anterior, and parafascicular nuclei. Additionally, this MD-centric definition requires that one be able to clearly define the MD – yet the MD had not been defined in all mammals (see Mogensen and Divac, 1982). The MD projection to the frontal

lobe spans many cytoarchitectonic areas, which are thought to subserve different functions (see Dalley et al., 2004; Goldstein and Volkow, 2011).

Recognizing the limitations of a MD-based definition of the PFC, Divac sought to identify other defining features of a prefrontal cortex. Divac was able to demonstrate a dopaminergic innervation of the frontal area innervated by the MD in three species: the rat, opossum, and tree shrew (1978a). In a separate analysis, Divac and colleagues were able to show, using retrograde tracing techniques, that projections from the MD, ventral mesencephalon, and basolateral amygdala were present in the same areas of the frontal cortex (1978b); this convergence of inputs was only seen in the PFC, but not other cortices. Accordingly, Divac proposed that the prefrontal cortex could be defined across mammals (and perhaps other species) as the cortical area in which axons of mediodorsal thalamic, basolateral amygdaloid, and midbrain dopaminergic neurons converge. The MD, BLA, and dopaminergic midbrain projections have all been observed in the dorsal bank of the rhinal sulcus. However, Divac's studies relied on relatively large retrograde tracer deposits, which invaded multiple cytoarchitectonic territories and were subject to uptake by axons-of-passage. To this day, the degree to which these three projections converge in the OFC is unclear and we are not aware of any direct examination of the spatial convergence of these neurons in the orbitofrontal region.

The orbitofrontal cortex (OFC) is referred to as a prefrontal cortical area. However, the afferents to this region have not been systematically analyzed. In this thesis, I will discuss the afferents to the OFC in the rat, with a particular focus on the orbitofrontal dopamine innervation.

CHAPTER 2

THE ORBITOFRONTAL CORTEX

The orbitofrontal cortex (OFC) is found within the ventral surface of the frontal lobe in the human. Following reports of Phineas Gage's injury, the various behavioral changes that Gage exhibited were largely attributed to the damage of the prefrontal cortex; it has since been shown that the OFC was one of the greatest-affected areas, and thus has often been thought of as a prefrontal area (see Ongür and Price, 2000). In Mesulam's foreword to the book entitled *The Orbitofrontal Cortex* (2006), he highlights that lesions of the OFC, similar to lesions of other prefrontal areas, do not produce overt motor, speech, or sensory alterations; instead, there is a complex combination of subtle changes that arise following lesions involving the OFC.

The OFC has received scant attention, as compared to the medial prefrontal cortex, particularly in the rodent. Despite the fact that an MD innervation of the OFC has been described in a wide variety of species, including the rat, mouse, hamster, sheep, and primate, thus defining the OFC as a prefrontal cortex, relatively little is known about this area as compared to its medial counterpart (Divac et al., 1978a; Krettek & Price, 1977b; Leonard, 1969; Ray and Price, 1992; Reep and Winans, 1982; Rose and Woolsey, 1948b).

The OFC, which occupies the ventrolateral frontal cortices in the rat, has been variously designated the sulcal cortex (Leonard, 1969), sulcal prefrontal cortex (Siegel et al., 1977), suprarhinal cortex (Divac, 1978a), agranular insular cortex (Krettek and Price, 1977b), lateral prefrontal cortex (Siegel et al., 1977), lateral orbitofrontal cortex (Krettek & Price, 1977b), or simply the orbitofrontal cortex (OFC; Krettek and Price, 1977a; Cooch et al., 2015). For simplicity, I will use the term orbitofrontal cortex to broadly discuss the ventrolateral frontal

cortex in the rat; when discussing specific areas within the OFC, I will use the terminology of van de Werd and Uylings (2008) (see Figure 1).
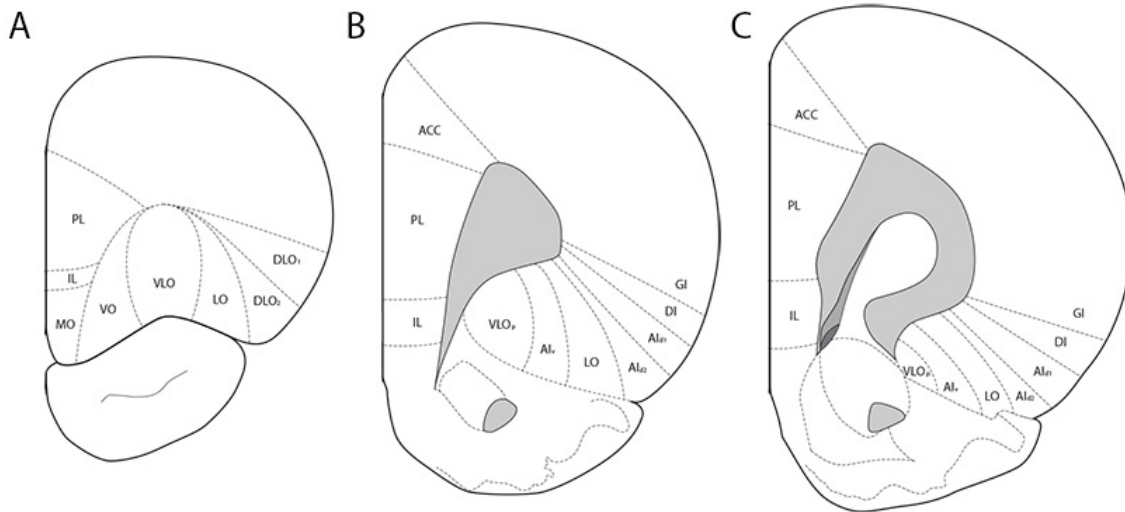
Figure 1. Borders used to describe the OFC at a rostral (A), mid (B), and caudal (C) level of the vlFC. Parcellation of OFC adopted from Van De Werd & Uylings (2008).

Defining the OFC

Cytoarchitectonics and Structure.

Brodmann (1909) highlighted the heterogeneity of the orbitofrontal region and referred to this broad region as areas 47 and 11, but suggested that further subdivisions would be useful (see Petrides and Mackey, 2006). In the atlas of von Economo and Koskinas (2008) Brodmann's area 47 became area FℱF, which included numerous "cortical types" and "modifications" of these

cortical types, further highlighting the heterogeneity within this region. All parcellations of the human OFC, however, noted that both granular and agranular areas are present within this expanse. In his atlas of the macaque brain, Walker subdivided the OFC, but did not explicitly compare the OFC in the macaque and human (Petrides & Mackey, 2006; Walker, 1940).

In the rat brain, the orbital areas have been most clearly and extensively delineated by van de Werd & Uylings (2008). Using a combination of cytoarchitectonics and

9
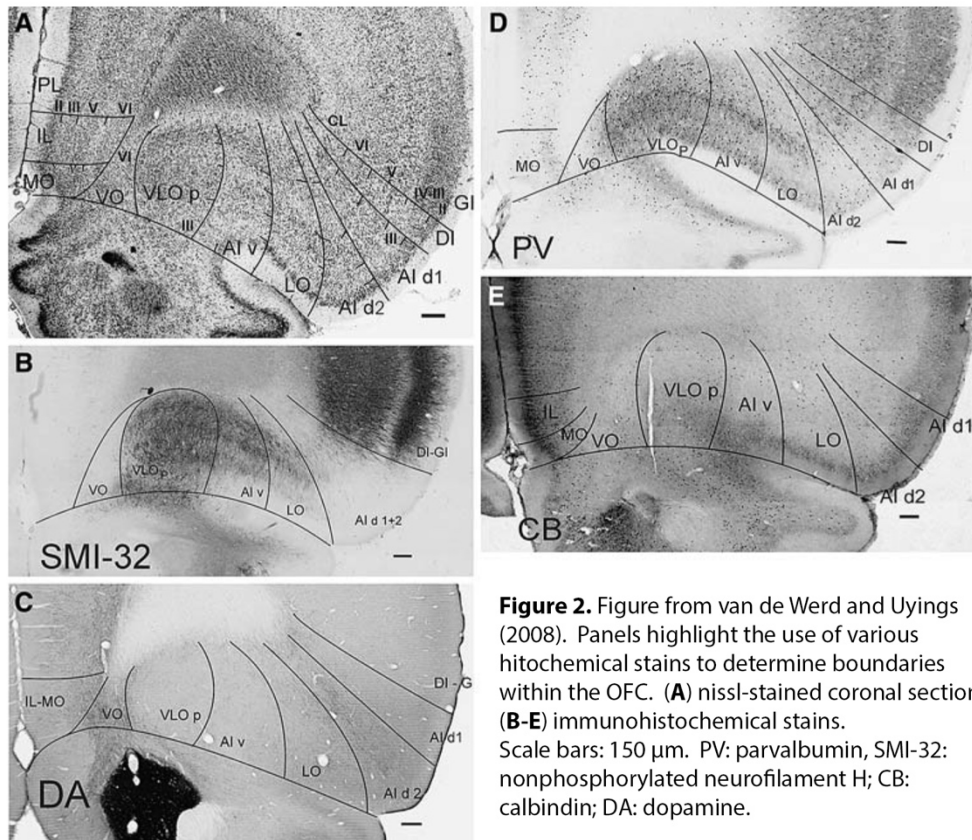
Figure 2. Figure from van de Werd and Uyings (2008). Panels highlight the use of various hitochemical stains to determine boundaries within the OFC. (**A**) nissl-stained coronal section (**B-E**) immunohistochemical stains. Scale bars: 150 μm. PV: parvalbumin, SMI-32: nonphosphorylated neurofilament H; CB: calbindin; DA: dopamine.

immunohistochemical stains, van De Werd and Uylings separated the OFC into fourteen distinct areas. These areas included both classical orbitofrontal areas such as the medial orbital (MO), ventral orbital (VO), ventrolateral orbital (VLO), lateral orbital (LO), and dorsolateral orbital (DLO) cortices as well as insular areas including the agranular insular cortex (AI), dysgranular insular cortex (DI), and granular insular cortex (GI). Some of these areas were then further subdivided into dorsal, ventral, and/or posterior subdivisions. The borders between regions were delineated using nissl-stained sections to identify the cytoarchitectonics, as well as different combinations of calbindin, parvalbumin, non-phosphorylated neurofilament H (SMI-32), and dopamine immunohistochemistry (see Figure 2). To discern the dorsolateral orbital cortex (DLO) from the medially-adjacent lateral orbitofrontal cortex (LO), for example, nissl staining illuminated differences in cell size in layer 2 and cell packing in layers 3 and 5. In addition to

these relatively subtle cytoarchitectonic differences, dopamine and parvalbumin immunohistochemical stains confirmed and clarified this border. In all of the areas defined within this analysis, various combinations of immunostains are used in conjunction with the nissl stain to define the borders.

Afferents.

In both the rat and the primate, the OFC receives an innervation from the mediodorsal nucleus of the thalamus (MD) (Krettek and Price, 1977b; Goldman-Rakic and Porrino, 1985). In the rodent, the MD innervation involves the only medial wall rostrally; caudally this innervation extends along the dorsal bank of the rhinal sulcus, through the OFC, excluding only AId_1, DI, and GI (see Figure 3). A direct projection of the basolateral amygdala (BLA) to the frontal cortices was first reported by Krettek and Price in 1974 and subsequently elaborated by these investigators (Krettek and Price, 1977a). The projections of the BLA complex (including the basolateral and lateral nuclei) are seen only in the dorsolateral aspects of this region. This innervation exits from the ventrolateral edge of the forceps and runs diagonally to the pial surface on the dorsal bank of the rhinal sulcus, encompassing the AId_2, AId_1, and dysgranular insular areas (see Figure 3).
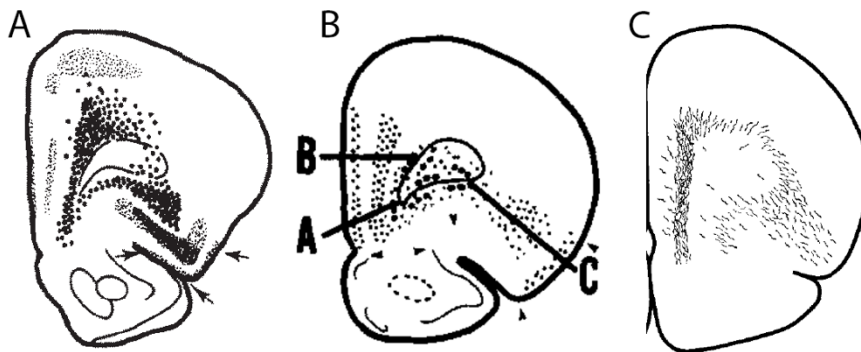
Figure 3. Representative figures of subcortical innervation of the frontal cortices. (**A**) Mediodorsal innervation from Groenewegen, 1988. (**B**) Basolateral amygdala innervation from Krettek and Price, 1977a. (**C**) Dopaminergic innervation from Lindvall et al., 1978.

The OFC in the rat also receives a dopamine innervation. This input to the OFC has received little attention relative to medial PFC (Gerfen and Clavier, 1979; Kalsbeek et al., 1988; Thompson et al., 2017; van der Werd and Uylings, 2008; van de Werd et al., 2010; van Eden et al., 1987). The orbitofrontal dopamine innervation is restricted to a small area centered in the ventral portion of the dorsal agranular insular cortex (AId$_2$) (van de Werd and Uylings, 2008). In one of the few systematic analyses of afferents of this region of the OFC, Gerfen and Clavier (1979), using horseradish peroxidase, suggested that the dopamine input to the OFC originates in the supramammillary nucleus, located at the rostral extent of the midbrain dopamine neurons.

Despite the fact that the MD, BLA, and dopaminergic midbrain all innervate this ventrolateral area of the OFC, there have been no contemporary analyses of the convergence of the MD, BLA, and dopaminergic inputs within this area, nor has there been an analysis of the collateralization of these inputs to the medial prefrontal and orbitofrontal areas.

Thus far, I have focused on the orbitofrontal innervation from the MD, BLA, and dopaminergic midbrain largely due to their critical importance in defining a prefrontal area. However, there are many other inputs to the OFC. In most cases, the OFC is not the primary focus of the examination. For example, in studies of the submedius nucleus of the thalamus (Yoshida et al., 1992) and the perirhinal cortex (Hwang et al., 2017), it was found that both densely innervate components of the OFC as well as other brain areas. There have been very few anatomical studies of the connections of the OFC (Gerfen and Clavier, 1979; Hoover and Vertes, 2011; Reep et al., 1996), and none that systemically determine and compare afferents to the many areas of the OFC. We have therefore examined the afferent organization across the rat OFC, paying particular attention to the dopaminergic innervation.

Methods

Animals. Adult male Sprague–Dawley rats (Envigo; Indianapolis, IN) were group-housed with food and water available *ad libitum*. All experiments were performed in accordance with the Guide for the Care and Use of Laboratory Animals as promulgated by the National Institutes of Health and under the oversight of the Vanderbilt University Institutional Animal Care and Use Committee.

Immunohistochemical procedures. Both immunofluorescence and immunoperoxidase methods were used. Immunoperoxidase procedures were used to visualize boundaries and layers within the OFC and immunofluorescence was used to analyze the dopamine innervation of the OFC.

Sections stained using immunoperoxidase methods were incubated in methanolic peroxide for 20 min, washed in 50 mM Tris-buffered saline (TBS), and blocked in TBS containing 4% normal horse serum (Gibco; ThermoFisher Scientific, Waltham, MA), and 0.2% Triton X-100 (TBS^{++}) before being incubated in the primary antibody overnight at room temperature. Sections were then washed repeatedly in TBS^{++} and incubated in biotinylated secondary antibody in TBS^{++} (1:1000; Jackson ImmunoResearch, West Grove, PA) for 2 hours at room temperature, washed, and incubated in HRP-conjugated streptavidin (1:1600; Jackson ImmunoResearch) prepared in TBS containing 0.2% Triton X-100 for 90 minutes. After being washed, sections were developed in a 0.025% diaminobenzidine tetrahydrochloride (DAB) solution in TBS containing 0.05% DAB with 0.009% hydrogen peroxide to yield a brown reaction product. Sections were then mounted onto subbed slides, cleared, and coverslipped. See Table 1 for an overview of the antibodies used here, as well as in all experiments described.

Table 1. Primary Antibodies

Antigen	Immunogen	Source	Manufacturer	Dilution
Cholera Toxin, subunit B	Choleragenoid	Goat, polyclonal	List Biologicals, #903, RRID: AB_231637	1:9,000
Fluoro-gold	Fluoro-gold (Hydroxystilbamidine)	Rabbit, polyclonal	Fluorochrome, RRID: AB_2314408	1:50,000 (immunoperoxidase) 1:20,000 (immunofluorescence)
Tyrosine Hydroxylase (TH)	Native TH from rat pheochromocytoma	Sheep, polyclonal	Millipore, AB1542, RRID: AB_90755	1:1,000
	TH purified from rat PC12 cells	Mouse, monoclonal	Immunostar, 22941, RRID: AB_572268	1:6,000

In cases involving immunofluorescent detection, sections were pre-treated in 0.25% trypsin (Sigma-Aldrich, St. Louis, MO) for 7 min at 37°C, then washed, incubated in TBS^{++} for 30 minutes, then incubated in sheep anti-TH primary antibody (AB1542, Lot 2896740, RRID: AB_90755, Millipore, Billerica, MA) at a dilution of 1:1000 overnight at room temperature. Following primary antibody incubation, sections were washed and placed in an Alexa 488-conjugated donkey anti-sheep secondary antibody (1:1500, Jackson ImmunoResearch) for two hours. Sections were then washed and mounted in Prolong Antifade (ThermoFisher Scientific, Waltham, MA).

Images were acquired using a Nikon Eclipse N*i*-U microscope. The brightness and contrast of some figures was adjusted; in all cases in which these parameters were modified the entire image was adjusted.

Monoamine concentrations in the OFC. The OFC was dissected from 1.0 mm thick coronal sections of four rats; this tissue sample spread from lateral ventrolateral orbital cortex (VLO) to the dysgranular insular cortex of the OFC, thus covering the lateral half of the OFC (see Fig. 5). Concentrations of dopamine and its acidic metabolites 3,4-dihydroxyphenylacetic acid (DOPAC) and homovanillic acid (HVA), as well as norepinephrine and serotonin, were measured by HPLC with electrochemical detection, following our previously described methods (Deutch and Cameron, 1992).

Results

The organization of the ventrolateral frontal cortex is complex, with the boundaries of the various cytoarchitectonic areas in the OFC difficult to discern and subject to different definitions. As previously mentioned, we followed the nomenclature of van de Werd and Uylings (2008) for the frontal cortices, which expands on the terminology of Krettek and Price (1977a,b) and Ray and Price (1992) for frontal cortical areas (see Fig. 1).

Dopaminergic innervation of the OFC. Dopaminergic axons medial to the rostral pole of the nucleus accumbens entered the white matter of the forceps minor in the ventromedial frontal cortex (see Fig. 4). Axons coursed dorsally along the margins of the white matter of the forceps to innervate mPFC regions. A stream of TH-ir axons continued along the medial and dorsal aspect of the forceps to exit at the ventrolateral border of the white matter, where the labeled axons entered the OFC and fanned out as they streamed toward the pial surface. The dopamine innervation of the OFC subjectively appeared to be substantially less dense than that of the mPFC.

Dopamine axons in the OFC were distributed throughout the AId_2, fanning out from a relatively compact cluster where they entered layer 6 (L6) as a bundle ~350 μm in width to distribute TH-ir axons throughout AId_2 (Fig. 4). The TH-ir axons fanned out to invade but not fill the lateral orbital (LO) cortex medially and AId_1 laterally. The dopaminergic innervation of these areas flanking AId_2 was broader in the more caudal aspects of the OFC, and narrowed rostrally.

Figure 4. Dopaminergic innervation of the OFC as revealed by TH immunoreactivity. (**A-C**) The distribution of TH-ir axons is shown at three different rostrocaudal levels. Note the sweeping band of TH-ir axons in the ventrolateral frontal cortex, running diagonally from the white matter to the pial surface. Scale bar (panels A-C), 1000μm. (**D-F**) TH-ir axons in layers 6 (panel D), 5 (E), and 3 (F). Scale bar (panels D-F), 50μm.

The morphology of OFC dopamine axons resembled those of mPFC dopamine axons. Relatively smooth, thick TH-ir axons exited the white matter to enter L6 (Fig. 4) and continued into deep L5. In superficial L5 the dopamine axons ramified and thin axons with small varicosities and large intervaricose segments were present. In L2/3 both smooth and highly varicose TH-ir axons were present (Fig. 4).

Monoamine concentrations in the OFC. The concentration of dopamine in the OFC was 0.96 ± 0.12 ng/mg protein, which was not significantly different from that in the mPFC (1.18 ± 0.13 ng/mg protein; Fig. 5). Acidic metabolites of dopamine were also detected in the OFC: the 3,4-dihydroxyphenylacetic acid concentration was 0.33 ± 0.10 ng/mg protein (vs 0.35 ± 0.09 ng/mg in the mPFC), and the homovanillic acid concentration was 0.57 ± 0.10 (vs 0.60 ± 0.11 ng/mg in the mPFC).

The norepinephrine (NE) concentration of the OFC was about five times greater than that of dopamine, while serotonin concentrations in the OFC were also much greater than that of dopamine (see Fig. 5).
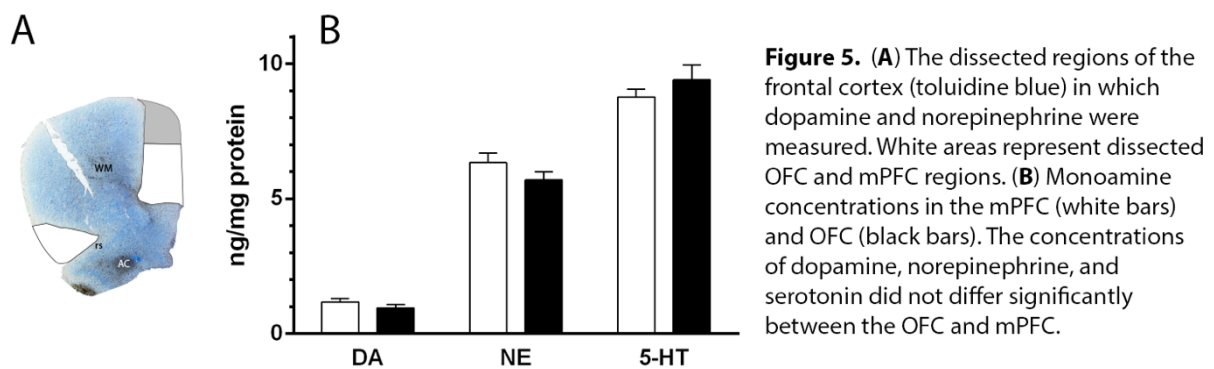
Figure 5. (**A**) The dissected regions of the frontal cortex (toluidine blue) in which dopamine and norepinephrine were measured. White areas represent dissected OFC and mPFC regions. (**B**) Monoamine concentrations in the mPFC (white bars) and OFC (black bars). The concentrations of dopamine, norepinephrine, and serotonin did not differ significantly between the OFC and mPFC.

Discussion

Subareas of the OFC. The orbitofrontal cortex is comprised of a large number of cytoarchitectonic areas, the borders of which are often difficult to discern. In general, we largely agree with the nomenclature scheme proposed van de Werd and Uylings (2008), given that we are able to identify the same cytoarchitectonic and immunohistochemical borders in our tissue samples. There is, however, one area in the inferior convexity of the white matter on which we disagree with the designation of van de Werd and Uylings: the claustrum.   At the time of the publication of the van de Werd and Uylings paper (2008), the area abutting the inferior convexity

of the forceps minor was designated the claustrum, with little-to-no attention to the placement of layer 6 of the cortices that were distal to the claustrum. However, the following year Mathur et al. (2009), using proteomic imaging methods and tract tracing, reported that the claustrum does not extend rostrally beyond the level of the genu, i.e., there is no claustrum at frontal cortical levels. This is a notable exception, because the presence of the claustrum is one of the key features differentiating the dorsolateral orbitofrontal cortex (DLO) from the more posterior dorsal agranular insular cortex (AId).

The dopaminergic innervation of OFC. We used tyrosine hydroxylase as a marker for the dopamine innervations of the frontal cortices. Although tyrosine hydroxylase is the rate-limiting step of catecholamine biosynthesis and should therefore label both dopaminergic and noradrenergic axons, multiple studies in both primate and rodent cortices have reported that TH antibodies preferentially label dopaminergic but not noradrenergic fibers (Gaspar et al., 1989; Noack and Lewis, 1989; Venator et al., 1999). Although the precise percentage of noradrenergic axons that are TH-positive depends on both the TH antibody used and the area of brain examined, in all cases studied the great majority of TH-ir axons are not labeled by a dopamine-beta-hydroxylase antibody (Noack and Lewis, 1989).

We observed a discrete group of TH-ir axons in the OFC, in contrast the broad pattern of staining revealed by dopamine-ß-hydroxylase or norepinephrine transporter antibodies (Bradshaw et al., 2016; Radley et al., 2008). The pattern of axonal TH labeling agrees well with previous data using high affinity uptake of [^{3}H]-dopamine uptake (Berger et al., 1976; Descarries et al., 1987; Lindvall et al., 1978), histofluorescent methods such as the Falk-Hillarp or glyoxylic acid techniques (Berger et al., 1976; Lindvall and Bjorklund, 1974), TH immunohistochemistry

(Febvret et al., 1991; Hökfelt et al., 1977, 1984), and dopamine immunohistochemistry (Kalsbeek et al., 1988; van de Werd and Uylings, 2008; van Eden et al., 1987). Specifically, we observed a relatively dense band of TH-ir axons that covered AId_2 and appeared to extend somewhat into LO and AId_1, consistent with the findings of van de Werd and Uylings (2008) using dopamine immunohistochemistry.

The density of the dopaminergic innervation of the OFC appears to be substantially lower than that observed in the medial PFC. This subjective impression is consistent with the quantitative data of Descarries et al. (1987), who reported that the density of the innervation of the dopamine-enriched area of the OFC (primarily AId) was less than one third that of the prelimbic cortex in the medial PFC.

The apparent differences in the density of the dopamine innervation of the medial and ventrolateral cortex, as revealed by anatomical techniques, contrast sharply with our biochemical data. We found that concentrations of dopamine and norepinephrine did not differ across the mPFC and OFC. Similarly, Slopsema et al. (1982), using a punch microdissection, found the levels of dopamine were similar in the OFC and the medial precentral cortex of the mPFC (which was not included in our dissection of the mPFC). Two other groups have also found there to be no significant difference in dopamine concentration in the OFC and mPFC (Kheramin et al., 2004; Fitoussi et al. 2013), though the cytoarchitectonic areas included within the "OFC" samples varied dramatically between groups. In contrast, Jones et al. (1986) found that dopamine concentrations were roughly twice as high in the mPFC than OFC. The lack of consistent results on the relative concentrations of dopamine in the mPFC and OFC likely reflect differences in the dissection procedures.

The differences in the relative abundance of dopamine as reflected by anatomical and biochemical measures reflect the fact that TH-ir axon density is not indicative of the amount of dopamine present. The activity of the TH enzyme is determined by phosphorylation of the enzyme at four different serine residues. In particular, phosphorylation of the ser40 site of TH leads to decreased affinity for catecholamines (competitive inhibitors for the tetrahydrobiopterin binding site). Therefore, phosphorylation at this site leads to greater activation of the enzyme (over 20-fold increase) (see Dauber et al., 2011). If the phosphorylation state of the TH enzyme was not consistent between the mPFC and OFC, it is possible that less TH could be present, while dopamine concentration was the same, as we see here. Future studies using antibodies that recognize TH phosphorylated at different serine residues may help resolve the difference between biochemical and anatomical data.

Dopamine receptors of the OFC.

Several studies have mapped the distribution of dopamine receptors in the frontal cortex, including the OFC (Gaspar et al., 1995; Santana et al., 2009; Wei et al., 2017). In general, however, most studies of dopamine receptor localization in the frontal cortices focus on the mPFC, not the OFC, and therefore limited information about laminar localization or co-expression of receptors is available. In the OFC, dopamine receptors D_1 and D_2 have been shown to be present within the agranular insular areas (Weiner et al., 1991; Santana et al., 2009). We are not aware of any systematic studies of D_3, D_4, or D_5 receptor distribution in the rodent OFC. It is interesting to note that the distributions of dopamine receptor transcripts may extend beyond the regions of dopamine innervation (Gaspar et al., 1995; Thompson et al., 2016; Wei et al., 2017).

In humans, all five dopamine receptors are expressed in the orbitofrontal cortex (BA 11) and dopamine receptors D_3 and D_4 have been shown to be decreased in brains of patients with schizophrenia by *in situ* hybridization (Meador-Woodruff et al., 1997). Similarly, all five dopamine receptors are present in the non-human primate orbitofrontal cortex as well. In non-human primate PFC, D_1 receptor expression is more prevalent and widespread than D_2 receptor expression, similar to our results in the rat (Lidow et al., 1998).

CHAPTER 3

AFFERENTS TO THE ORBITOFRONTAL CORTEX

The orbitofrontal cortex (OFC) is heterogeneous in terms of both cytoarchitectonics and function. Although there have been some studies of the connections of discrete parts of the OFC, such as the medial and ventral orbital cortices (Hoover and Vertes, 2011), a comprehensive examination of the afferents to the OFC is lacking.

In order to systematically examine the functions of the various areas within the OFC, it is critical to understand the connections of these areas. We have therefore compared the projections to the many areas within the OFC (see Figure 1).

Methods

Animals. Adult male Sprague–Dawley rats (Envigo; Indianapolis, IN) were group-housed with food and water available *ad libitum*. All experiments were performed in accordance with the Guide for the Care and Use of Laboratory Animals as promulgated by the National Institutes of Health and under the oversight of the Vanderbilt University Institutional Animal Care and Use Committee.

Tracer deposition. 21 animals received retrograde tracer deposits into various sites in the OFC. Both FluoroGold (FG; Fluorochrome, Denver, CO) and AlexaFluor 555-conjugated cholera toxin subunit B (CTB; ThermoFisher Scientific, Waltham, MA) were used. In two of the animals the tracer ejection failed, resulting in 19 cases being analyzed. FluoroGold was iontophoretically deposited through fiber-filled pipettes (15-25 µm tip diameter) by applying +2.0 µA current for

15 min (7 sec on/off). Cholera toxin B (75 nl of a 1.5% solution in .05M phosphate buffer, pH 7.4) was injected through a 27g cannula at a rate of 25 nL/min.

Seven to ten days post-operatively, animals were overdosed with isofluorane and transcardially perfused with phosphate-buffered saline (pH 7.4) followed by 4% paraformaldehyde in PBS. Brains were removed and post-fixed in 4% paraformaldehyde before being cryoprotected in 30% sucrose. Frozen sections were then cut at 40μm and collected into six alternating sets.

Immunohistochemistry. Immunoperoxidase methods used were largely outlined in chapter 2. In some cases, sections were developed in a 0.025% diaminobenzidine tetrahydrochloride (DAB) solution in TBS containing 1.5% nickel ammonium sulfate and 0.15% cobalt chloride with 0.0009% hydrogen peroxide, which resulted in a blue-black reaction product, as opposed to the brown reaction product previously outlined. The antibodies used for the CTB immunoperoxidase included goat anti-cholera toxin, subunit B (CTB; List Biological Laboratories, Cambell, CA; #703, Lot 7032AA, RRID: AB_231637) at a dilution of 1:9,000 (primary antibody), donkey anti-goat IgG (1:50, Jackson ImmunoReseach, 705-001-003, lot 55430,) (secondary antibody), and peroxidase-anti-peroxidase complex (1:400; Jackson ImmunoReseach, 123-005-024, lot 87203). For detection of fluorogold within our sections, we used a rabbit anti-FG antibody (Lot 529600, RRID: AB_2314408) from Fluorochrome (Denver, CO) at a dilution of 1:50,000 (primary antibody), followed by a biotin-conjugated donkey anti-rabbit secondary antibody (1:1000, Jackson ImmunoResearch , #711-065-152, lot 131559), and lastly, horseradish-peroxidase-conjugated streptavidin (1:1600, Jackson ImmunoResearch , #016-030084, lot 123649).

Charting of afferents. Retrogradely-labeled cells were charted manually onto templates adapted from the Paxinos and Watson rat brain atlas (2007) and van de Werd and Uylings (2008) using a Nikon Eclipse N*i*-U microscope.

Results

The distributions of retrogradely-labeled cells observed after tracer deposits into the ventrolateral frontal cortex are discussed for cases that involve different sites in the OFC. A schematic representation of all retrograde tracer deposits is shown in Figure 6.
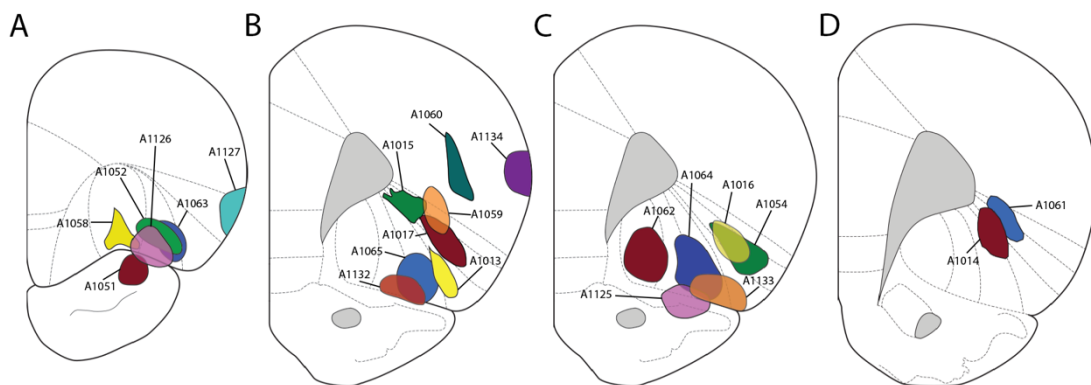
Figure 6. Schematic representation of the core of the tracer deposits into the OFC and surrounding regions, illustrated at the level of maximal deposit.

Afferents to the medial segments of OFC: VLO, AI$_v$ and LO.

Case A1062. The core of the tracer deposit (see Figures 7B, 8) was centered in the mid-anterior OFC and crossed the rhinal fissure to involve the rostral medial pyriform cortex. Within the OFC the core of the FG deposit was in the posterior ventrolateral orbital cortex (VLO$_p$), with some extension into the ventral agranular insular cortex (AI$_v$).
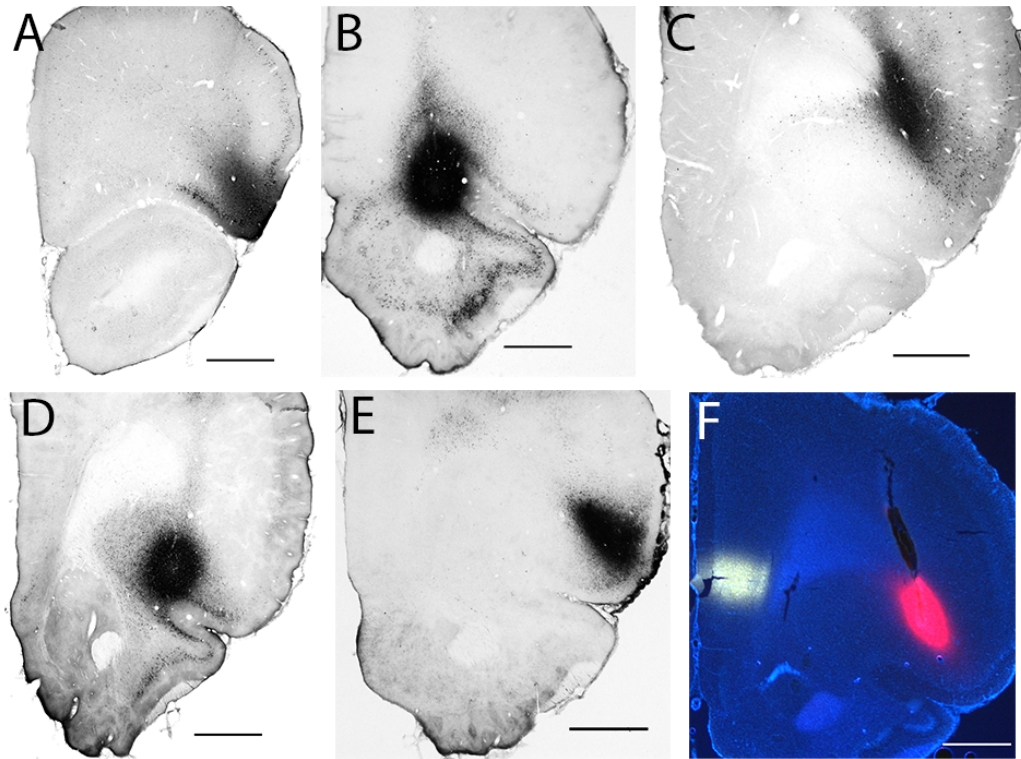
Figure 7. Photomicrographs of tracer deposits centered in (**A**) DLO (case A1013), (**B**) VLO$_p$ (A1062), (**C**) DI-GI (A1061), (**D**) LO (A1065), (**E**) AId$_1$ (A1054). (**F**) A dual retrograde tracer deposit in the frontal cortices, with the Fluoro-Gold deposit into the prelimbic cortex in the mPFC (white) and tetramethylrhodamine-cholera toxin B injected into the AId$_2$ of the OFC (case A1014). Scale bar: 1000 µm.

Cortical Afferents. Ipsilateral to the tracer deposit retrograde labeling was mainly observed in the medial aspects of the frontal lobe, involving the medial orbital, rostral prelimbic, pregenual anterior cingulate, and medial precentral cortices; additional scattered cells were seen rostral to the injection site, in the ventrolateral orbital cortex (VLO) and LO and rare labeled cells were seen in the dorsolateral orbital area (DLO) and AId. More posterior the prelimbic (PL) and infralimbic (IL) cortices were notable for their lack of labeling, the exception being a band of cells along the white matter, extending from the tenia tecta into the IL, PL, and more dorsal regions. A dense collection of retrogradely-labeled cells was seen in the ipsilateral pyriform cortex.

Contralateral to the injection site, labeling was seen in the more medial OFC, extending from the MO, VO, VLO, and AI$_v$ (Fig. 9A). Retrogradely-labeled cells were present in the contralateral LO, but less frequently in the DLO and AId (see Fig. 8). In the medial wall of the contralateral frontal cortex, only rare labeled cells were seen in the IL and PL, with a slightly greater number more dorsally in the anterior cingulate and medial precentral cortices. A low density of labeled cells was present in the rostral somatomotor cortex.

Caudal to the genu, cortical labeling was mainly seen in the perirhinal and pyriform cortices and the entire rostrocaudal extent of the cingulate cortex. At levels rostral to the crossing of the anterior commissure, a moderate number of labeled cells was present in the agranular insular cortex with fewer extending into the dysgranular and granular cortices; few claustral cells were labeled. The pyriform cortex was densely labeled. More caudally, the density of labelling dorsal to the rhinal fissure increased but there were fewer cells ventral to the fissure, in the pyriform cortex. At these levels a moderate number of retrogradely-labeled neurons were seen in the visceral areas, and still more posteriorly filled cells in the rostral pole of the entorhinal cortex, the rostral auditory cortex, and the ventral somatosensory cortex were observed. The neurons in the rostral entorhinal cortex did not extend posteriorly to the rest of the entorhinal cortex.

Retrograde labeling contralateral to the tracer deposit mirrored that of the ipsilateral hemisphere, albeit with a much-reduced density of labeling.

Amygdala and Hippocampus. The basolateral amygdala was almost devoid of retrograde labeling; this stands in sharp contrast to other cases with more lateral tracer deposits. Similarly, the hippocampus and subiculum did not contain back-filled cells.

Case A1062
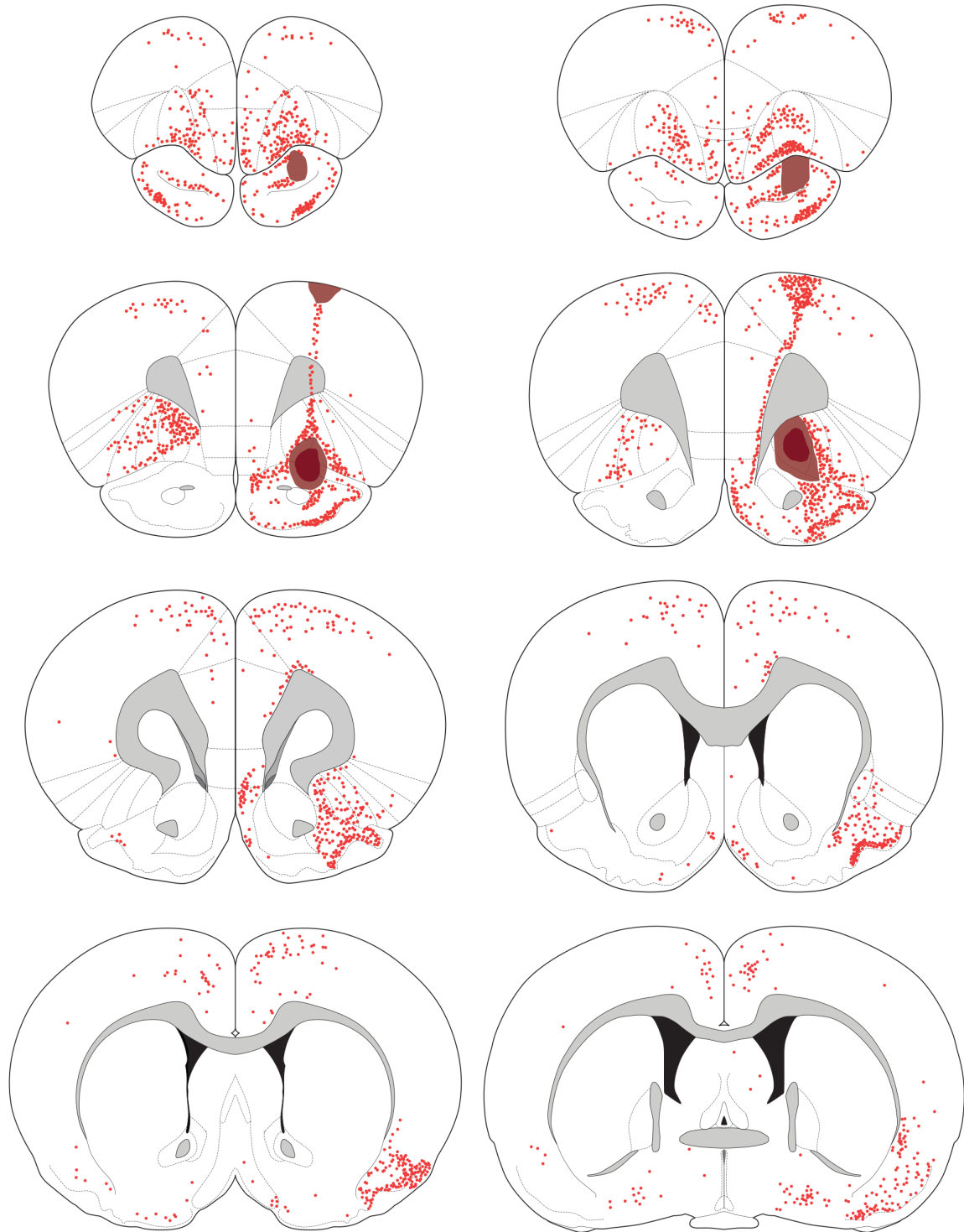
Figure 8. The distribution of retrogradely-labeled cells after a tracer deposit into the VLO$_p$ region (case A1062). Darkly shaded region represents tracer deposit core, with the lighter shading depicting the penumbra of tracer deposit. The chartings were made onto plates modified from Paxinos & Watson (2007).

Case A1062
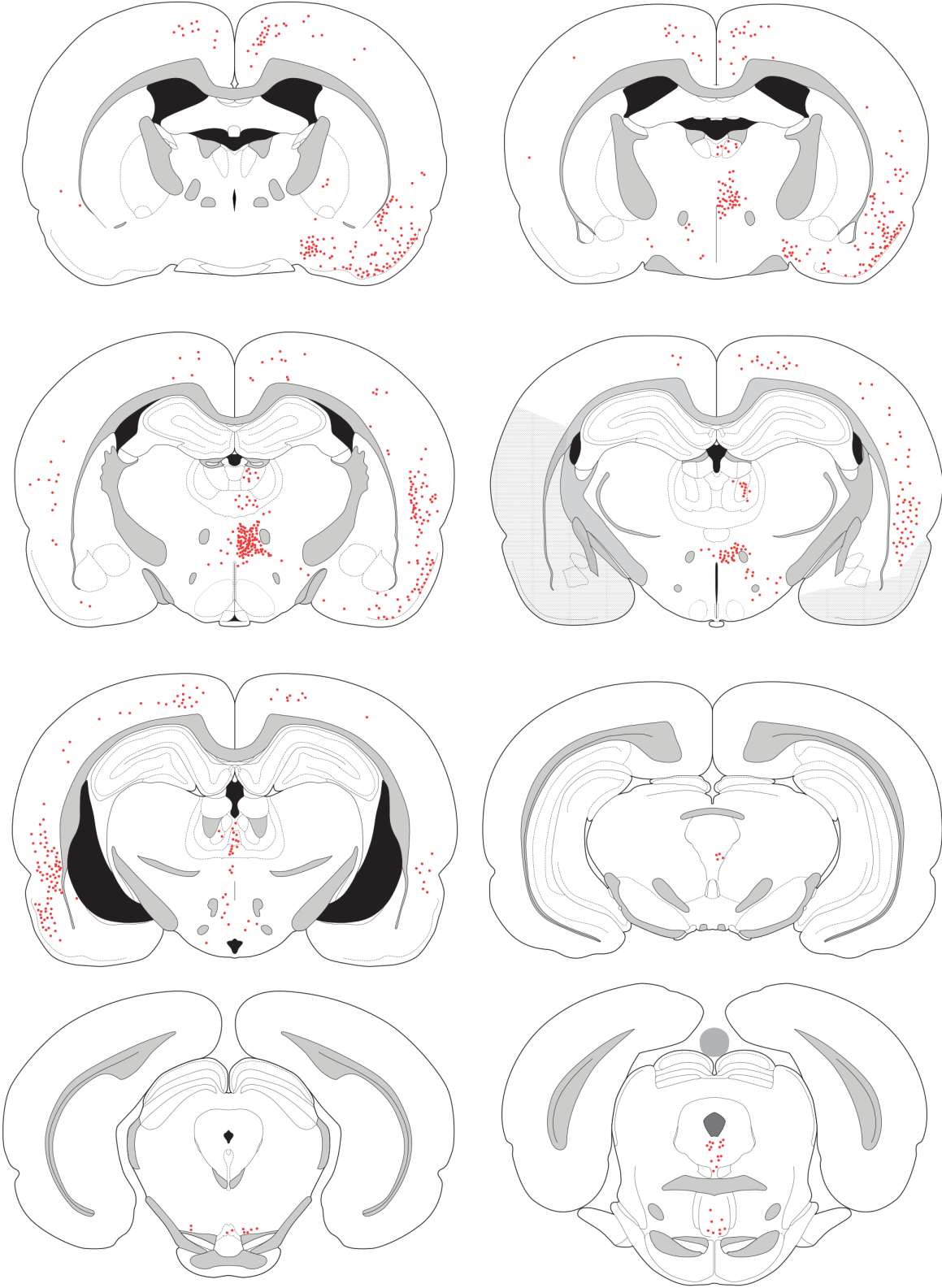
Figure 8. Distribution of retrogradely-labeled calles following a deposit in VLO$_p$ (case A1062).

Diencephalon. Retrograde labeling was most prevalent in the ipsilateral thalamus, with a dense aggregate of labeled cells seen in the nucleus submedius and in the reuniens. In contrast, relatively few labeled cells were seen in the MD, where they were concentrated in the central segment. A small number of cells was present in most of the midline nuclei and in the thalamic paraventricular nucleus (PVT), particularly its posterior (bilateral) half. A small number of labeled cells was present in the central medial (CM) nucleus; very few labeled neurons were in the parafascicular nucleus (PF), with most being concentrated in the posterior and ventral PF. Some retrogradely labeled cells were present in the parataenial nucleus. There was almost no labeling in the contralateral MD and adjacent areas.

In the hypothalamus, few retrogradely-labeled cells were seen in the parasubthalamic and preparasubthalamic nuclei (see Swanson et al., 2005) of the lateral hypothalamus (LH); almost no labeled cells were seen in the perifornical area.

Mesencephalon. Sparse labeling was observed in the supramammillary nucleus, and the VTA exhibited few labeled cells. Moving caudally, some labeled cells were present in the caudal linear nucleus, and a small cluster of FG-positive cells was seen in the posterior parabrachial nucleus. A moderate number of back-filled cells were in the ventral periaqueductal gray and the medial dorsal raphe.

The A10 dopamine neurons are located in a broad band extending from the supramammillary nucleus to the VTA and thence to the dorsal raphe. We therefore determined if any of the retrogradely-labeled cells were dopaminergic, using tyrosine hydroxylase-immunoreactivity to mark dopamine neurons. Of the retrogradely-labeled cells in this case, only 2.4% also expressed TH, i.e., were dopaminergic.
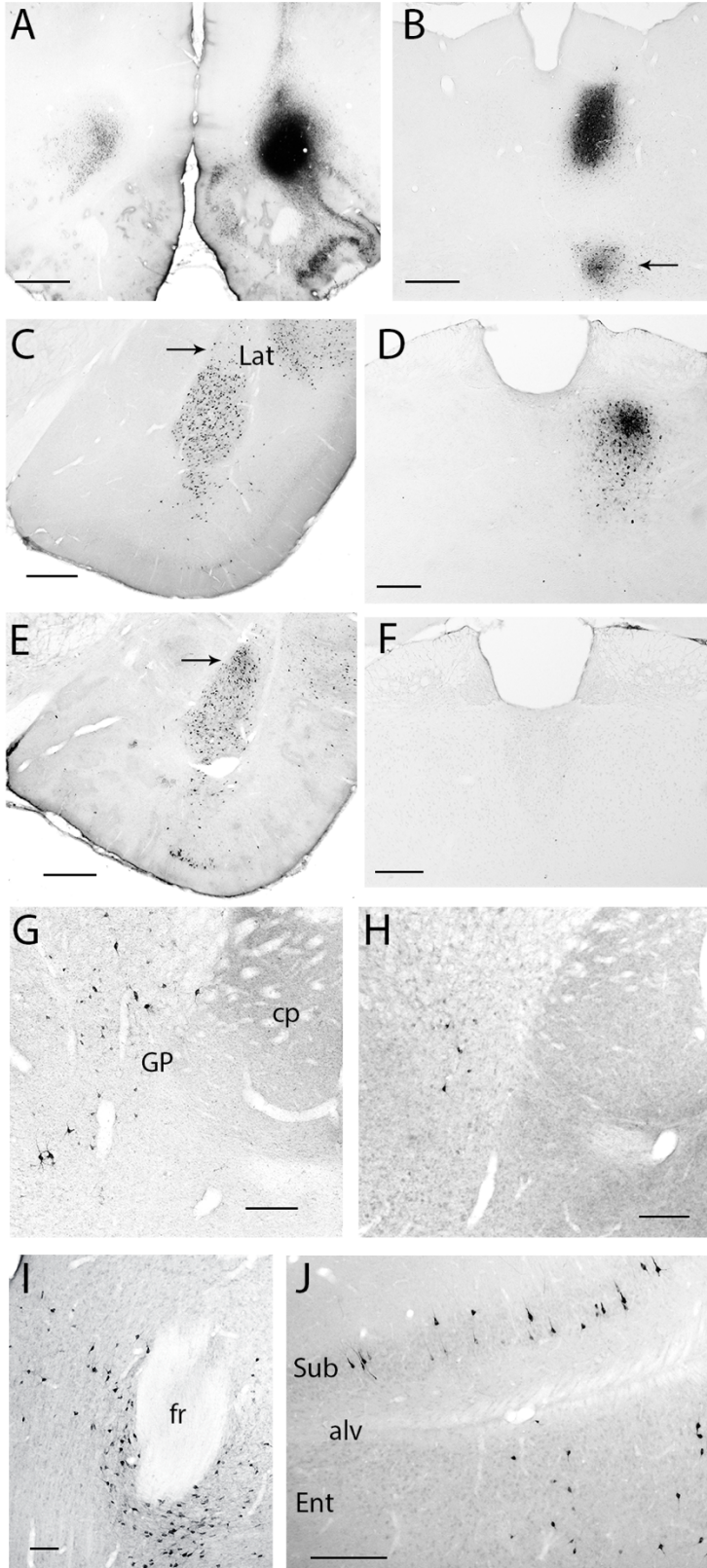
Figure 9. Retrograde labeling following tracer deposits into the OFC. (**A**) Tracer deposit into VLO$_p$ and contralateral labeling (case A1062). (**B**) Dense retrograde labeling in case A1052 in the central segment of MD, with the arrow pointing to labeling in the submedius nucleus. (**C, E**) Retrograde labeling in the amygdala following tracer deposits in AId$_2$ (C; A1014) and LO (E; A1064). Note the greater density of labeled cells in the lateral nucleus after FG was iontophoresed into LO. (**D, F**) Retrograde labeling in the MD following tracer deposits into either LO (D; A1065) or DI-GI (F; A1060). (**G, H**) Retrogradely-labeled cells in the globus pallidus and substantia innominata following a deposit into AId (G; A1016) or DI-GI (H; A1061). Labeled neurons in the parafascicular nucleus (**I**) and subiculum and entorhinal cortex (**J**) in case A1014 (AId$_2$ deposit). Scale bars: (A) 1000 μm; (B, C, E) 500 μm; (D, F-H, J) 250 μm; (I) 250 μm. Abbreviations: alv, alveus; CP, caudatoputamen (striatum); fr, fasciculus retroflexus; ENT, entorhinal cortex; GP, globus pallidus; Lat, lateral amygdala nucleus; PF, parafascicular nucleus; Sub, subiculum.

Other areas. Labeling was seen in both the horizontal and vertical limb of the diagonal band of Broca (DBB). Labeled cells were also seen in the substantia innominata (SI) and in the ventral aspects of the globus pallidus (GP). There appeared to be two types of labeled pallidal cells, one with a large cross-sectional soma ($298.6 \pm 19.9 \ \mu m^2$) and the other with much smaller soma ($128.1 \pm 14.8 \ \mu m^2$). Rare back-filled cells were seen in the ventrolateral septum.

<u>Case A1065.</u> The core of the deposit was centered in the superficial layers of the lateral orbital cortex (LO) and extended medially into the superficial AI_v and laterally into the dorsal agranular insular cortex, ventral part (AId_2; Fig. 7D, 10). The penumbra surrounding the tracer core involved the deep layers of the LO and slightly extended into rostral pyriform cortex, ventral to the rhinal fissure.

Cortical Afferents. Retrogradely-labeled cells were seen across the medial and lateral regions of the ipsilateral frontal cortex. Within the orbital regions, labeling was seen in the VO, VLO, AI_v, and LO, with scattered labeling in AId_2 (Fig. 10). In the medial wall of the hemisphere, there was a dense accumulation of retrogradely-labeled cells in the rostral MO. More caudally in the medial frontal lobe, the density of labeled neurons decreased, with a few small clusters of labeled neurons in the rostral IL, PL, pregenual cingulate, and medial precentral cortices. The tracer deposit extended slightly into to the rhinal fissure, resulting in dense labeling of cells in the rostrocaudal extent of the pyriform cortex.

Labeling in the contralateral frontal cortices largely mirrored that of the ipsilateral cortex but with fewer labeled cells present. However, the caudal half of the contralateral infralimbic region was largely devoid of labeled cells.

Case A1065
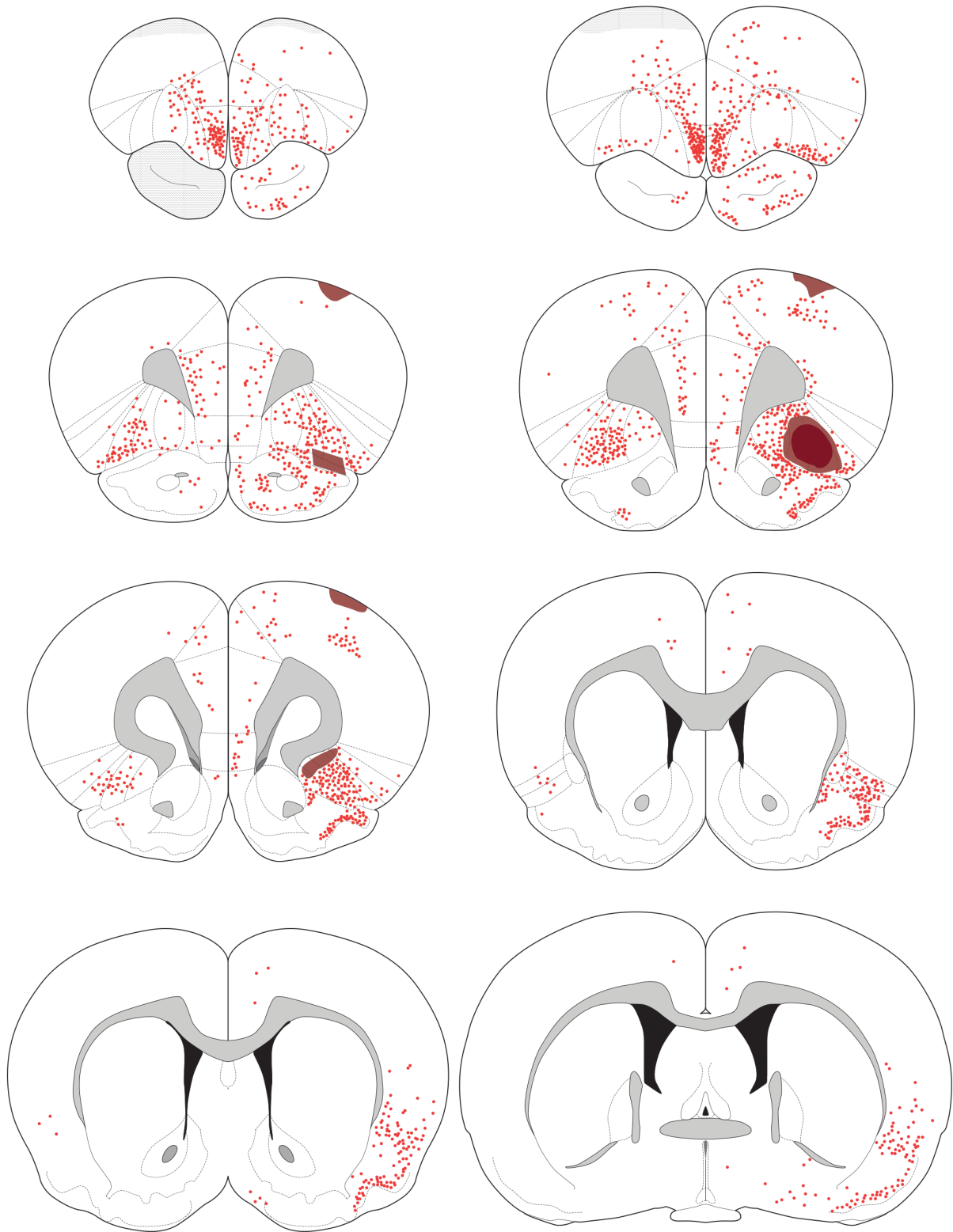
Figure 10. The distribution of retrogradely-labeled cells after a tracer deposit of the LO (case A1065).

Case A1065
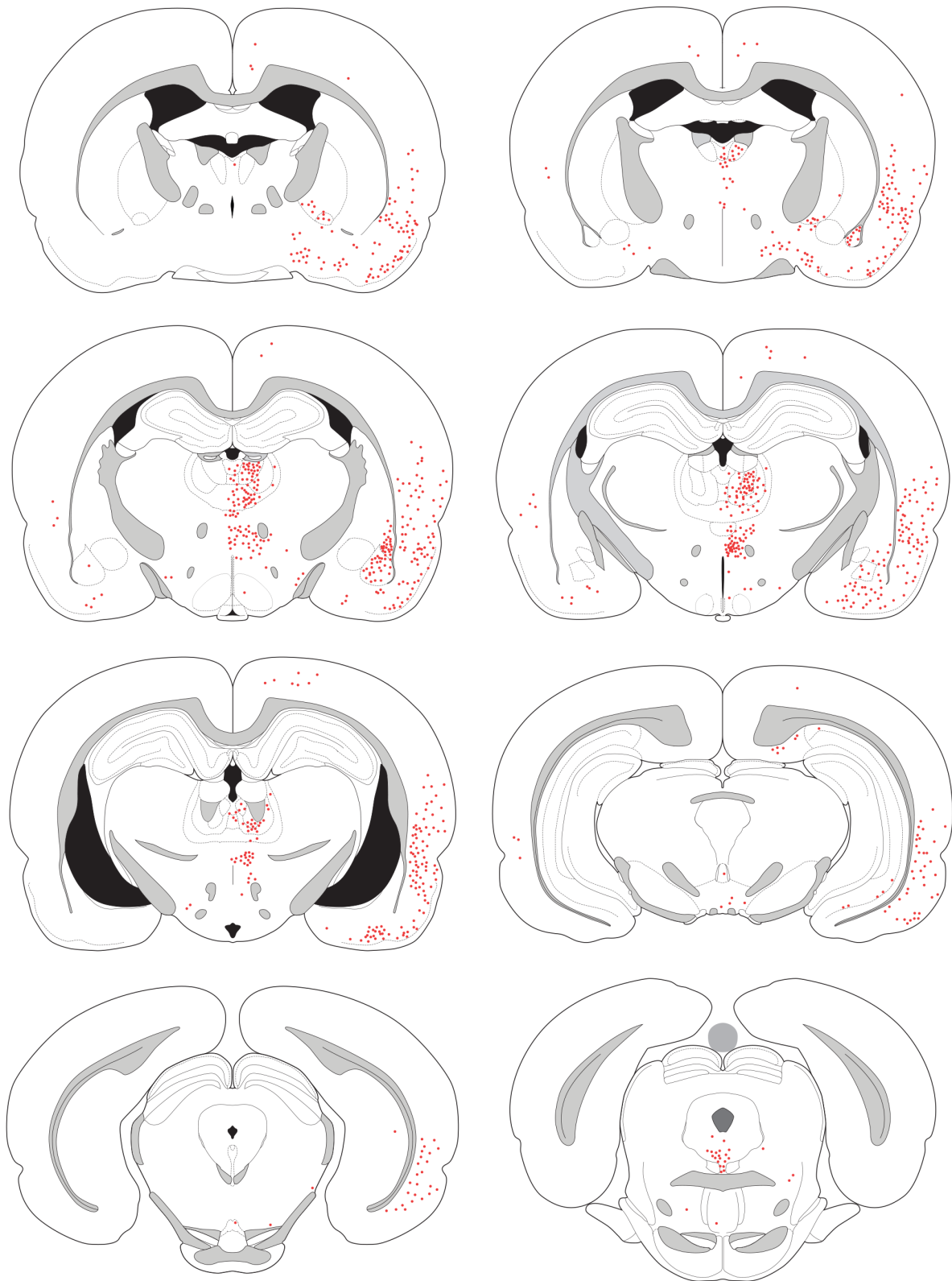
Figure 10. The distribution of retrogradely-labeled cells after a tracer deposit of the LO (case A1065).

Posterior to the genu, retrograde labeling was most predominant in the peri- and entorhinal cortices, with sparse labeling in the cingulate cortex (Fig. 10). At mid-rostral striatal levels, retrogradely-labeled cells were present in the ipsilateral agranular insular cortex across L2/3 and L5, as well as in the dysgranular and granular cortices. Labeling ventral to the rhinal fissure, in the pyriform cortex, was progressively less dense along the anterior-posterior domain. More caudally, the posterior insular cortex had some labeled cells, with a very low density of back-filled cells more dorsally, in the auditory cortex. In the entorhinal region retrogradely-labeled cells were present in area 25 and the lateral entorhinal cortex, with minimal labeling in the medial entorhinal zone.

In the contralateral hemisphere, there was sparse of labeling in the granular, dysgranular and agranular insular cortices and perirhinal cortex; only rarely were labeled cells present in the contralateral entorhinal cortex.

Amygdala and Hippocampus. Retrograde labeling was detected through the rostro-caudal extent of the ipsilateral amygdala (Fig. 10). Labeling was present in the BLA and extended dorsally into the lateral nucleus. Retrograde labeling appeared roughly comparable in the lateral and basolateral nuclei. In addition, the density of labeled cells appeared somewhat greater in the dorsal than ventral aspects of the basolateral nucleus. A few labeled cells were also seen in the anterior amygdaloid area and the basomedial amygdala (BMA). No labeled cells were observed in the central nucleus. Retrograde labeling of the amygdala was almost exclusively ipsilateral to the injection site.

Light labeling was detected in the hippocampus. In particular, clusters of retrogradely-labeled cells were seen in both the subiculum and to a lesser degree in the CA1 field of the ipsilateral hippocampus.

Diencephalon. Many retrogradely-labeled cells were present in the ipsilateral thalamus, most densely in the MD and nucleus submedius; minimal labeling was seen in the contralateral thalamus. Labeled cells in the anterior MD were mainly concentrated in the central portion of the structure, with some extension into the medial and lateral segments. More caudally, labeled MD neurons were primarily localized to the central and lateral aspects of the nucleus, with a dorsal bias (see Fig. 9D). Moderately dense labeling of the parataenial nucleus was observed. Along the midline, scattered labeled cells were present in the anterior PVT; labeling decreased as one moved caudally in the PVT. In the intermediodorsal (IMD) nucleus, ventral to the PVT, a somewhat greater number of filled neurons were seen; scattered retrogradely-labeled cells were present in the reuniens and rhomboid nuclei. Dense labeling was seen in the nucleus submedius.

Retrograde labeling was seen in the central medial-parafascicular (CM-PF) complex, primarily in the central medial (CM) and paracentral (PC) portions. Moderately dense labeling was present in the parafascicular nucleus, particularly in the medial PF (Fig. 10).

In the hypothalamus, a very small number of retrogradely-labeled cells was observed in the dorsal perifornical area (Fig. 10). In contrast to case A1014, only rarely were labeled cells seen in the remainder of the LH, where they were restricted to the ventrolateral area.

Mesencephalon. Sparse retrograde labeling was seen in the VTA, primarily in the nucleus parabrachialis. Labeled cells were also present in the rostral linear nucleus, and increased in number as one moved posteriorly to the caudal linear nucleus. Rare labeled cells were seen in the interpeduncular nucleus, pars lateralis of the substantia nigra, and retrorubral field.

Caudally, in the dorsocaudal extension of the A10 cell group (A10dc; Hökfelt et al, 1984), where the caudal linear nucleus merges dorsally with the ventral periaqueductal gray, a few retrogradely-labeled cells were present. These cells were continuous with a more dense collection of filled cells in the dorsal raphe. We observed a single labeled cell in the median raphe.

Of the small number of retrogradely-labeled cells observed in the VTA and A10dc region, 29.5% of these neurons expressed TH, i.e., were dopaminergic.

Other areas. Retrogradely-labeled cells were detected in several other forebrain areas. A few labeled neurons were present in the DBB. Labeled cells were also seen in the substantia innominata and nucleus basalis, but rarely did labeling extend dorsally into the globus pallidus. The nucleus basalis differed from most other subcortical nuclei by displaying bilateral labeling after LO injections, although the density of labeling in the contralateral hemisphere was less than observed ipsilaterally.

Afferents to the central segments of OFC: DLO and AId_2

Case A1014. The dense core of the tracer deposit primarily involved the deep layers of the dorsal agranular cortices, with the penumbra surrounding the core extending from L2-L6 (Fig. 7F, 11). In addition to $AId_{1/2}$, the core of the deposit extended rostrally into the dorsal aspect of the dorsolateral orbital cortex 1 (DLO_1; see Fig. 11) and minimally into the LO.

Cortical Afferents. Retrogradely labeled cells were seen in much of the ispilateral frontal cortex, with prominent labeling seen across the cortex above the rhinal sulcus, from the ventrolateral orbital cortex (VLO) into the lateral aspect of the LO (see Fig. 11); a moderate number of labeled cells was seen in the anterior pyriform cortex, ventral to the rhinal sulcus.

Case 1014
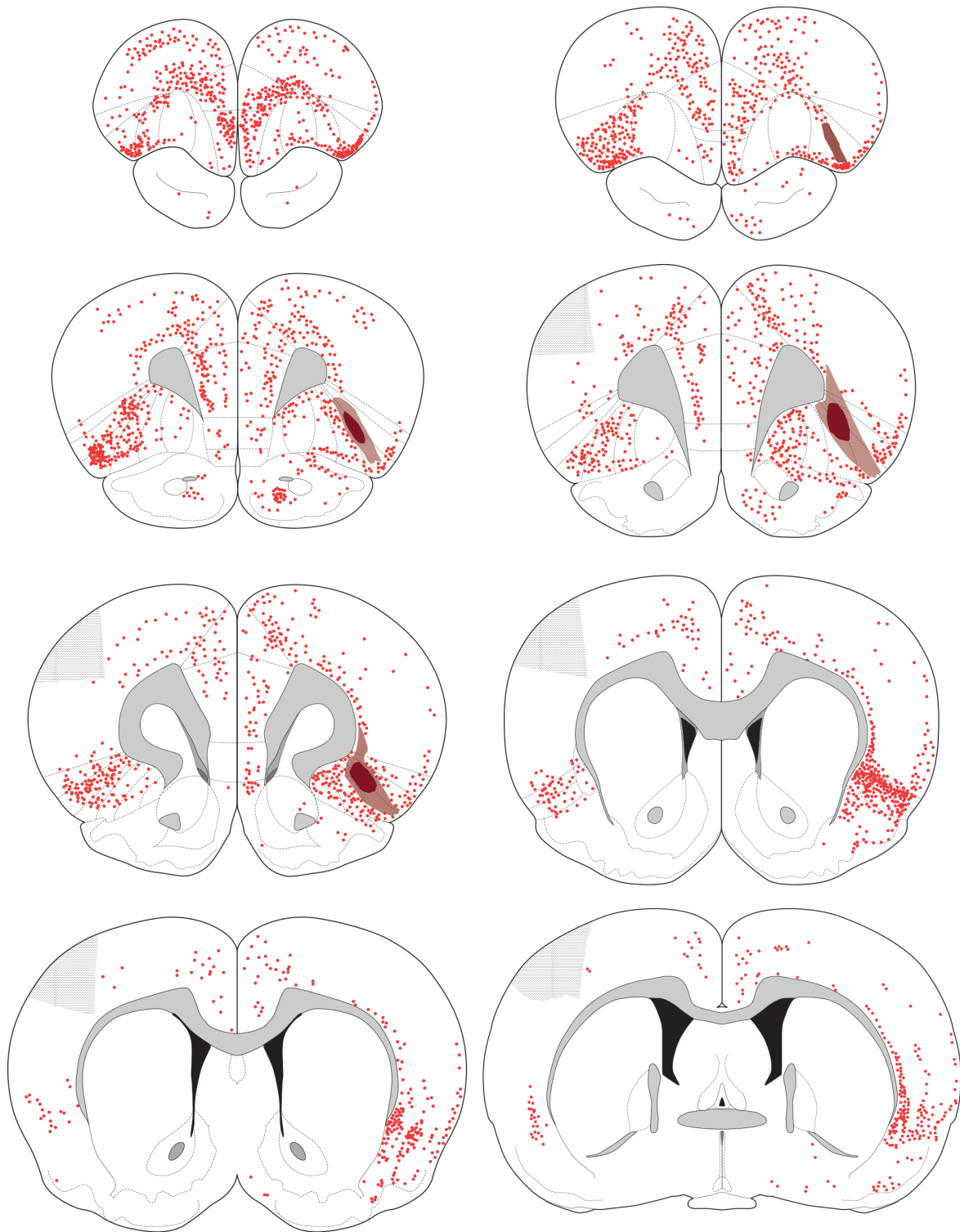
Figure 11. Retrograde labeling following a tracer deposit into AId$_2$ (case A1014).

Case A1014
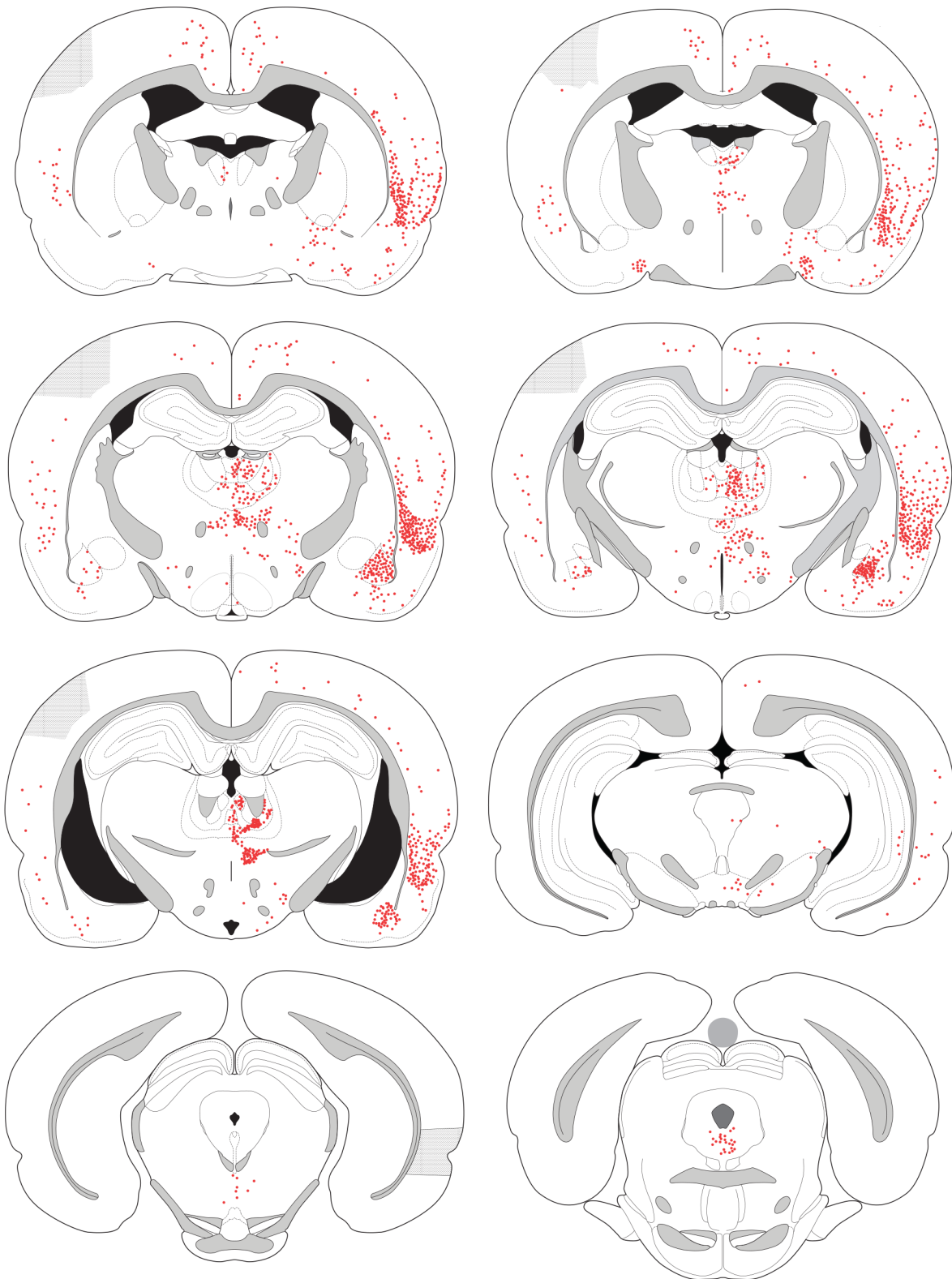
Figure 11. Retrograde labeling following a tracer deposit into AId$_2$ (case A1014).

The entire medial wall of the ipsilateral hemisphere showed moderate labeling, including the MO, layer 5 of the infralimbic (IL), prelimbic (PL), pregenual anterior cingulate, and medial precentral cortices, extending into the forelimb representation of the motor cortex.

In most frontal areas, the density of labeling was roughly comparable in the ipsilateral and contralateral hemispheres. Very dense labeling was present in the AId_1 and AId_2 cortices contralaterally, extending rostrally to the DLO and medially into the LO. In contrast to the largely symmetric labeling across the two hemispheres in the OFC regions, in the caudal aspects of the contralateral mPFC there were very few labeled cells in the ventral PL and IL cortices (Fig. 11). Labeling was largely absent in the rostral somatosensory cortices. In the posterior aspects of the frontal cortex retrogradely-labeled cells were present in the pyriform cortex.

Posterior to the genu of the corpus callosum, cortical labeling was largely restricted to two broad regions: the peri- and ento-rhinal cortices laterally, and the cingulate cortices dorsomedially. There was extensive labeling of neurons across the granular, dysgranular, and agranular insular cortices (Fig. 11). Ventral to the insula, there was light-to-moderate labeling of the pyriform cortex. The dorsal half of the anterior claustrum contained scattered retrogradely-labeled cells; in the more posterior claustrum labeling was more dense and uniformly distributed. Dorsal to the granular insular cortex was a thin band of deep layer neurons that followed the curve of the white matter to the motor cortex. In addition, a small number of labeled neurons were present in the auditory cortex.

Labeling was also present in the entorhinal cortex (ENT), primarily in the deep layers of the lateral entorhinal area (Fig. 9J, 11); far fewer cells were seen in the medial ENT.

Retrograde labeling was seen across the rostrocaudal extent of the cingulate cortex, from the pregenual aspects to the retrosplenial cortex; labeled cells were present in both the deep (L5) and superficial layers, with few labeled cells seen in the medial-most motor cortex.

Amygdala and Hippocampus. Ipsilaterally, dense labeling was seen in the basolateral (BLA) nucleus, with labeling of the lateral nucleus being less dense (Fig. 9C, 11). Labeling in the contralateral BLA was sparse. A few scattered cells were present in the intercalated nuclei and AST. The entire mediolateral extent of the basolateral complex contained labeled cells, with no apparent mediolateral bias. Moving caudally in the amygdala, light to moderate labeling was present in the basomedial nucleus (BMA). Only rarely were labeled cells seen in the corticomedial amygdala.

Moderate labeling of pyramidal cells in the hippocampal formation was observed. These labeled neurons were restricted to the CA1 field and the subiculum and presubiculum (Fig. 9J, 11).

Diencephalon. Retrograde labeling was dense in the ipsilateral thalamus, primarily in the mediodorsal nucleus (MD) and midline intralaminar nuclei, with less dense labeling in the central medial complex. There was relatively little labeling in the contralateral thalamus. Retrogradely-labeled cells were present in the lateral hypothalamus (LH) and contiguous nuclei.

Dense but heterogeneous labeling was seen in the MD (Fig. 11), with more cells labeled in the medial MD and spilling over into the central part of the MD; fewer labeled cells were seen in the lateral MD. A moderately dense group of labeled cells was present in the parataenial nucleus, but only rare filled cells were seen in the anteromedial nucleus. Retrogradely-labeled cells were also present medial to the MD, in the thalamic paraventricular nucleus (PVT); the density of labeled cells was greater in the posterior PVT (where the nucleus bifurcates) than

rostral PVT. Other midline thalamic nuclei, including the intermediodorsal (IMD) and interanteromedial (IAM) nuclei, as well as the rhomboid and reuniens, also contained labeled cells (Fig. 11). The nucleus submedius contained numerous labeled cells.

Labeled neurons were detected across in the central medial-parafascicular complex. These retrogradely-filled cells were moderately dense in the CM, and diminished in number moving laterally to the paracentral (PC) and central lateral (CL) nuclei. Posteriorly, the medial parafascicular nucleus was densely labeled (Fig. 9I, 11).

In the ventral diencephalon a small number of retrogradely-labeled cells was seen in the lateral hypothalamic region. A small cluster of labeled cells was present in the dorsal perifornical area (Fig. 11). More scattered cells were seen in other territories of the lateral hypothalamus, particularly in more lateral areas of the LH, with most of these seen in the parasubthalamic and preparasubthalamic nuclei (see Swanson et al., 2005). Very rare labeled neurons were seen in the ventromedial nucleus and the posterior hypothalamus.

Mesencephalon. Light labeling was seen in the midbrain dopamine cell-rich areas. Scattered cells were present medially in the ventral tegmental area (VTA), with cells mainly present in the nucleus parabrachialis and nucleus paranigralis; a few labeled neurons were seen in the rostral linear nucleus. Further caudally, a substantially greater number of retrogradely-labeled cells was present, primarily in the caudal linear nucleus, the ventral periaqueductal gray, and the dorsal raphe. Few labeled cells were seen in the medial substantia nigra, with rare back-filled neurons seen in the medial retrorubral field (Fig. 11). Of the retrogradely-labeled cells seen across the rostrocaudal extent of the A10 cell group, 22% were also TH-ir, i.e., about one fifth of the midbrain neurons innervating the OFC were dopaminergic.

Other Areas. Some other areas of the brain contained retrogradely-labeled neurons. Labeled cells were seen in the DBB, mainly in the vertical limb. Moving posteriorly cells were seen in the substantia innominata and extending dorsally with a few labeled cells in the ventral-most globus pallidus. Retrogradely labeled cells were not seen in the nucleus accumbens or the septal nuclei.

Afferents to areas dorsolateral to the zone of dopamine innervation (AId_1, DI, and GI)

<u>Case A1054.</u> The Fluoro-Gold deposit primarily involved AId_1 and DI (see Figures 7E, 12). The core of the deposit was in the mid-anteroposterior level of AId_1 and DI, with the penumbra extending rostrally into DLO_1.

Cortical Afferents. Moderate labeling of the pyriform cortex was observed. More back-filled cells were seen in the posterior pyriform cortex rather than the anterior pyriform area. In the ipsilateral frontal lobe, a narrow band of retrogradely-labeled FG cells was seen in the prelimbic cortex, but only rarely did these cells extend ventrally into the infralimbic cortex; the exception to this rule was that there was appreciable labeling in the caudal infralimbic region. A moderate number of labeled cells was present in both the superficial and deep layers of the medial precentral and anterior cingulate cortices. Labeled somatosensory cells extended dorsally from the FG deposit. The density of labeled cells was greater in the more anterior frontal regions, and showed a marked decrease caudally. Rare labeling was present in the anterior (pregenual) pyriform cortex, particularly ipsilateral to the tracer deposit.

Labeling in the contralateral frontal areas mirrored that seen ipsilaterally, but was less dense. In the contralateral homotypic areas, the density of FG-labeled cells was appreciably greater in the dysgranular than granular cortices, and a moderate density of cells also present in AId_1.

Case A1054

Figure 12. Retrograde labeling following a tracer deposit into AId$_1$ (case A1054).

Case A1054
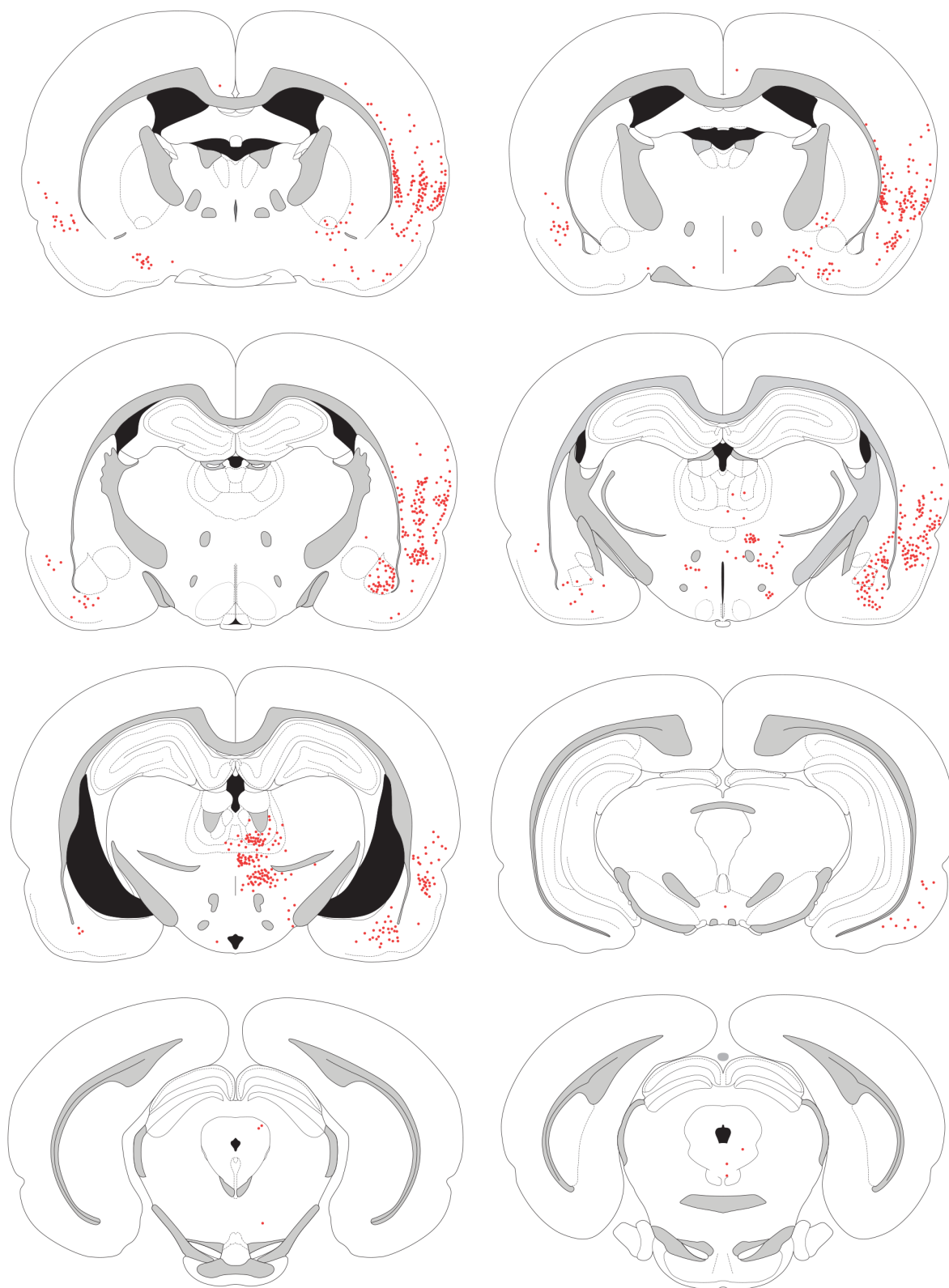
Figure 12. Retrograde labeling following a tracer deposit into AId$_1$ (case A1054).

Posterior to the genu, moderate labeling was seen in the ipsilateral insular cortices and in the pyriform cortex. Although the claustrum was nearly devoid of labeling except in its most dorsal aspect, the endopyriform cortex was densely filled with retrogradely-labeled cells.

Amygdala and Hippocampus. The basolateral amygdala contained a moderate number of retrogradely-labeled cells. Most of these neurons were located in the BLA, with less seen in the lateral nucleus; fewer labeled neurons were seen in the basomedial nucleus. There was no significant labeling of cells in the hippocampal formation, with the exception of a low-to-moderate density of filled cells in the lateral entorhinal cortex.

Diencephalon. In the mediodorsal thalamus a small number of FG-positive cells was seen in the ventral parts of the central and medial MD. Very few filled cells were seen in the thalamic paraventricular nucleus; cells in the rhomboid and reuniens nuclei were also observed. The nucleus submedius was not labeled. Finally, a moderate density of back-filled cells was present in the ventral posterior medial (VPM) and particularly ventromedial (VM) thalamic nuclei.

A moderate number of retrogradely-labeled cells were seen in the CM-PF complex. In the central medial nucleus back-filled neurons were more frequently encountered than in the paracentral and central lateral nuclei. There was a moderately high density of FG-positive cells in the parafascicular nucleus.

Rare retrogradely-labeled cells were seen in the perifornical area and the lateral hypothalamus. A somewhat greater number of back-filled cells were seen in the posterior lateral hypothalamus.

Mesencephalon. A moderately-dense cluster of FG-positive cells was present in the supramammillary nucleus. Occasionally, back-filled cells were seen in the VTA, where they were almost exclusively located in the parabrachial nucleus. A few labeled cells were seen in the

anterior pole of the dorsal raphe. Of the retrogradely-labeled neurons in the ventral midbrain, 17.5% were dopaminergic, as defined by expression of TH-ir.

Other areas. Very rare FG-positive cells were seen in the olfactory tubercle. There was a moderate density of retrogradely-labeled neurons in the ventral pallidum, clustering at the border of the ventral pallidum and dorsal (globus) pallidus at rostral GP levels, but with labeled cells seen extending into the GP proper for 500-1000 μm.

A small cluster of FG-positive cells was observed in the preoptic area, just dorsolateral to the optic tract.

Case A1060. The core of the tracer deposit was located in AId_1 and the dysgranular insular cortex dorsal to AId_1, with some involvement of the granular insular cortex (GI) (Fig. 13). The deposit involved most cortical layers, with the anterior portion invading the superficial layers and extending dorsocaudally into the deep layers. The penumbra extended anteriorly to encroach on the DLO_1 and ventrally into AId_2.

Cortical Afferents. Scattered retrogradely-labeled cells were present in the lateral half of the ipsilateral frontal pole, but few were seen along the medial wall. Rare labeling was found in the rostral MO. In the PL, only scattered retrogradely-labeled cells were observed. Moderate labeling was observed in the medial precentral (shoulder) and cingulate cortices.

Contralateral to the injection site the pattern of retrograde labeling was largely comparable to that seen in the ipsilateral areas. In contrast to the other cases, the subjective density of labeled cells in the contralateral somatomotor, medial precentral, and cingulate cortex appeared slightly greater than that in the corresponding ipsilateral areas.
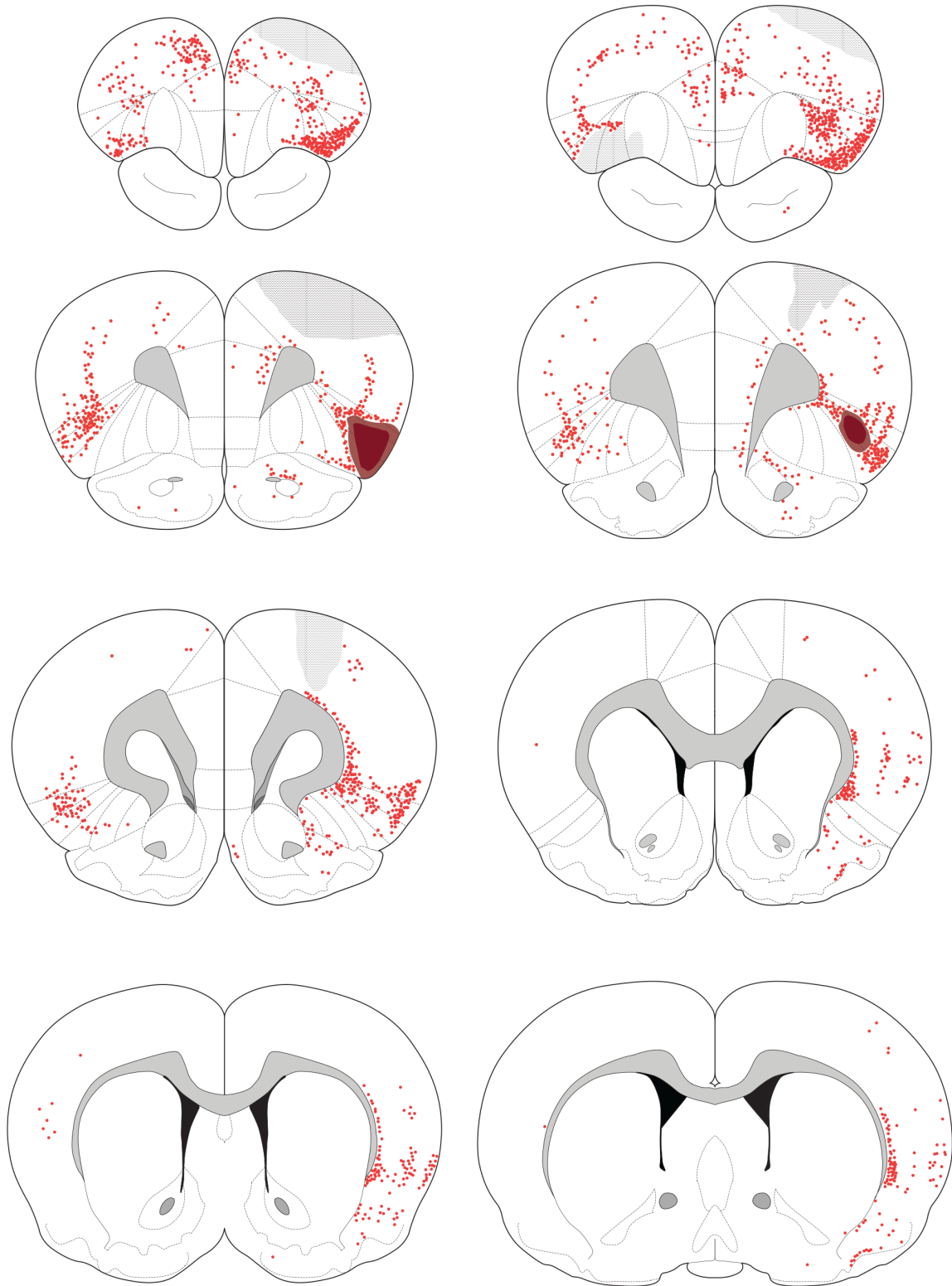
Case A1060

Figure 13. Retrograde labeling following a tracer deposit into DI-GI (case A1060).

Case A1060
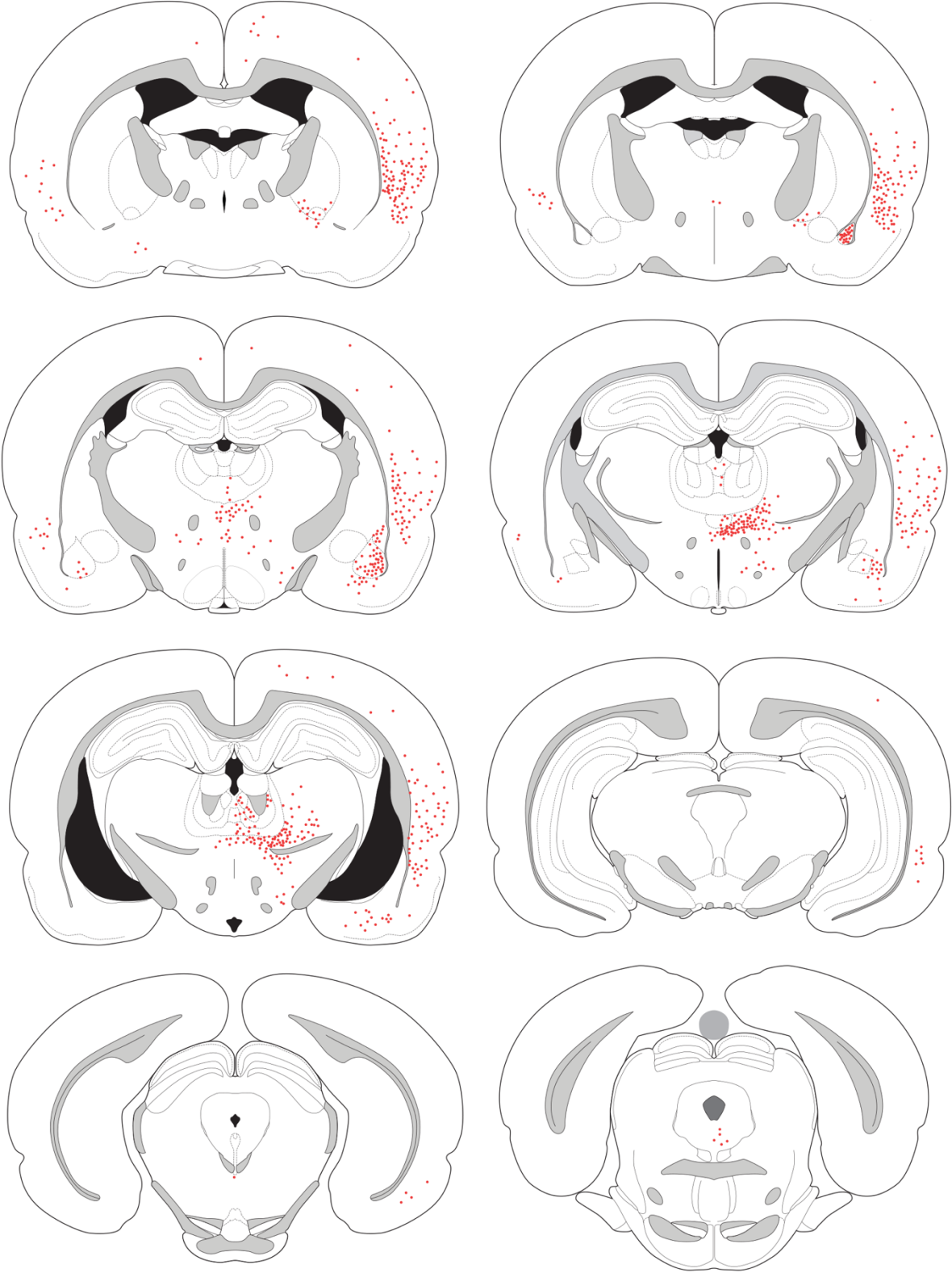
Figure 13. Retrograde labeling following a tracer deposit into DI-GI (case A1060).

Retrograde labeling in cortical areas posterior to the genu was predominantly observed in the peri- and ento-rhinal cortices, with sparse labeling in the cingulate areas. In the cortex surrounding the rhinal fissure, retrograde labeling was dense in the ipsilateral AI, DI, and GI, and extended dorsally into the somatomotor cortex; scattered cells were seen in the claustrum. Labeling in the contralateral insular cortex was much less dense and primarily involved the GI. No retrogradely-labeled cells were seen in the pyriform cortex. Labeling in the entorhinal cortex was scattered, and mainly found in the lateral entorhinal area.

Amygdala and Hippocampus. Retrogradely-labeled cells populated the basolateral and lateral nuclei of the amygdala. There was a greater density of retrograde labeling in the anterior BLA complex, with few labeled cells present in the posterior BLA. Labeling was slightly more dense in the basolateral nucleus, as compared to the lateral nucleus. Scattered cells were seen in the basomedial nucleus. Very few retrogradely-labeled cells were detected in the contralateral amygdala.

The hippocampus, including subiculum and CA1 field, rarely contained retrogradely-labeled neurons.

Diencephalon. In contrast to the more medial cases previously discussed, retrograde labeling was minimal in the MD. Although a few scattered retrogradely labeled cells were present in the thalamic paraventricular nucleus and other midline nuclei, the MD was conspicuous by its absence of labeling (see Fig. 9F). Sparse retrograde labeling was observed in the central medial nucleus, with a moderate density of filled cells present in the medial parafascicular (PF) nucleus. Moderate numbers of retrogradely-labeled cells were seen across the ventromedial, ventral posterior, and posterior thalamic nuclei.

In the hypothalamus, infrequent retrogradely-labeled cells were scattered dorsal and lateral to the fornix, where they abutted the ventral aspect of the zona incerta, with few filled cells in most lateral aspects of the LH, near the border with the subthalamic nucleus.

Mesencephalon. Almost no retrogradely-labeled cells were seen in the VTA. More caudally there was a moderate number of retrogradely-labeled cells in the dorsal raphe region, with less frequent labeling of cells in the periaqueductal gray, and rare labeled neurons in the in the caudal linear nucleus. In this case, none of the retrogradely-labeled cells also expressed TH, i.e., none were dopaminergic.

Other areas. Retrograde labeling was seen at the border of the globus pallidus and nucleus basalis and ventral pallidum.

Case A1061. The core of the tracer deposit was centered in the dysgranular and granular insular cortices (DI and GI), mainly involving the deep layers but with some L2/3 involvement rostrally. The deposit extended dorsally into the deep layers of the somatosensory cortex.

Cortical Afferents. Retrogradely labeled cells were widely distributed across much of the ipsilateral and contralateral frontal cortices (see Figures 7C, 14). Moderately dense labeling was seen in the ipsilateral rostral somatomotor region, decreasing medially, with few retrogradely-labeled cells seen in the shoulder cortex, pregenual cingulate, prelimbic, and infralimbic cortices on the site of the tracer deposit.

Retrograde labeling was more dense in the contralateral frontal area, particularly the rostral aspects of the somatomotor and M2 motor regions. Scattered back-filled cells were present in the contralateral mPFC, including the prelimbic and infralimbic cortices. The
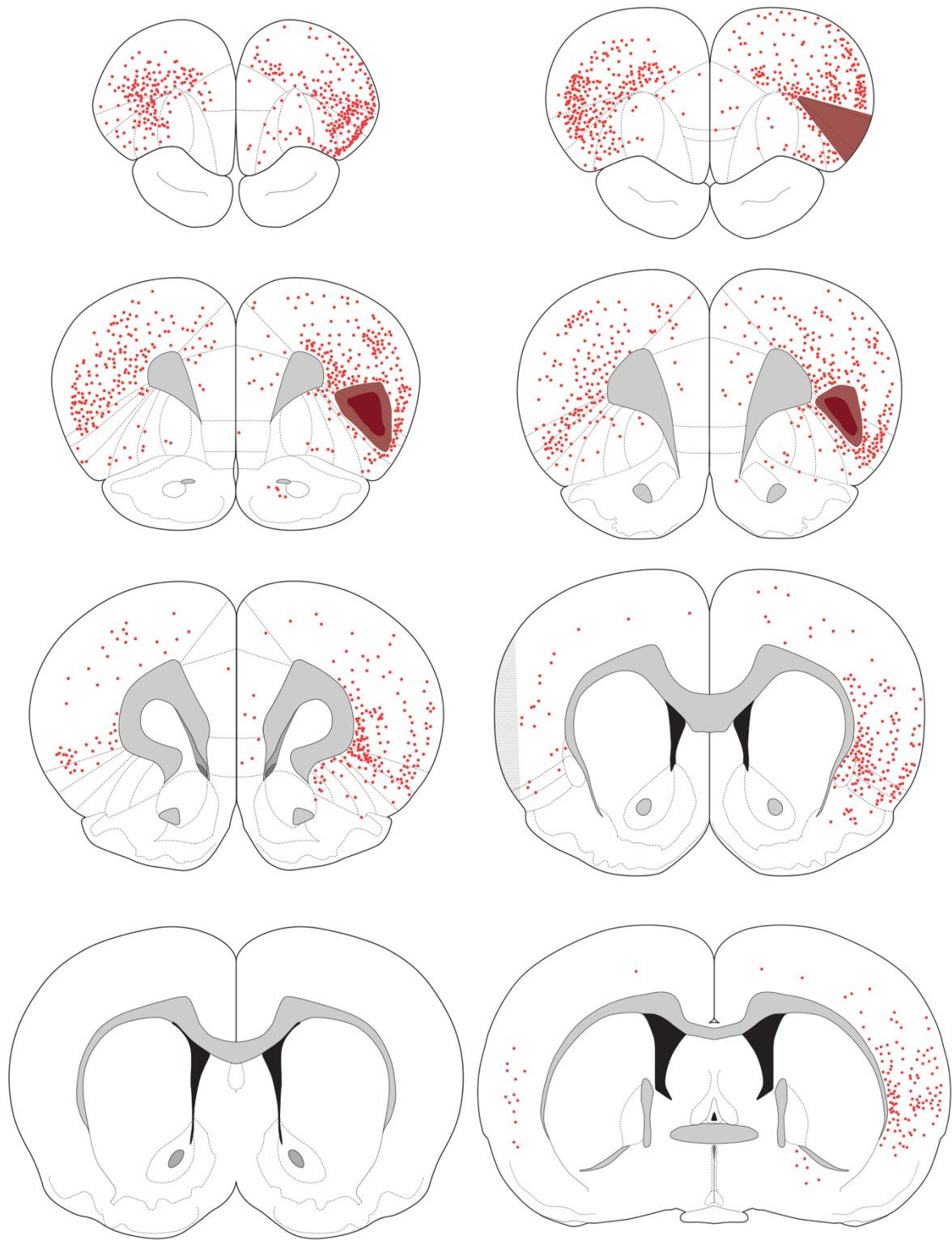
Case A1061
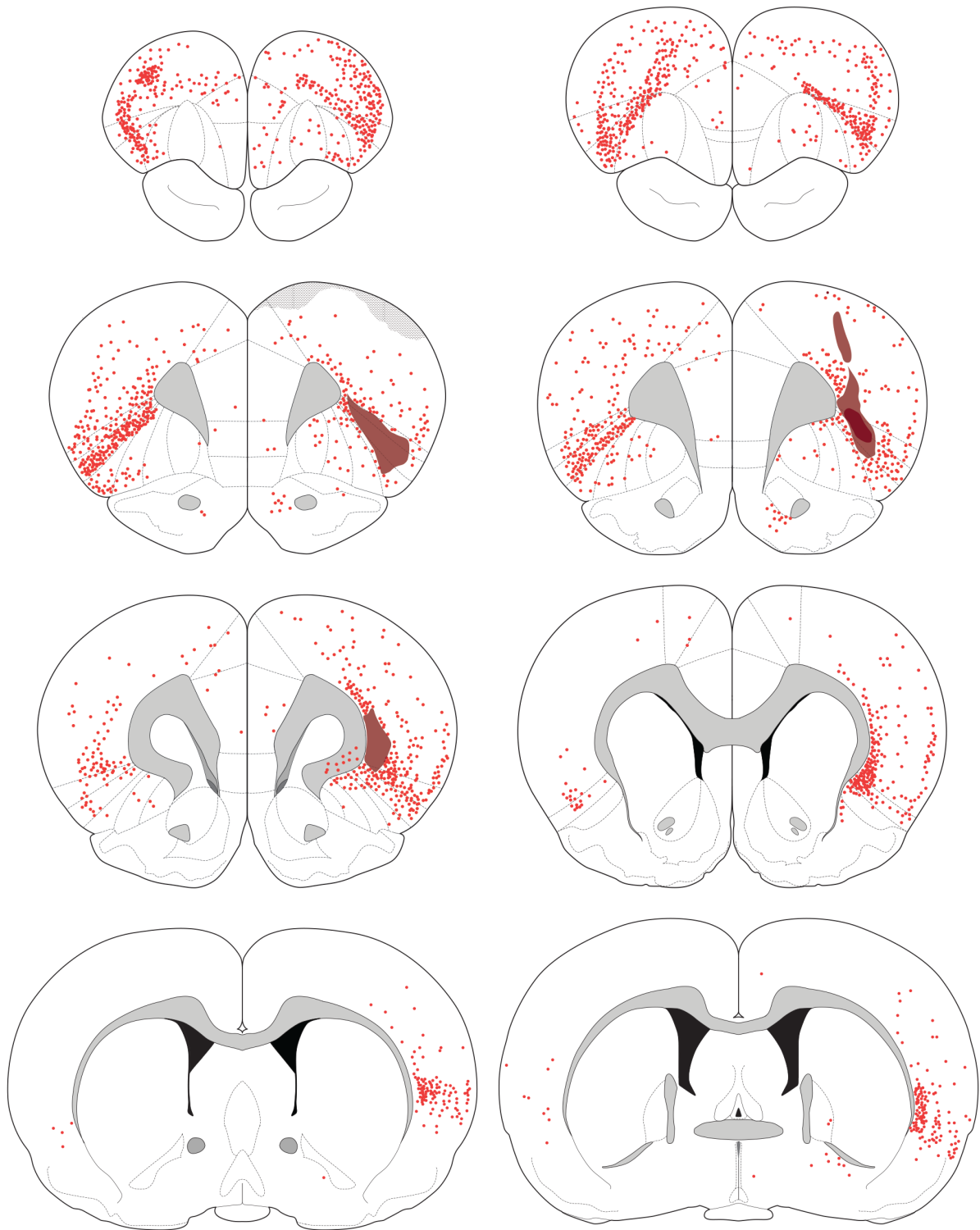
Figure 14. Retrograde labeling following a tracer deposit into DI-GI (case A1061).

Case A1061
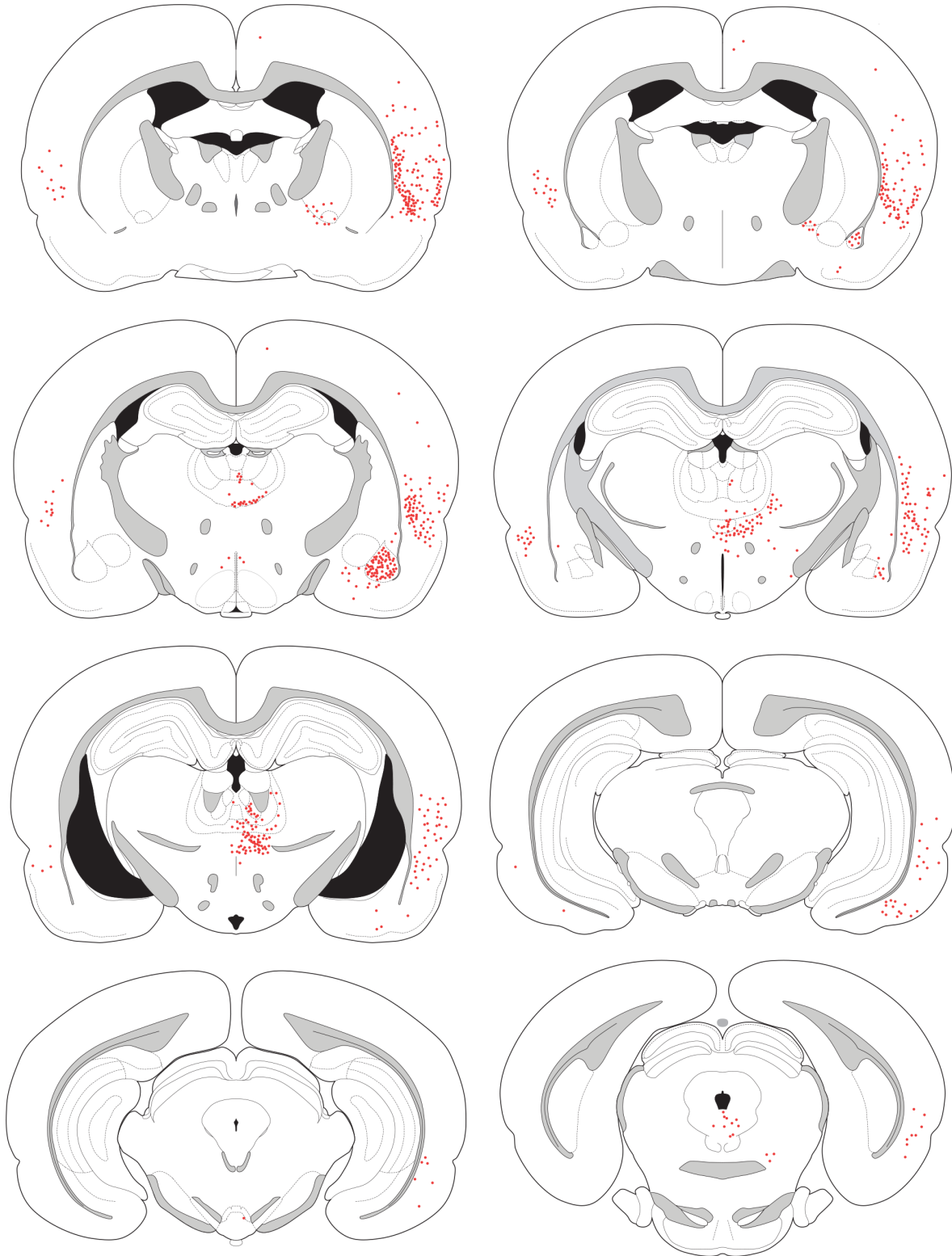
Figure 14. Retrograde labeling following a tracer deposit into DI-GI (case A1061).

contralateral GI and particularly DI were densely labeled; less densely labeled were DLO_1, $AId_{1/2}$, and LO, bilaterally.

Posterior to the genu, ipsilateral cortical labeling was largely restricted to the cortices dorsal to the rhinal sulcus, where labeling was seen in the perirhinal cortex as well as gustatory and visceral fields, particularly in the deep layers.

Contralaterally, there were considerably fewer retrogradely-labeled cells. The claustrum harbored a very low density of retrogradely-labeled neurons, but moderate numbers of deep layer cells dorsal to claustrum were seen. In contrast to other cases discussed, only rarely were retrogradely-labeled cells seen in the pyriform cortex.

More caudally, fewer filled cells were present in the insular and gustatory cortices; labeled cells extended dorsally from the GI into the ventral (secondary) somatosensory cortex. Retrogradely-labeled neurons were not present in the posterior cingulate and retrosplenial cortices; a small number of filled neurons were seen in the lateral entorhinal cortex.

Amygdala and Hippocampus. Labeling of the amygdala differed from cases involving LO deposits in that there was a moderate density of filled cells in the BLA but significantly fewer in the lateral nucleus. Moreover, labeling in the BLA was strongly biased to the anterior parts of the basolateral complex, with very few back-filled cells seen in the more posterior BLA. There was light labeling in the basomedial nucleus.

Retrogradely-labeled cells were not seen in the hippocampus or subiculum.

Diencephalon. Labeling in the thalamus was more prominent along the midline than laterally, with very few retrogradely-labeled cells seen in the MD. A moderate number of back-filled neurons were present in the intermediodorsal nucleus and in the paraventricular thalamic

nucleus, particularly its posterior (bilateral) aspects. A few scattered cells were present in the more ventral midline nuclei, including the rhomboid and reuniens.

Retrograde labeling was present in the CM-PF complex. Most of the labeling was seen in the central medial nucleus, particularly in the midline where the nucleus has a modest dorsal extension; fewer filled cells were seen in the paracentral and especially central lateral parts of the CM complex. Retrogradely-labeled PF neurons were also present in moderate density; they were more frequently encountered in the ventral PF.

The nucleus submedius was not labeled, and only rare retrogradely-labeled neurons were present in the hypothalamus.

Mesencephalon. Almost no retrogradely-labeled cells were seen in the VTA. There was a modest number of labeled cells in the lateral supramammillary nucleus. More posteriorly, in the A10dc region, no back-filled cells were seen in the caudal linear nucleus, but were present in the posterior periaqueductal gray and the dorsal raphe. Of the retrogradely-labeled neurons in the A10 cell group (almost entirely limited to those neurons located in the A10dc and A10vr regions), none expressed TH-ir, i.e., none were dopaminergic.

Other Areas. A few retrogradely-labeled cells were seen in the substantia innominata and ventral pallidum; these cells appeared to be continuous with labeled cells extending dorsally into the GP. Overall, there were fewer cells in this group of substantia innominata-pallidal neurons than seen in case A1054.

Other Cases. The various cytoarchitectonic areas that comprise the OFC are relatively small and tightly clustered, and thus tracer deposits targeting these areas often invade adjacent areas. It is

therefore quite useful to compare the data from the cases not discussed above to arrive at general statements concerning the organization of afferents to the OFC.

The core of the tracer deposits in a large number of cases extended not only across different cytoarchitectonic regions in the OFC, but beyond the OFC. In a number of cases there appeared to be incidental involvement of the anterior pyriform cortex, although on occasion it was difficult to differentiate the retrograde labeling of the pyriform (primary olfactory) cortex resulting from tracer deposits into the OFC (secondary olfactory area) from direct tracer spread into the pyriform cortex. In case A1051, the Fluoro-Gold deposit was restricted to the pyriform cortex beneath the rhinal sulcus (see Fig. 6). Compared to cases involving tracer deposits into the OFC, retrograde labeling across the brain was quite limited. A moderate density of labeled cells was seen in the ventrolateral orbital area, extending slightly into the lateral and ventral orbital cortices, particularly ipsilateral to the FG deposit. Dense labeling throughout the anteroposterior extent of the pyriform cortex was seen. In addition, a moderate density of FG-positive cells was seen in the olfactory tubercle; a few cells were present in the horizontal limb of the diagonal band complex. Moderate retrograde labeling of the subiculum and CA1 of the hippocampus was present bilaterally. However, in contrast to cases involving OFC deposits, there was no labeling of the basolateral amygdala, mediodorsal thalamus, or the midbrain.

The impressions gleaned from the cases that we have not discussed in detail confirm in large part our observations in the cases we discussed earlier. However, comparing the additional cases allowed us to detect evidence of topographic relationships between the OFC and afferents from the MD and BLA, both within part of the OFC (such as the medial OFC, including the VLO and LO) and across the entire OFC.

The ventrolateral orbital cortex (VLO) is the medial-most region of the OFC that we will

discuss. Some investigators include the medial orbital cortex (MO) as part of the OFC. However, the MO is directly ventral to mPFC regions (the prelimbic or infralimbic cortices, depending upon the anteroposterior level of the frontal lobe). Moreover, Hoover and Vertes (2011), in their study of MO efferents, argued that the pattern of MO projections resembles that of the mPFC and is distinct from that of the OFC.

In case A1062 the core of the tracer deposit was mainly in the posterior VLO. The density of retrogradely-labeled neurons in the medial mPFC (prelimbic and infralimbic cortices) was substantially less than seen after FG deposits into the LO in case A1065. Moreover, the density of FG-positive cells in the basolateral amygdala was greater after tracer injections of the (more lateral) LO than VLO. Interestingly, in both these and other VLO and LO cases, there appeared to be a greater labeling in the lateral nucleus than the basolateral nucleus. In contrast, tracer deposits into lateral OFC (from AId_1 to GI) resulted in roughly comparable labeling in the lateral and basolateral nuclei.

Moving laterally, we compared the pattern of retrograde labeling after tracer deposits centered in the LO (case A1064) and the insular AId_2 regions (case A1014). In the former case MD labeling was mainly seen in the central MD but with some medial MD labeling. In contrast, the AId_2 deposit yielded more medial MD labeling. Another difference in the afferents to the LO and the more lateral AId_2 was the greater labeling of neurons in temporal cortical areas dorsal to the rhinal fissure (including the GI, DI, and somatosensory cortices and, posteriorly, the auditory cortex) after tracer deposit into insular cortices. There was little difference in the overall density of labeling of the basolateral complex, but the lateral nucleus exhibited more filled cells than did the basolateral nucleus in case A1064.

Case A1014 was a relatively large injection in which most of the core of the tracer deposit was in AId_2. The FG deposit in case A1054 was more laterally placed, centered in AId_1 and DI. Labeling of the medial frontal areas, including the prelimbic area, was substantially greater after deposits into AId_2. Importantly, MD labeling was much more sparse in case A1054 (AId_1 and DI) than A1014. In turn, we compared the same AId_1-DI case (A1054) with two animals (A1060 and A1061) in which FG was deposited more laterally, into the DI and GI. Both DI-GI tracer deposits (cases A1060 and A1061) resulted in a greater degree of BLA labeling, but a marked decrease in the density of MD labeling.

While labeling of the basolateral complex increased as tracer deposits were placed into progressively more lateral areas of the OFC, labeling of the basomedial amygdala was greater after FG deposits of the agranular insular areas (cases A1014 and A1016) that seen with injection of the far lateral cases (A1060 and A1061).

Although there appeared to be a mediolateral topographic organization of thalamic and amygdaloid projections to the OFC, we were not able to discern any such relationship of midbrain afferents to the OFC. The two largest groups of cells in the midbrain that project to the OFC were in the supramammillary nucleus and a caudal area extending from the caudal linear nucleus to the central gray to the anterior dorsal raphe, with few cells in the VTA proper, as defined by Phillipson (1979).

Similarly, other areas that were unexpectedly labeled, such as the globus pallidus (GP), also did not vary as a function of mediolateral position of the tracer deposit into the OFC. Globus pallidus labeling was prominent after tracer deposits into the AId_1, AId_2, and DI (A1016, A1014, and A1060, respectively) compared to other cases. However, these cases involve OFC deposits

into the central and lateral OFC, but not in the far lateral OFC, and thus GP labeling does not appear to follow a medio-lateral topography.

In contrast to the data supporting a general mediolateral topographic organization of thalamic and amygdaloid afferents to the OFC, it is more difficult to discern a consistent difference in the distribution of these projections to the rostral versus caudal OFC. Case A1016 involved a tracer deposit centered in AId_2 and AId_1. In another case (A1013) in which the tracer was centered in DLO_1 and DLO_2 (see Fig. 7A), rostral to case A1016, there was considerably less labeling in than seen after the caudal tracer deposit, although pregenual cingulate labeling was roughly comparable across the two hemispheres. However, we lacked sufficient number of far rostral tracer deposits to be able to confidently describe a rostrocaudal topography.

Discussion

Technical considerations.

We used retrograde tracing to determine the inputs to the orbitofrontal cortex. In most cases, we iontophoresed Fluoro-Gold, using a moderate current intensity to deliver the tracer. While this approach minimizes tracer uptake by axons-of-passage, we cannot exclude in any given case tracer accumulation by axons. Our limited anterograde data (shown in Chapter 5), which was primarily generated in order to examine OFC overlap of axons from thalamic, amygdaloid, and midbrain neurons, in some cases provided a means of confirming the retrograde tract tracing data.

We have assumed that transport occurs from the dense core of the deposit and not the penumbra, as suggested by Brog et al. (1993). Nonetheless, in most cases tracer deposits extended beyond the small dimensions of the cytoarchitectonically-defined areas that comprise

the OFC. The issue of spread of the tracer is of particular concern in the deep layers of most OFC areas. For example, the dopaminergic innervation of the agranular insular cortices enters the OFC as a tight bundle of axons of ~350 μm width before fanning out to invest the more superficial layers, thus requiring deep layer tracer deposits of <350 μm in size to restrict labeling to inputs of one cytoarchitectonic area. However, the analysis of cases involving overlapping tracer deposits across successive areas of the OFC provided a means of assessing afferents to a particular area.

Afferents to the OFC.

Afferents to the OFC arise from a large number of cortical and subcortical sites. Among the OFC afferents are those originating in the MD, BLA, and midbrain. Our data are largely consistent with and extend earlier reports on afferents from the MD and BLA complex to the rostral agranular insular cortex and surrounding regions (Alcaraz et al., 2016; Gerfen and Clavier, 1979; Krettek and Price, 1977a,b; Leonard, 2016; Mátyás et al., 2014; Reep and Winans, 1982; Reep et al., 1996).

Our data largely agree with previous studies of the thalamo-frontal projections, which have indicated that the MD projection to the OFC primarily originates in the central MD (Groenewegen, 1988; Kuramoto et al, 2016). However, as noted by Kuramoto and colleagues (2016) in their elegant single-cell reconstructions of thalamocortical projections, neurons in the medial or lateral MD also contribute to the OFC innervation. For example, in case A1014 our tracer deposit was centered in AId_2 but extended somewhat into the LO medially, resulting in retrograde labeling in the medial and lateral as well as the central sectors of the MD.

Our data also offer new insights into the nature of the amygdala projection to the OFC. Previous studies have emphasized that the basolateral complex, including both the basolateral

59

nucleus and the lateral nucleus, projects to the frontal cortices. We observed differences in the contribution of these two nuclei, mirroring functional differences in the lateral and basolateral nuclei (Pape et al., 1998; Yang and Wang, 2017). Tracer deposits of the AId_2 labeled substantially more basolateral than lateral nucleus neurons, while injections involving the LO labeled more lateral than basolateral cells. A deposit in the VLO_p failed to label significant numbers of cells in either basolateral or lateral nuclei, consistent with our anterograde observations. However, Reep et al. (1996) observed retrograde labeling in the BLA after rostral VLO tracer injections.

Just as the MD is not the sole source of thalamic projections to the prefrontal cortices, there are amygdaloid nuclei in addition to the basolateral complex that innervate the OFC. The basomedial nucleus, which has been previously noted to provide an input to the ventral mPFC (Petrovich et al., 1996) was labeled, particularly after tracer deposits into the central OFC, including the agranular insular regions AId_2 and $AId_1.$ The OFC input from the basomedial complex is consistent with the anterograde data of Petrovich et al. (1996), who reported that the BMA projection to the OFC was substantially less dense than that targeting the mPFC. Our observation that retrograde labeling of the BMA is more prominent after tracer deposits of the central (AId_2) OFC contrasts with the BLA efferents, which primarily target lateral OFC areas, including the dysgranular and granular insular cortices caudally and the DLO_1 rostrally.

We observed retrogradely-labeled midbrain neurons in a broad swath extending from the supramammillary nucleus to the dorsal raphe (DR), including the VTA. In general, the rostral and caudal poles of this territory housed the greatest density of labeled cells (although in absolute terms this was a small number of neurons). Cells in the VTA were few in number and

most often seen in the nucleus parabrachialis and the caudal linear nucleus (CL). The labeled cells in the CL were continuous with cells in the periaqueductal gray and anterior DR.

The overall density of retrograde labeling within the VTA did not vary markedly across different OFC tracer deposits, although there was a trend toward AId_2 tracer deposits yielding more labeled midbrain cells than did injections of sites lateral or medial to the AId_2. This is consistent with the dopamine innervation of the OFC being most dense in AId_2. Moreover, tracer injections of AId_2 resulted in greater retrograde labeling in the caudal linear nucleus (CL) than did deposits into other OFC areas. The anterior DR was retrogradely labeled after tracer deposits into all parts of the OFC, presumably reflecting filling of serotonergic neurons.

The projections from the midbrain to the OFC included dopaminergic and non-dopaminergic inputs. Previous studies had determined that the dopamine inputs to the frontal cortices arise exclusive from midbrain neurons and not diencephalic or other neurons. In an animal with tracer deposited into AId_2 (case A1014), 22% of the retrogradely-labeled cells in the midbrain were dopaminergic. Similarly, a deposit into the LO region that extended slightly into AId_2 (case A1065) retrogradely-labeled both dopaminergic neurons (29.5% of the total number of filled cells) and non-dopaminergic midbrain neurons. In both cases, most of these dopaminergic cells were in the caudal and dorsal extension of the A10 cell group (A10dc) in the CL and DR. This observation is similar to the pattern seen after mPFC tracer injections, in that Swanson (1982) determined that the percentage of midbrain dopamine neurons retrogradely-labeled after mPFC tracer deposits was markedly higher in the caudal linear than more rostral VTA areas. Yoshida et al. (1989) also concluded that dopamine neurons in the dorsal raphe were a major source of the PFC dopamine innervation.

Our studies revealed substantial differences in afferents to the OFC, including those

originating in various cortices. For example, there were major differences in the degree of

retrograde labeling of the mPFC after tracer deposits into various OFC sites. Labeling of neurons

in the caudal (but not rostral) prelimbic and infralimbic cortices was much greater after tracer

deposits into the AId_2 than into other OFC areas. This observation agrees with general

descriptions of mPFC projections to the OFC region in the hamster (Reep and Winans, 1982),

rabbit (Buchanan et al., 1994), and rat (Sesack et al., 1989).

Retrograde labeling of the auditory cortex was almost exclusively seen after AId_2

injections. This labeling was confined to the rostral auditory cortex, and has not been previously

reported in the rat. In contrast to our observations, Reep et al. (1996) commented that they were

unable to detect consistent reciprocal labeling of auditory areas following OFC tracer deposits.

However, the presence of an input from the auditory cortex suggests a feedback loop involving

the OFC and A1 region, consistent with a recent evidence for a direct OFC-A1 projection that is

involved in determining the receptive fields of auditory cortex neurons (Winkowski et al., 2017).

It is interesting to note that the presence of an auditory cortex projection to the OFC in primates

is uncertain (Price, 2006).

A subcortical area that provides an OFC input is the hypothalamus. Projections from the

lateral hypothalamus, including the perifornical area, to the mPFC have been previously reported

(Fadel et al., 2002; Hoover and Vertes, 2007). Comparable data on the OFC are lacking,

although Allen et al. (1991) reported a moderately dense projection to the posterior agranular

insular cortex. We found that retrogradely-labeled cells were present in the lateral hypothalamus

(LH), including the perifornical area (PFA), after tracer deposits of the OFC. Fluoro-Gold

deposits into medial orbitofrontal areas, including the VLO and LO, only rarely retrogradely

labeled LH neurons. Similarly, filled cells were rarely seen after FG deposits of the lateral OFC (AId$_1$ and DI/GI). However, with tracer deposits into AId$_2$ we observed a small number of LH cells that were back filled. Most of these neurons were in the lateral aspects of the LH. In some cases, a cluster of retrogradely-labeled cells was seen in the PFA.

The paucity of labeling in the PFA was unexpected in light of the presence of orexin (hypocretin) neurons in the dorsal perifornical and adjacent regions, which provide projections to all neocortical regions, including the OFC (Peyron et al., 1998). Thus, we would have expected orexin cells in the PFA to broadly innervate the OFC. One possible explanation is that there is a small number of orexin cells (Allard et al., 2004), and among this total population are discrete sub-populations that project to different areas of brain (Fadel et al., 2002).

We observed retrogradely-labeled neurons in the globus pallidus after OFC tracer deposits. Previous studies have noted projections from the basal forebrain to the mPFC and OFC, with neurons seen in the midposterior ventral pallidum and substantia innominata and nucleus basalis (Chandler et al., 2013; Grove, 1988; Hoover and Vertes, 2007; Reep et al., 1996). However, in contrast to our material, earlier studies did not report that the cluster of basal forebrain cells extends dorsally into the GP, on occasion for more than a millimeter. We were unable to discern a topographic organization of the GP projection to the OFC, although it appeared that the density of the pallidal labeling was greatest after tracer deposits into the AId$_2$.

CHAPTER 4

COLLATERALIZATION OF INPUTS TO THE mPFC AND OFC

The rat medial prefrontal cortex (mPFC) receives afferents from the mediodorsal nucleus of the thalamus (MD), basolateral amygdala (BLA), and dopaminergic midbrain (Krettek and Price, 1977a,b; Lindvall et al., 1978). My results in Chapter 3, along with previous studied (Groenewegen, 1988; Krettek and Price, 1977a,b; Lindvall et al., 1978), have shown that neurons from the MD, BLA, and dopaminergic midbrain also innervate the orbitofrontal cortex (OFC).

The mPFC receives its MD innervation primarily from the medial segment of MD, with some involvement of the lateral segment (Krettek and Price, 1977b). My results show that the innervation of AId_2 primarily originates in the medial MD, while the innervation of the VLO, LO, and AI_v derives from the central MD, consistent with the observations of Gronewegen (1988).

The mPFC and OFC are also innervated by BLA neurons, without any discernible topography (see Chapter 3; Reppucci and Petrovich, 2016). The dopamine innervation of the medial PFC arises from the nucleus parabrachialis of the ventral tegmental area (VTA), as well as A10 dopamine neurons located caudal to the VTA in the dorsal raphe (Yoshida et al., 1989). In our studies, we observed that the majority of the orbitofrontal dopamine innervation seems to originate along the dorsocaudal extent of the A10 cell group, including the caudal linear nucleus (CL) and dorsal raphe (DR).

However, it is unclear if the MD, BLA, and dopaminergic midbrain neurons collateralize to innervate the mPFC and OFC or if these afferents arise from separate neuronal populations. We

64

used dual retrograde tract tracing to assess the collateralization of MD, BLA, and A10dc neurons collateralize to innervate both the mPFC and OFC.

Methods

Animals. Adult Sprague-Dawley rats were used for these experiments and all experiments were performed in accordance with institutional and national guidelines.

Tracer deposition. Tracers were placed into the OFC and mPFC. In these experiments, 8 animals received Fluoro-Gold (FG) and Alexa555-conjugated cholera toxin, subunit B (CTB) deposits into the mPFC and OFC. Because a portion of the dopamine innervation of the OFC courses through the deep layers of the mPFC *en route* to the orbitofrontal cortex, the issue of potential uptake of the tracer placed in the mPFC by fibers-of-passage was of concern. We therefore iontophoretically deposited FG, using a relatively low current intensity (+2.0 μA) as outlined in Chapter 3.

Results

Retrogradely-labeled cells were observed throughout the brain, as described in Chapter 3. In order to better understand the collateralization and topography of cells projecting to the mPFC and OFC, we focused on labeled neurons in the MD, BLA, and midbrain. Fluoro-Gold was deposited in the mPFC and all tracer deposits involved the prelimbic area, though some also involved the ventrally-positioned infralimbic cortex. CTB tracer deposits involved multiple areas within the OFC, including the LO, DLO, AId_2, AId_1, DI, and GI (see Fig. 7F for Case A1014).

We determined if individual neurons in any of the three major subcortical nuclei that innervate the OFC collateralized to innervate both the OFC and mPFC, by the presence of dual-labeled neurons. Labeling was analyzed in five animals. We did not observe any neurons in the MD or midline thalamic nuclei that branched to innervate both the orbitofrontal and medial frontal territories. In the ventral midbrain, including the posterior extension of the VTA to the central gray matter and dorsal raphe, we observed two neurons that accumulated both retrograde tracers and thus projected to both the mPFC and OFC. Similarly, in the basolateral complex, we found four neurons across the five cases analyzed that were double-labeled (see Fig. 15).

Figure 15. Localization of retrogradely-labeled cells in the (**B**) mediodorsal thalamus, (**C**) basolateral amygdala, and (**D**) midbrain (including rostral dorsal raphe) after (**A**) depositing Fluoro-Gold into the mPFC (blue) and cholera toxin B into the OFC (red) in case A1014. The filled blue circles indicate neurons retrogradely-labeled from the mPFC and red filled circles indicate cells retrogradely-labeled from the OFC; yellow stars depict double-labeled cells. A single midbrain cell and two amygdala cells (yellow stars) were double labeled.

Discussion

We did not observe double-labeled cells in the MD or PVT of animals with dual retrograde tracer deposits into the medial and lateral frontal territories, and saw only four double-labeled BLA cells and two double-labeled VTA neurons. These data suggest that neurons of

three major subcortical areas that innervate the OFC do not branch to also innervate the mPFC. While we have found only rarely do these neurons collateralize to innervate the mPFC and OFC, Chandler et al. (2013) reported the a somewhat larger percentage of double-labeled VTA cells after dual injections into the mPFC and OFC. However, their tracer deposits appeared to target OFC regions situated more rostral than the locations of most of our tracer injections.

Our findings are consistent with the early studies of Fallon and colleagues (Fallon, 1981; Loughlin and Fallon, 1984) and Swanson (1982), who noted that there is little collateralization of VTA neurons to innervate more than one forebrain target in the rodent. In studies specifically examining if midbrain neurons projected to both the mPFC and OFC, both Sarter and Markowitsch (1984) and Sobel and Corbett (1984) reported that there was a very small population of double-labeled neurons in the VTA of rats receiving tracer injections into the mPFC and OFC. While there is a consensus that very few midbrain dopamine neurons in the rat collateralize to provide multiple telencephalic inputs, in the primate it appears that collateralization of mesotelencephalic dopamine neurons is relatively common (Willliams and Goldman-Rakic, 1998).

Krettek and Price (1977b) reported that the MD projection to the OFC is not homogeneous, but targets different subregions; this finding was elegantly confirmed by Kuramoto et al. (2016), using Sindbis virus-transfected cells to reconstruct single MD neurons in different parts of the MD. Sarter and Markowitsch (1984) noted that MD neurons do not collateralize to innervate the mPFC and OFC, consistent with our observations. Moreover, we did not observe double-labeled cells in the thalamic paraventricular nucleus, although single PVT neurons collateralize extensively to innervate the mPFC and other forebrain targets (Bubser and Deutch, 1998).

We found an average of approximately one double-labeled cell per animal after tracer deposits into the medial and lateral frontal cortical fields. This stands in contrast to the observation of Sarter and Markowitsch (1984), who reported that a substantial population of anterior BLA cells is double-labeled after injections of Fast Blue and Nuclear Yellow into the mPFC and OFC. Although these older tracers are avidly accumulated by axons of passage, in contrast to contemporary tracers such as (iontophoretically deposited) FG, Sarter and Markowitsch did not observe double-labeled thalamic or midbrain neurons, suggesting that uptake of axons traversing the medial frontal cortex may not explain the differences in the two studies.

We assessed possible collateralization of three major afferents to the OFC and mPFC. We did not systematically explore other areas that may harbor single neurons that branch to innervate both frontal cortical targets, such as the hippocampus (see Verwer et al., 1997).

The lack of collateralization of dopamine neurons innervating the OFC or mPFC has functional implications. The fact that separate midbrain dopamine neurons innervate the mPFC and OFC may explain why of lesions of the OFC do not disrupt working memory in rodents or humans (Dalley et al., 2004; Divac et al., 1975; Mishkin, 1964; Zald and Rausch, 2006), yet mPFC lesions cause working memory deficits with perseverative errors. Moreover, because single dopamine cells do not branch to innervate the OFC and mPFC, the dopaminergic contribution to the frontal cortices cannot be coordinately regulated by tegmentocortical projections. Instead, functional dopaminergic actions in the OFC and mPFC may be coordinated through reciprocal connections of the mPFC and OFC (predominantly involving AId_2), or via long-loop feedback projections to the VTA.

CHAPTER 5

CONVERGENCE OF SUBCORTICAL AFFERENTS IN THE OFC

The PFC is most often defined by its innervation from the mediodorsal nucleus of the thalamus (MD), a definition which originated in 1948 with the publication of Rose and Woolsey's seminal analysis of projection targets of the MD.

During the characterization of the thalamic innervation of the frontal cortex it was noted that certain extra-thalamic nuclei also innervate the frontal cortex, overlapping the distribution of MD axons. Krettek and Price (1974) reported that the basolateral amygdala (BLA) projects to the frontal cortex. Although these BLA-derived afferents to the frontal cortex extend into areas not innervated by the MD, both MD and BLA neurons innervate the prelimbic cortex (Divac et al., 1978a). Similarly, Beckstead (1976) and Divac et al. (1978b) reported that both the MD and the midbrain ventral tegmental area (VTA) project to the prelimbic and pregenual cingulate cortices. Based on these and other data, Divac and colleagues (1978a,b) suggested that the convergence of MD, BLA, and dopaminergic midbrain afferents defines the PFC across species. Despite regularly being referred to as the lateral prefrontal cortex, there has been no examination of the convergence of these afferents within the OFC.

Methods

Animals. Adult Sprague-Dawley rats were used for these experiments and all experiments were performed in accordance with institutional and national guidelines.

Tracer Deposition. Anterograde tracing experiments (N=16) were performed to determine if the MD, BLA, and dopamine neurons of the midbrain sent convergent axonal projections to the OFC. In these cases, MiniRuby (lysine-fixable tetramethylrhodamine-conjugated biotinylated dextran amine, 10,000 MW; Molecular Probes, Waltham, MA; 10% in 10mM sodium phosphate buffer) was iontophoretically deposited (+5.0 µA (pulsed 7sec on/off) for 30 min through micropipette tips of 15-30 µm diameter) into the MD or BLA, and MiniEmerald (lysine-fixable flourescein-congugated biotinylated dextran amine, 10,000 MW (Molecular Probes)) into the other subcortical site. The contribution of the midbrain dopamine neurons was evaluated by examining the distribution of tyrosine hydroxylase-immunoreactive (-ir) axons in the OFC (see Noack and Lewis, 1989).

Seven to ten days post-operatively, animals were overdosed with isofluorane and transcardially perfused with phosphate-buffered saline (pH 7.4) followed by 4% paraformaldehyde in phosphate-buffered saline. Brains were removed and post-fixed in 4% paraformaldehyde before being cryoprotected in 30% sucrose. Frozen sections were then cut at 40µm and collected into six alternating sets.

Immunohistochemical procedures. Immunofluorescence protocols were used as previously explained in Chapter 2. Dopaminergic fibers were visualized by TH-ir, using a sheep anti-TH (AB1542, Lot 2896740, RRID: AB_90755) from Millipore (Billerica, MA), at a dilution of 1:1000. Afferents from MD and BLA were visualized by the deposited fluorophore-conjugated BDA, without immunohistochemistry.

Results

The possible convergence of subcortical afferents to the OFC was examined by examining animals in which BDA conjugated to different fluorophores was deposited into the basolateral amygdala and mediodorsal thalamus, and immunohistochemical detection of TH-ir axons was used to mark dopaminergic afferents from the midbrain. An example is shown for case A1115, in which BDA conjugated to fluorescein was iontophoresed into the amygdala, with the deposit primarily involving the BLA and to a lesser extent the lateral nucleus. In the case of thalamic tracing, BDA conjugated to tetramethylrhodamine was deposited in the mid-posterior MD, involving the lateral segment and extending into the ventral aspect of the central MD.

The MD projection to the OFC covered an obliquely-positioned swath of the OFC, running from the VLO medially to the AId_2 (Fig. 16). This band of labeled axons ran parallel to the rhinal sulcus and about 300 μm dorsal to the sulcus. Interestingly, there was an inhomogeneity in the mediolaterally oriented band of labeled axons, with a clear separation into two areas of axons separated by an area in which anterogradely-labeled thalamic axons were very sparse (see Fig. 16). The MD projection onto the PFC decreased in density at more rostral levels.

Axons of basolateral amygdala neurons were mainly distributed to the deep layers of AId_2 and across the dysgranular and granular insular cortices. There was a second minor investment of BLA-derived axons in L2/3 of the AId_2.

Consistent with our examination of the distribution of dopaminergic axons in the OFC (see above), dopamine axons in the OFC largely filled AId_2 with some extension medially to partially invest the LO and laterally into the caudal $AId_1;$ a smaller contingent of dopaminergic axons extended rostrally to invade parts of DLO_1 and DLO_2.

71

Overall, convergence of thalamic, amygdaloid, and ventral mesencephalic axons in the OFC was quite restricted (see Fig. 16D, H). The BLA inputs to the AId_2 were segregated from the MD innervation. Within the AId_2 a narrow band of dopaminergic axons was positioned between the more ventral MD-derived axons and the dorsolateral- situated BLA axons. It is, however, important to note that these different clusters of axons largely distributed to different lamina of AId_2 and thus there was little convergence *sensu stricto*.

In six cases either the thalamic or amygdaloid tracer deposit failed or was misplaced. However, in all of these cases the other BDA injection (into either the BLA or MD) was successful and we therefore compared the distributions of the midbrain dopamine input and the thalamic or amygdaloid input. These cases also indicated that the three major subcortical inputs to the OFC largely targeted different areas within the ventrolateral frontal areas.

For example, case A1109 involved a BDA deposit into the mid-caudal MD, primarily in the lateral segment but also impinging on the central MD and the central lateral nucleus of the CM-PF complex. In this case, MD-derived axons at caudal levels were primarily seen in the medial aspects of the OFC (AI_v), about 300 µm dorsal to the rhinal sulcus, and flanked ventrally and dorsally by zones of low density dopamine axons. More rostrally, the MD-derived inputs separated into two discontinuous areas, with the more lateral cluster of fibers largely separated from the dopamine axons in the AId_2 or (at rostral levels) DLO_2. In the rostral OFC, axons originating in the MD were largely absent.

In case A1112, in which the thalamic deposit primarily involved medial MD and slightly impinged on the central MD, anterogradely-labeled axons also displayed a discontinuous OFC innervation, with the more lateral of the two clusters of MD axons fibers extending to the LO, adjacent to the dopamine-innervated areas of AId_2 and, more rostrally, DLO_2 (Fig. 16I-K).

Neurons on the basolateral amygdala were largely segregated from the dopamine

innervation of the OFC. For example, in case A1129, which involved a BDA deposit restricted

to the BLA with no appreciable involvement of the lateral nucleus, axons from the BLA were

found dorsal and lateral to the dopaminergic innervation of the AId_1 and, at rostral levels, in the

far lateral OFC in DLO_1 and the granular cortex dorsal to DLO_1 (Fig. 16L). Thus, the amygdala

projection to the OFC was mainly distributed to the area dorsal and lateral to the dopamine

innervation, whereas the thalamic innervation as mainly confined to territories medial to the

dopamine axons.
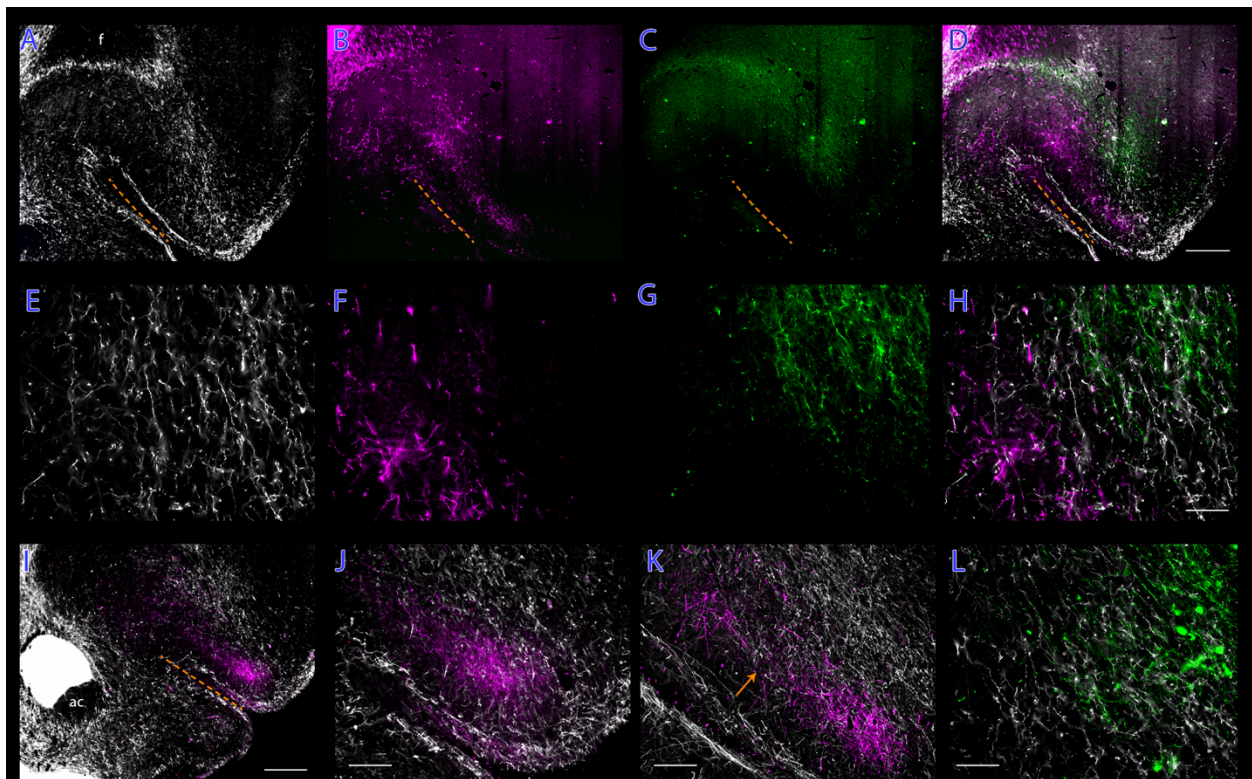
Figure 16. The distributions of OFC axons anterogradely-labeled from the mediodorsal nucleus (**B,F**; magenta) and basolateral amygdala (**C,G**; green), with TH-ir (dopaminergic) axons shows in white (**A,E**). The three inputs to the OFC are largely segregated, with the dopaminergic innervation of AId_2 and surrounding areas being flanked medially by the thalamic input and laterally by the amygdaloid projection. While the three innervations are, in large part, to spatially distinct areas of the OFC, there is some overlap of axons that can be appreciated in the higher- power photomicrographs in panels E, F, G, and (**H**) the merge image. Panels **I, J,** and **K** depict another case (A1112) with axons originating in the mediodorsal thalamus (magenta) being ventrally positioned relative to the TH-ir (dopaminergic) axons. The arrow in panel K points to a discontinuity in the thalamic innervation, which was characteristic of inputs from the mediodorsal nucleus, which is invested with a small cluster of dopaminergic axons. Panel (**L**) indicates a zone of overlap in the lateral OFC of midbrain dopaminergic axons (white) and basolateral amygdala (green) fibers in case A1129. Scale bars: A-D and I, 500 μm; E-H and L, 100 μm; J and K, 200 μm.

Discussion

Defining the PFC on the basis of MD afferents posed early problems to investigators interested in cortical function across species: MD projections label different frontal areas of different species (Divac et al., 1978b). Divac (1978a,b) argued that the PFC could be defined across all mammals (and perhaps even birds [Divac and Mogenson, 1985; Mogenson and Divac, 1982]) by the convergence of projections originating in the MD, BLA, and dopaminergic cells of the midbrain.

The idea of convergent inputs was predominantly based on labeling of two or more subcortical regions after single retrograde tracer deposits into a cortical field. However, anterograde transport studies suggest that the pattern of labeling in the OFC from the MD may be spatially distinct from that of axons labeled after transport from the amygdala (Groenewegen, 1988; Kita and Kitai, 1990; Krettek and Price, 1977a,b).

To examine potential convergence of the major subcortical inputs to the OFC, we anterogradely labeled projections of the MD and BLA, and examined in the same cases the distribution of TH-ir axons in the cortex. We used TH-ir axons as a marker of the VTA input based on the data of Divac et al. (1978b), who found that dopamine axons in the frontal lobe are restricted to those areas that were innervated by the MD. It is possible that different results may be obtained if a third anterograde tracer, such as PHA-L, was placed in the VTA. However, such an approach would fail to label most of the large area (which extends from the mesodiencephalic juncture to the dorsal raphe) from which frontal cortical dopamine projections originate.

We observed that MD, BLA, and TH-ir axons were all present in the ventrolateral frontal cortex, but largely in different parts of the OFC. For example, the MD projection was primarily

distributed to the more medial aspects of the OFC, from VLO to AId_2. Moreover, anterogradely-labeled MD axons were primarily present in the superficial layers, consistent with the data of Krettek and Price (1977b). In contrast, axons labeled anterogradely from the amygdala were present in the more lateral aspects of the OFC, extending from areas dorsal to the DI to AId_2. The distributions of axons in the OFC revealed TH-ir (dopamine) axons filled AId_2, and were flanked medially by MD axons and laterally by BLA axons, particularly in L2/3. However, all three types of axons were present in L1. This renders discussion of the "convergence" of MD, BLA, and VTA axons a matter that requires ultrastructural data to clarify. In the PFC, Kuroda et al. (1996) examined the convergence of VTA and MD axons on L5 neurons of the mPFC, finding that VTA axons synapsed preferentially on proximal dendrites while MD axon synapsed onto more distal dendrites.

Similar ultrastructural and physiological studies of the OFC will be required to help unravel the organization of microcircuits in AId_2 and other OFC regions. However, because our data suggest that there is a general lack of spatial overlap of thalamic, amygdaloid, and midbrain dopamine inputs to much of the OFC, only AId_2 can be considered a "prefrontal" cortex as defined by Divac and colleagues (1978b).

CHAPTER 6

CORTICOSTRIATAL CONNECTIONS OF THE OFC

The striatum receives topographically-organized inputs from the entire cerebral cortex. Projections from the frontal lobe to the striatum have been implicated in the pathophysiology of a number of neuropsychiatric disorders, including schizophrenia (Dandash et al., 2017) and obsessive-compulsive disorder (Figee et al., 2016). In rodent models of obsessive-compulsive behavior, the orbitofrontal efferents to the striatum are though to subserve overgrooming behaviors (Ahmari et al., 2013; Burguière et al., 2013).

Different cortical areas innervate distinct striatal territories. For example, as small anterograde tracer deposits are made at successively more dorsal positions in the medial prefrontal cortex, from infralimbic to pregenual anterior cingulate and medial precentral cortex, anterograde labeling in the striatal complex is positioned progressively more lateral, moving from the medial shell to the lateral core of the nucleus accumbens (Sesack et al., 1989; Berendse et al., 1992).   The striatal afferents originating in the OFC have not been extensively characterized. Both Berendse et al. (1992) and Schilman et al. (2008) examined projections from the OFC to the cortex, but neither report focused on AId_2, the OFC area which also receives a dopaminergic innervation.   In a limited number of cases we examined projections from the OFC to the striatal complex, focusing attention on AId_2.

Methods

Surgical methods were used as described in chapter 2. Cholera toxin subunit B (CTB) was deposited into various areas within the OFC. Five cases were examined. Because CTB can

act as both a retrograde and anterograde tracer, it was possible to visualize striatal afferents following these deposits, which were also used for retrograde studies.

Results

The orbitofrontal innervation of the striatum was examined in seven cases. The tracer deposits of these cases involved central and lateral OFC areas, including AId_2, AId_1, DI, and GI.
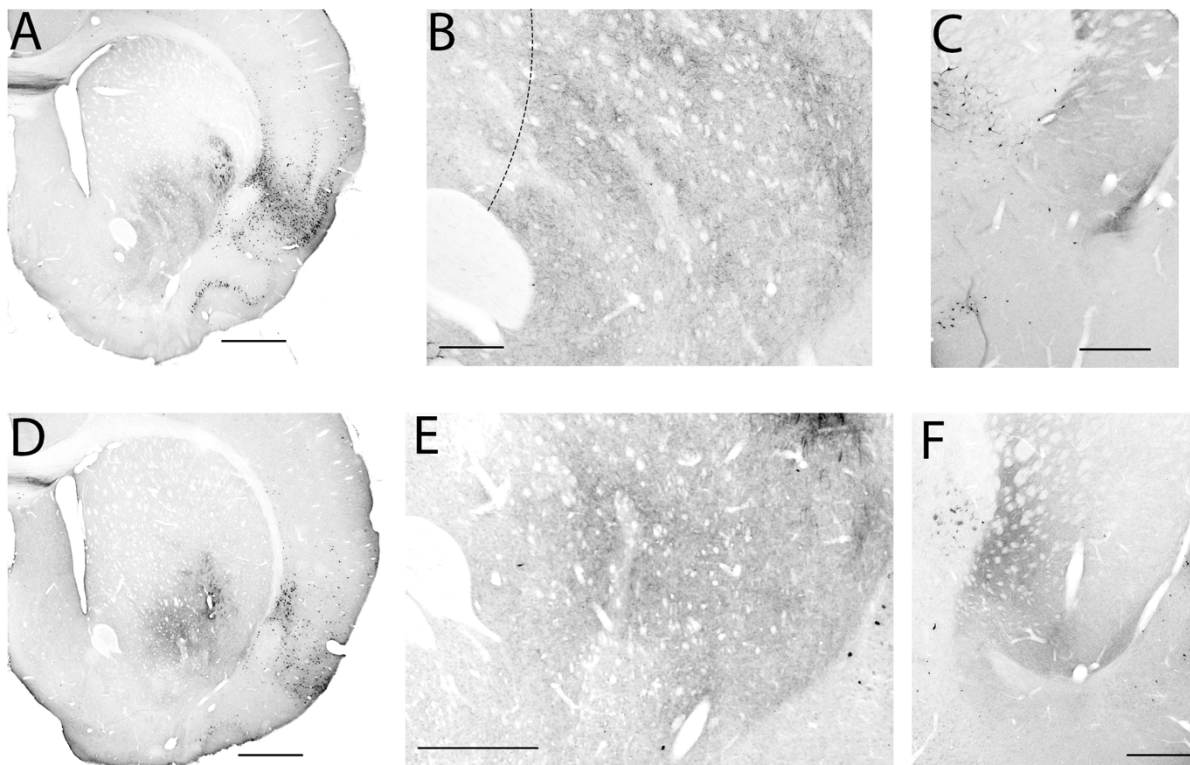
Figure 17. Following a tracer deposit into AId_2, innervation of the nucleus accumbens core (NAS) is striated (Case A1017; **A, B**). In the NAS core, there is a border in which labeling is seen laterally, but not medially (dotted line; B). Striations are not seen following a tracer deposit into AId_1 and DI and the extent of innervation of the NAS core is unclear (Case A1059; **D, E**). In both cases, labeled fibers are seen in the caudal striatum, but drop off sharply at the border of the globus pallidus (GP), most of the labeled fibers seen in the GP are present in fiber bundles (**C, F**). Scale bars (A, D) 1000 μm;

Following a tracer deposit into AId$_2$ and AId$_1$ (case A1017; see Fig. 6), anterograde labeling was seen in the ventral caudatoputmaen and the lateral core of the nucleus accumbens (NAS), but did not invade the medial core or the shell. There is a sharp border directly dorsal to the anterior commissure in the rostral NAS in which labeling is seen laterally, but not medially (see Fig. 17B). Anterogradely-labeled axons formed a striated banding pattern in the striatum with streaks of densely-labeled axons interdigitating with zones in which few labeled axons were seen. A similar pattern of labeling was also detected in the NAS following a deposit into the deep layers of AId$_2$ (case A1014; see Fig. 6, 7F).

Caudal to the NAS, anterogradely-labeled fibers were primarily present in the ventral aspects of the caudatoputamen, midway between the bed nucleus of the stria terminalis and the external capsule. The density of labeled axons fiber terminals was largely restricted to striatal territories and dropped off dramatically at the striatum-GP border (see Fig. 17). Some labeled fiber bundles entered the pallidum. Anterogradely-labeling of the striatum was bilateral, with labeled axons being more dense ipsilateral to the tracer deposit.

In case A1059, CTB was injected into AId$_1$ and DI (see Fig. 6). The penumbra of the tracer deposit extended ventrally into the deep layers of AId$_2$ and LO. Labeled fibers could be seen exiting the OFC into the lateral tip of the forceps. At the rostral pole of the striatum, fiber bundles were seen in the dorsolateral territories, but no terminal arbors

Figure 18. Following a deposit into AId$_1$ (Case A1059), labeled fibers are present in the central area of the ventral aspect of the striatum at the level of the crossing of the anterior commissure. Scale bar: 1000 μm.

were seen. Anterogradely-labeled fibers were seen in the ventral striatum, and appeared to primarily involve the same ventral and central aspects of the caudatoputamen and invade the lateral core. It appeared that the density of labeled axons was less than in case A1017, and no striated patterning was seen within the NAS. Caudally, at the level of the crossing of the anterior commissure, there was a single cluster of anterogradely-labeled fibers in the central area of the ventral-most striatum, just dorsal to the temporal limbs of the anterior commissure (see Fig. 18). Labeled fibers were again seen bilaterally, though density was lower in the hemisphere contralateral to the tracer deposit. In another case, involving a deposit into DI and GI (A1060; Fig. 6), anterograde labeling avoided the nucleus accumbens, but was found in the ventrolateral striatal territories caudally.

Discussion

Following deposits of CTB into the OFC, anterograde labeling was present in both the ventral (nucleus accumbens) and dorsal (caudatoputamen) striatum. No labeling was seen in the rostral pole of the striatum, nor was accumbal labeling seen in the septal pole of the NAS. Labeling in the nucleus accumbens primarily involved the lateral core compartment, and was seen only when deposits involved AId_2. However, all of the CTB injection sites were in the central and lateral OFC, so we are unable to comment on the striatal innervation of medial orbitofrontal territories. Moreover, our CTB injections were into the caudal half of the OFC, and did not involve rostral OFC territories.

Schilman et al. (2008) reported no significant innervation of the nucleus accumbens following anterograde tracer deposits into the OFC. However, the tracer injections in this study were limited to the most rostral OFC. Berendse et al. (1992) used PHA-L to labeled fronto-

striatal projections; they described two tracer deposits into the OFC. Their description of these two cases was very similar to the labeling we observed, with striated innervation of the accumbens core. Retrograde tracer studies of accumbal afferents corroborate that the central OFC projects to the lateral core and contiguous caudatoputamen. For example, Brog et al. (1993) reported dense retrograde labeling of the agranular insular cortex following Fluoro-Gold deposits into the accumbens core.

In all of the cases described here, we have used cholera toxin, subunit B (CTB) as the anterograde tracer. Because the CTB was deposited by pressure injection, most deposits were relatively large and spanned multiple cytoarchitectonic regions. However, using multiple overlapping deposits, we were able to arrive at the conclusion that the central orbitofrontal territories, particularly AId_2, innervate a striatal area including the lateral core and contiguous caudatoputamen. This conclusion agrees well with the data Berendse et al. (1992) and Brog and colleagues (1993) using different anatomical methods.

CHAPTER 7

THE OFC ACROSS SPECIES

Defining homologous cortical areas across species largely relies on three major criteria: cyto- and chemo-architectonics, connections with other brain areas (hodology), and functional equivalence. In order to compare the OFC of rodents and primates, I will briefly discuss the three of these criteria, drawing primarily from studies of rats and several different primate species, including humans.

Particularly in rodent studies, the nomenclature of the ventrolateral frontal cortices has been notoriously inconsistent, with some investigators using the term OFC to refer to the entire area dorsal to the rhinal sulcus, while others use the term to refer to the more medial structures and do not include the agranular areas. I will use the term OFC in its broadest sense, incorporating all of the territories dorsal to the rhinal sulcus, including the insular areas.

Cytoarchitectonics

The cyto- and chemo-architectonics of the orbitofrontal cortex have been investigated in many species, including rodents (van de Werd & Uylings, 2008), several different non-human primates (Carmichael & Price, 1994), and humans (Öngür et al., 2003). The most obvious difference between the orbitofrontal cortex of primates and rodents is the presence of a granular layer IV throughout most of the OFC in primates, which is either lacking or very difficult to discern in the rodent. The agranular insular cortex (AI) of the rat and mouse, located in the caudal-most orbitofrontal territory, is the exception, it is agranular in both the primate and rodent. In the macaque (*macaca fascicularis, macaca mulatta,* and *macaca nemestrina*),

Carmichael and Price (1994) divided the AI into five areas using a complement of histochemical and immunohistochemical stains including nissl, non-phosphorylated neurofilament H (SMI-32), parvalbumin, and acetylcholinesterase. Using the same complement of stains, Öngür and colleagues (2003) identified four of these same areas within the human brain. In Öngür's architectonic analysis of the human brain, however, the fifth area was caudal to the brain tissue available for the study and therefore could not be examined or compared to the macaque. For the four comparable examined areas of the agranular insular cortex, there were strong similarities between the macaque and human brains.

More recently, van de Werd and Uylings (2008) divided the rat agranular insular cortex into four areas as well, using a combination of histochemical and immunohistochemical stains, including nissl, SMI-32, dopamine, parvalbumin, and calbindin. However, the nomenclature and relative location of the defined areas differ from those of the primate. While all of the primate AI areas are contiguous, at its rostral extent the rat ventral AI (AI_v) is flanked by two orbital areas, the VLO and LO. The rat caudal AI_v, however, is contiguous with the dorsal AI (AI_d), similar to the primate agranular insular areas.

Connections of the OFC

In the primate, areas of the prefrontal cortex are often grouped together and referred to as the orbital and medial prefrontal cortex (collectively abbreviated OMPFC; Price, 2006a,b; Öngür et al., 2003). Within the OMPFC, two systems have been described: a medial and an orbital network. A majority of orbitofrontal cortical areas are, unsurprisingly, assigned to the orbital network. However, the connections of the medial-most orbital areas are often ascribed to the

medial network (Price, 2006b), as has been the medial orbital cortex in the rat (Hoover & Vertes, 2011).

Thalamic Connections.

The primate OFC receives afferents from a number of thalamic nuclei. The thalamic innervation from the mediodorsal nucleus (MD) has become the defining characteristic of prefrontal cortices (Carlen, 2017). In primate species, most of the MD projection to the OFC originates in the magnocellular (medial) MD. The rodent OFC also receives a major input from the MD (see Fig. 19), with projections from the medial sector of the nucleus projecting heavily to AId_2, and more medial orbitofrontal areas receiving inputs from the central MD (see Chapter 3; Groenewegen, 1988; Kuramoto et al., 2017).
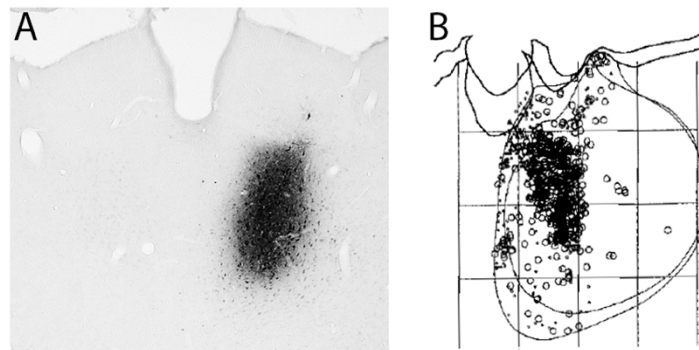
Figure 19. Pattern of retrograde labeling within the MD is similar in the rat (**A**; Case A1052) and the macaque (**B**; Adapted from Ray & Price, 1993) following tracer deposits in the rat LO (A) and the macaque Area 13 and AId (B).

Dopaminergic Innervation of the OFC

As discussed in Chapter 2, as well as in the cytoarchitectonics study of van de Werd and Uylings (2008), the dopaminergic innervation of the rat orbitofrontal cortex is most dense in a sub-area of the agranular insular cortex (AId_2). In fact, dopamine immunohistochemistry was

used as a defining feature of the AId$_2$ borders in this van de Werd and Uyling's analysis. In contrast, all areas in the non-human primate OFC receive a dopamine innervation, although the density of innervation varies across OFC areas (Lewis et al., 1988). There have been no published studies examining the distribution of dopamine axons in the human OFC.

Sensory Connections.

The primate orbital network appears to receive inputs from all five sensory cortices, though the auditory input is a point of contention (Carmichael and Price, 1995; Price, 2006b). Based in part of this extensive sensory-related input to the OFC, it has been hypothesized that the OFC in the primate plays a role in the sensory integration (Carmichael & Price, 1995b; Price, 2006b). As I have highlighted in Chapter 3, different parts of the rodent OFC receive inputs from the pyriform, auditory, and somatosensory cortices, highlighting the homology of this broad area across species. Notably, the auditory input to the OFC in the rat had not previously been described.

Connections of the agranular insular cortex

In the primate, the agranular insular cortex, though included in the orbital network, has connections that differ from other orbital areas (Price, 2006b). In general, the agranular insular cortex (AI) is more heavily connected with limbic areas, such as the amygdala, hippocampus, and entorhinal cortex, than the more medial orbitofrontal areas (Carmichael & Price, 1995a; Price, 2006b). We have shown here that this pattern follows in the rat; the afferents from the BLA and hippocampus are most prominent in dorsal agranular insular areas. The more medial orbitofrontal areas of the rat also receive afferents from limbic regions, but to a lesser extent than

84

the AId. In the primate, the agranular insular cortex is caudal to other areas of the orbitofrontal cortex. The same holds in the rat brain, with the dorsolateral orbitofrontal cortex (DLO) occupying lateral area dorsal to the rhinal sulcus, rostrally contiguous with the AI. Though our analysis of the rostral orbital areas was limited, we did find that the retrograde labeling following a tracer deposit into DLO (case A1013) differed from that of tracer deposits into the AI (cases A1014, A1016), leading to more restricted labeling of limbic areas including the BLA and hippocampus.

Function of the OFC

There have been relatively few rodent studies and even fewer primate studies into the function of the orbitofrontal cortex. Even within studies of the same species, targeted areas are often poorly defined and because of inconsistencies between groups, it is difficult to reconcile these analyses to arrive at functions of areas within the OFC. When comparing studies between species, different territories are often involved. In an excellent review of the comparative literature, Wallis (2011) highlights the need for precision when comparing areas of the OFC across species. Because of this, it is not possible to arrive at a meaningful comparison of function across species. The studies simply have not been done.

We are left with what can provide clues to orbitofrontal homologies: hodology and cyto- and chemo-architectonics. On these grounds, one can make limited comparisons between rodents and primates, particularly in the agranular insular cortices. As outlined here, and highlighted in other reports (Heilbronner et al., 2016; Pruess, 1995; Wallis, 2011), the OFC is quite comparable between rodents and primates. However, comparative studies of the functions within these areas are needed to establish homology.

CHAPTER 8

THE OFC AS A PREFRONTAL CORTEX

Topography of afferents and parcellation of the OFC

The pattern of retrograde labeling of thalamic and amygdaloid neurons from the OFC suggests that there is topographic organization of afferents, with MD neurons investing the medial OFC and amygdaloid neurons the lateral OFC.

Most of our tracer injections were not confined to one of the 14 cytoarchitectonic areas that comprise the rat OFC (see van der Werd and Uylings, 2008). This is not surprising, considering the small size (some less than 350 μm along the mediolateral domain) of the areas that comprise the OFC. However, because the locations of most of the injection sites overlapped with other injections, we were able to compare retrograde labeling from different areas of the OFC in order to determine differences between adjoining cytoarchitectonic areas. This allowed us to detect a general pattern in the organization of afferents, dividing the OFC into three sectors: medial, central, and lateral. We found that MD neurons were most heavily labeled after tracer deposits into the medial (VLO and LO) or central (AId_2) OFC. Our anterograde cases revealed that MD projections to the OFC were largely confined to the medial and central sectors of OFC, with very few axons extending laterally beyond AId_2. In contrast to our data indicating that the medial OFC is the primary target of MD projections, early anterograde tract tracing studies of MD projections that used relatively large tritiated amino acid injections reported a widespread innervation of the OFC, so extensive that at rostral levels the entire cortex was encircled by MD-derived axons. However, the large tritiated amino acid deposits were likely invaded thalamic nuclei outside of the MD, including the CM-PF complex.

Retrograde tract tracing revealed significant labeling of the basolateral nucleus of the amygdala (BLA) after injections into the central (AId$_2$) and lateral (AId$_1$, DI, and GI) aspects of the OFC; after tracer deposits into the medial OFC (VLO and LO), retrograde labeling within the BLA was much less dense or absent. Consistent with these observations, our anterograde cases indicated BLA projections were essentially limited to the central and lateral orbitofrontal areas, although some axons course through the medial areas of OFC to reach the lateral territories. It is worth noting that our BDA deposits for anterograde tracing were limited to the BLA, and did not involve the lateral nucleus, which lies immediately dorsal to the BLA.

We were unable to detect a topographic organization of midbrain projections to the OFC because there were so few cells labeled in the ventral midbrain dopamine regions. However, tyrosine hydroxylase-immunoreactive (TH-ir) axons were limited to the central OFC (centered in AId$_2$). Moreover, because of the large anteroposterior extent of the midbrain dopamine neurons, with clusters of labeled cells seen from supramamillary nucleus at the mesodiencephalic juncture to the rostral aspects of the dorsal raphe at the level of the pontomesencephalic transition, anterograde tracer deposits would have been too small to be informative.

These observations suggest a general organization of the ventrolateral frontal cortex that includes three (medial, central, and lateral) OFC territories (see Fig. 20), with the thalamic inputs defining the medial OFC, the BLA afferents defining the lateral OFC, and the dopaminergic innervation demarcating the central OFC. Because most inputs to the OFC are not strictly confined to areas defined by cytoarchitectonics but spread to invade adjacent areas, this organization scheme is an oversimplification, but one that may be a convenient heuristic for future studies of the OFC, particularly functional studies.
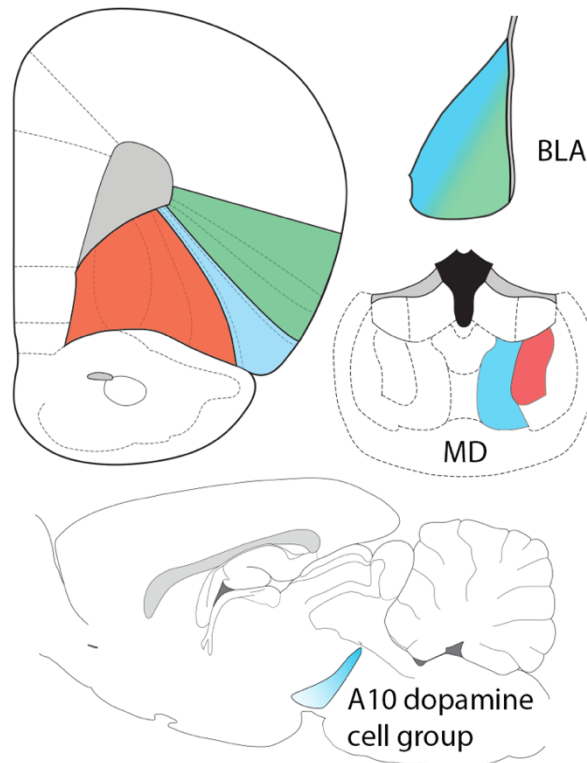
Figure 20. Schematic representation of proposed parcellation of the OFC based on organization of afferents. There are three major divisions of the OFC arranged medially to laterally. The most medial division, which encompasses the VLO and LO, received major inputs from the mediodorsal thalamus (red), primarily the central segment. The smallest of the divisions, which includes all of AId_2, receives inputs from the dopamine neurons in the midbrain A10 cells (blue), particularly those in the posterior DA cell region (A10dc) of the caudal linear, periaqueductal gray, and dorsal raphe regions. The input from the basolateral amygdala primarily targets the lateral OFC (green), including AId_1, DI, and GI. Thus, the central dopamine region is flanked by the thalamic and amygdaloid inputs. The assignments of afferents to specific cytoarchitectonic regions of the OFC are not strictly confined to cytoarchitectonic regions or the three OFC domains, but extend to invade adjacent territories to varying degrees. This can be seen most clearly in the case of the central OFC, in which the inputs to the AId_2, the boundaries of which are depicted by dotted lines, extend into the medial OFC (LO) and the lateral OFC (AId_1).

We have primarily based this cortical parcellation on the projections of the MD, BLA, and midbrain dopamine neurons. However, several other inputs appear to conform to this organizational scheme. For example, the basomedial nucleus of the amygdala (BMA) innervates the central (AId_2) OFC, with sparser retrograde labeling of this nucleus found following tracer deposits into either the medial or lateral sectors. Additionally, the orbitofrontal afferents from

the thalamic nucleus submedius are restricted to the medial and central OFC, and the auditory input is largely restricted to the central OFC.

This organizational scheme holds for the posterior two-thirds of the OFC. However, we lacked a sufficient number of anterior cases to be able to state that the rostral OFC (at the level of the anterior olfactory nucleus) follows this organization. However, our anterograde tracer cases suggest that the anterior OFC may differ from the posterior aspects that we have described here. As noted above, the MD innervation of posterior OFC primarily involved VLO, LO, and AId_2, but was largely absent from the DI and GI in the lateral OFC. In contrast, we did not observe a significant MD-derived innervation of the rostral OFC, including the rostral extensions of the VO, VLO, and LO. These findings are consistent with a tripartite organization of most of the OFC, but not including the rostral OFC.

Is the OFC a prefrontal cortex?

The prefrontal cortex is most often defined as the zone of innervation by the mediodorsal thalamic nucleus; a definition that dates back to the mid-20th century (see Chapter 1). By this common definition, the entirety of the medial and central sectors of the orbitofrontal cortex, from the VLO to the AId_2, can be considered prefrontal. However, it is clear that the medial OFC (VLO, LO) is also the target of projections from other thalamic nuclei, particularly the nucleus submedius. Additionally, these medial orbitofrontal areas receive MD projections primarily from the central segment of MD, as opposed to the medial MD that provides most of the mPFC innervation. The lateral sector of the OFC (AId_1, DI and GI), however, does not receive an MD innervation and therefore cannot be considered a prefrontal cortex by this common definition.

In 1978, Divac and colleagues (1978a,b) proposed that the convergence of MD, BLA, and dopaminergic midbrain afferents as a defining feature of the prefrontal cortex (see Chapter 1). Our data indicate that only the central sector (AId$_2$) of the OFC receives afferents from all three of these areas. Though these inputs do not all overlap *sensu stricto*, with the MD and BLA inputs flanking the dopaminergic innervation, all three inputs can be found within the cytoarchitectonic area of AId$_2$. Thus, by the convergence definition put forth by Divac and colleagues (1978a,b), only the central sector of the OFC can be considered prefrontal.

Future Directions and Functional Implications

This dissertation provides the first systematic examination of the afferents to the orbitofrontal cortex as well as a simplified segmentation of the OFC based upon these afferents. Future studies will determine if this parcellation of the OFC predicts functionally segregated divisions.

Connections of the OFC

Our studies are limited in several respects. We are unable to provide an understanding of the rostro-caudal topography of afferents. Many functional studies target anterior OFC areas (Ahmari et al., 2013; Burguière et al., 2013; Gremel et al., 2016) and rarely do these reports discuss the heterogeneity of the OFC across the rostro-caudal extent. In order to understand the diverse functions of the OFC, it is critical to understand how the afferents that we have described differ in more rostral areas. For example, in our anterograde studies, the MD innervation rarely invades the rostral territories despite the fact that there is a dense innervation of the caudally-adjacent VLO, LO, and AId$_2$. Given that areas related to all five senses innervate the macaque

OFC, it would be particularly interesting to determine if the auditory input to the rat OFC, which is first described in this thesis, is also present in rostral territories.

I have largely investigated the afferents to the OFC and only minimally discussed orbitofrontal efferents. In order to understand the functions of the OFC, it will be critical to determine the ways in which the OFC is connected with the rest of the brain, both in terms of its direct connections and the broader circuitry of this region. Anterograde tract-tracing can be used to uncover the direct connections of the OFC and more sophisticated viral-based targeting can be used to manipulate specific circuits to uncover their functions.

Dopamine in the OFC

Despite the wealth of information regarding dopamine in the medial PFC, the role of dopamine in the OFC is largely unknown. It is likely that dopamine is involved in a number of the behaviors within the OFC, specifically in the LO-AId$_2$ region that has been largely examined by Schoenbaum and colleagues (Cooch et al., 2015; Lucantonio et al., 2014; Takahashi et al. 2009). Future studies may use dopamine denervation techniques, such as, 6-hydroxydopamine or viral-based techniques, combined with behavioral assays to determine how dopamine subserves the functions of this area. The dopaminergic, thalamic, and amygdaloid projections to the mPFC and OFC arise from distinct neuronal populations within the same nuclei. Because of this, it will be interesting to see how the mPFC and OFC are coordinated. It is possible that these areas are regulated by direct connections, as we know that AId$_2$ also receives afferents from the prelimbic area, or it may be that feedback loops back into the MD, BLA, and dopaminergic midbrain are in place to coordinate these areas.

Prefrontal dopamine has been implicated in the pathophysiology of a number of psychiatric illnesses (Goldstein and Volkow, 2011; Howes and Kapur, 2009). A better understanding of the homologies between the dopaminergic innervation of the rodent and primate OFC, and specifically within the agranular insular cortices, is critical to further studies investigating the role of dopamine in the pathophysiology of orbitofrontal-related illnesses including OCD and addiction, as many studies are performed in rodents, yet it is still unclear how this will translate to human disease. In the dorsolateral PFC, for example, the dopamine innervation is decreased in patients diagnosed with schizophrenia (Akil et al., 1999). It is currently unknown if a similar denervation occurs in the OFC in various disease states.

We have proposed that only the central sector of the OFC may be considered prefrontal by the convergence definition put forth by Divac and colleagues (1978a,b). Historically, prefrontal territories have been associated with working memory function, but the OFC is not associated with these functions (Bechara et al., 2000). The OFC is, however, involved in other functions, such as impaired reversal learning, that lead to perseverative behavior. Because the central sector of the OFC is restricted in area, particularly in the deep layers, it will be difficult to target using traditional lesion methods. It may be beneficial to use viral techniques which can target specific projections, such as the orbitofrontal-ventromedial striatal projection targeted by Ahmari et al. (2013). Future studies using such techniques may be able to determine the functions of projections to either the mPFC or the OFC from the BLA for example, in which neighboring cells project to separate targets. Additionally, these types of studies will be instrumental for determining if there are functions common to both prefrontal cortices.

Functions of the OFC

The orbitofrontal cortex has been implicated in functions ranging from reversal learning to social behavior. In 1974, in a series of reports, Kolb (1974a,b,c) reported that lesions of the rat OFC, but not the mPFC, increased locomotor activity and resulted in changes in social behavior. In these early studies, aspiration lesions removed lateral half of the OFC, encompassing the LO, AId, DI, and GI, as well as a large portion of the dorsolateral somatomotor cortex. In contrast, Chudasama and Robbins (2003) reported that animals with excitotoxic lesions of the OFC were not hyperactive; however, the quinolinic acid lesions involved nearly the entire OFC (including medial aspects) and presumably spared axons. There is an implicit assumption that connections of the OFC would be reflected in the functions subserved by this region. Given that the various orbitofrontal sectors receive different afferents, shown in this dissertation, one would expect that these areas are involved in segregated functions as well. However, many studies refer to the entire orbitofrontal expanse as a homogeneous territory. Determining the segregated functions of orbitofrontal areas, will likely depend on discrete manipulations of particular areas or circuitry, as opposed to lesions of the entire territory as outlined here. For example, it is now possible to use combinatorial viral approaches (Gore et al., 2013) to specifically target neurons projecting from the BLA to the lateral orbitofrontal areas. Using these methods, it would be possible to examine the function of this specific projection and compare its function to the BLA-mPFC projection, or the MD-OFC projection.

In recent years, the introduction of optogenetic methods has made it possible to more precisely examine the functions of different orbitofrontal areas. A number of groups have suggested that the OFC is critically involved in the pathophysiology of obsessive compulsive disorder (OCD) (Baxter et al., 1987; Brambilla et al., 2002; Chamberlain et al., 2005). In a paper

published in *Science*, Ahmari et al. (2013) expressed channelrhodopsin 2 in an orbitofrontal-ventromedial striatum (VMS) projection in wild-type mice, then optically stimulated the projection and examined effects on grooming behavior. When the OFC-VMS projection was stimulated for five days (five minutes/day), mice exhibited a progressive increase in self-grooming behavior, which persisted for up to two weeks post-stimulation. Despite the fact that there were no changes in any other typical behaviors associated with OCD (anxiety or prepulse inhibition), excessive self-grooming was reversed with treatment with fluoxetine, a treatment for OCD.

In the same year in the journal *Science*, Burguière et al. (2013) used optogenetics to target orbitofrontal-striatal circuitry in the *Sapap3* mutant mouse, which exhibits excessive self-grooming and anxiety, and has been used as a model of OCD. To examine aberrant behavior, Burguiére and colleagues used a conditioning paradigm to trigger excessive self-grooming following a water drop applied to the mouse's forehead, and expressed channelrhodopsin in cortical neurons of the OFC. Optical activation of the OFC-striatal projection, from a fiber placed either within the OFC or in the striatum, led to an inhibition of aberrant self-grooming. In comparison, the results of Ahmari et al. (2013) and Burguière et al. (2013) seem paradoxical, with one paper reporting a causal role of the OFC in excessive grooming, and the other showing an important role of the OFC in the inhibition of excessive grooming. However, Ahmari et al. focused their attention on the rostral MO and VO areas of wild-type animals, while in the study of Burguière et al. the optical fiber was placed in the LO and DLO of *Sapap3* mutant mice, leading to difficulties reconciling these results.

The Schoenbaum lab has pioneered the interrogation into the function of the rodent OFC, and in particular, they have focused on the area that we have designated as the central sector,

which receives inputs from the MD, BLA, and dopaminergic midbrain. As described above, the OFC has been implicated in functions ranging from response inhibition to general activity levels and aggression, though the data supporting these claims vary dramatically. In a review entitled "What the orbitofrontal cortex does not do," Stalnaker, Cooch and Schoenbaum (2015) critically examined some of the proposed functions of the OFC. They found that, in many cases, the existing data was not sufficient to conclude that the role of the OFC in behavior could be explained by the simplified functions previously proposed, including response inhibition and encoding of value or emotion. They argued instead that the OFC might play a role in broader processes, such as cognitive mapping. The Schoenbaum group (Takahashi et al., 2009) previously showed that OFC neurons work together with the dopaminergic neurons of the VTA work together to signal reward prediction errors in a Pavlovian overexpectation task. However, orbitofrontal neurons alone did not signal errors in reward predictions, indicating that the OFC was not solely responsible for this function and instead may be responsible for broader functions that have implications in specific reward prediction paradigms.

A large body of data suggests that the OFC is involved in processes that are altered in addiction (substance use disorder in DSM-5; Volkow & Fowler, 2000; Schoenbaum et al., 2013). For example, Gremel et al. (2016) reported that the OFC, and specifically endocannabinoids within this region, is important for the balance between goal-directed behavior and habit formation, a process thought to be impaired in addiction (Goldstein and Volkow, 2011). The OFC has also been implicated in drug-seeking behavior, especially with relation to cocaine. Lasseter et al. (2014) were able to attenuate cocaine-seeking behaviors following a direct OFC infusion of the D1-like receptor antagonist, SCH23390, and showed that the OFC-BLA circuit is particularly important for these behaviors. Following this work, Arguello et al. (2017) showed

that the projection from OFC to the BLA, and not vice versa, is important for conditioned stimulus-induced reinstatement of cocaine-seeking. From the Schoenbaum laboratory, Lucantonio et al. (2014) showed that electrophysiological correlates of insight in the OFC were lacking following cocaine self-administration, but could be restored with optogenetic activation of the OFC, indicating that drugs of abuse may induce physiological changes within the OFC relevant to the pathophysiology of addiction, specifically relapse.

It is currently difficult to coherently link data on any of the multiple functional roles that have been proposed for the OFC. For example, the agranular insular cortex has been reported to sustain high rates of intracranial self- stimulation in the rat, apparently in a dopamine-dependent manner (Clavier and Gerfen, 1979). However, a subsequent study by the same investigators somewhat paradoxically reported that self-stimulation of the sulcal region did not depend on presynaptic release of dopamine (Gerfen and Clavier, 1981). Nonetheless, these reports anticipated a large number of investigations into the role of the OFC in drug abuse, ranging from studies of craving to perseverative behavior and response anticipation (see Goldstein et al., 2006; Schoenbaum et al., 2016).

It becomes even more difficult to place these studies into a consistent framework because different subregions within the OFC, including the rostral LO (Gremel et al., 2016), AI_v and medial LO (Lasseter et al., 2014), LO and AId_2 (Arguello et al., 2017), and AId_2 (Lucantonio et al., 2014), have been manipulated or evaluated. These studies varied as well in the degree of extra-target involvement (such a spread of channelopsin transfection or drug).

In turn, this will require that investigators define the precise area of the OFC: the term OFC has been ubiquitously used to describe a heterogeneous region that requires more precise definition (Murray et al., 2007). An excellent recent review by Izquierdo (2017), which

synthesizes the behavioral data on the OFC in response to various manipulations, may provide a

map for approaching a fine-grained understanding of the functional correlates of the rodent OFC.

Conclusions

The OFC is comprised of a number of anatomically distinct areas. The term OFC has

been used in recent literature to refer to any combination of areas or single area within the

ventral frontal cortex, and its definition varies between research groups. Our data indicate that

there are distinct differences in the OFC regions that can be defined on the basis of afferents, and

that the OFC is generally comprised of three segments: medial (including LO and VLO), central

(largely comprised of AId_2), and lateral (AId_1, DI and GI). Of these sectors, only the central

(AId_2) territory can be considered a prefrontal cortex by the convergence definition. The findings

reported here provide a new insight into the anatomy of the orbitofrontal cortex, and suggest that

specific terminology, as well as greater precision, are required in the design and interpretation of

functional studies across this fascinating brain region.

APPENDIX A

IMAGING MASS SPECTROMETRY OF THE OFC

The orbitofrontal cortex is comprised of multiple distinct areas, as illustrated in both cytoarchitectonics analyses (van de Werd and Uylings, 2008) and by our own examination of afferents. Given the heterogeneity of this region, we performed a preliminary experiment in which we using matrix-assisted laser desorption/ionization imaging mass spectrometry (MALDI IMS) to survey intact protein distributions across the OFC. This discovery-based technique allows for visualization of protein distribution across the tissue section. By focusing on the OFC, we are able to determine if any detected proteins were confined to or excluded from specific areas within the OFC.
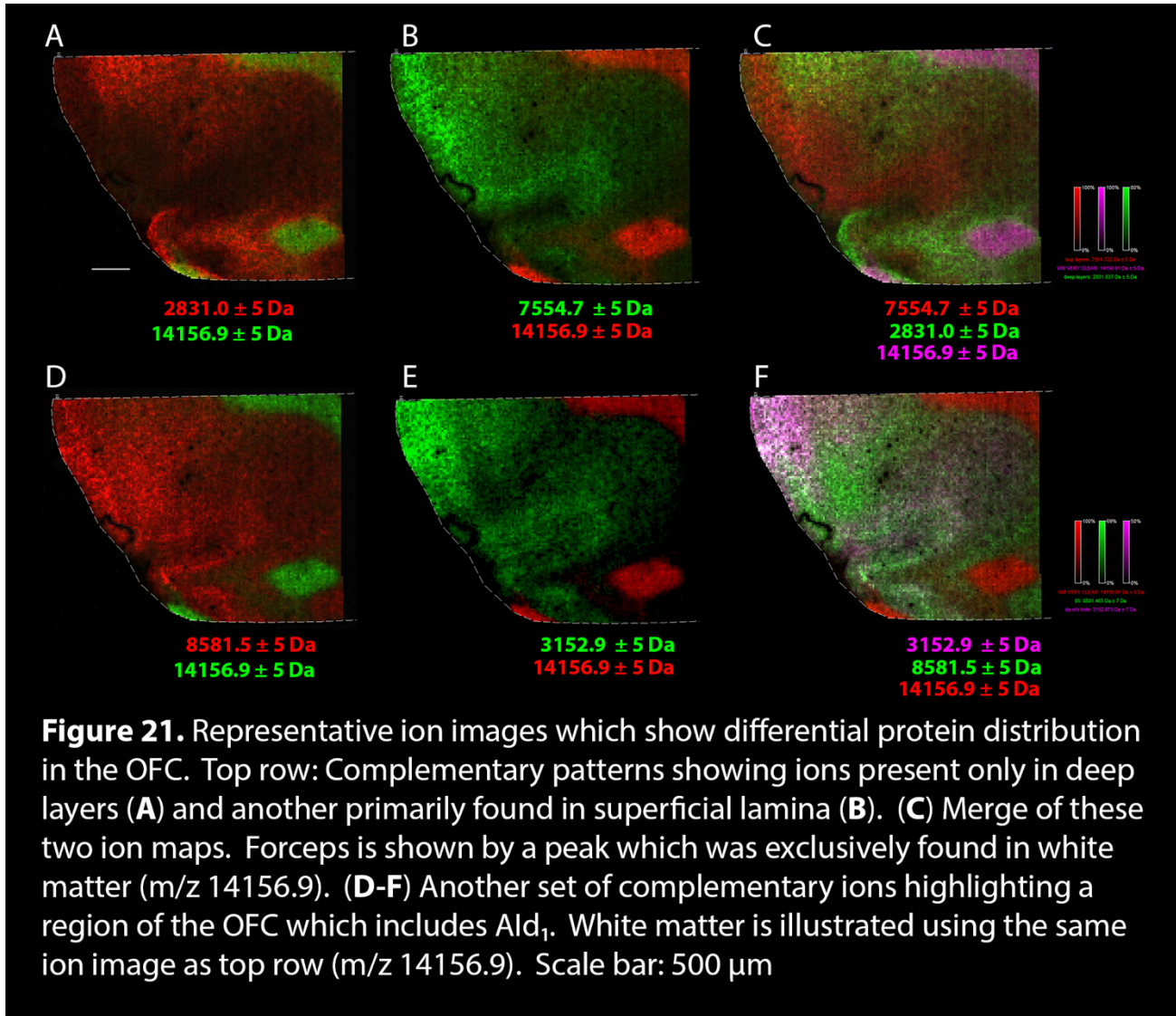
Methods

Sample preparation. Fresh frozen rat brain tissue was sectioned at 10 µm thickness and thaw-mounted onto indium-tin oxide-coated glass slides and stored in the -80ºC freezer until analysis. Frozen plates were allowed to come to room temperature prior to exposure to ambient air in order to minimize water condensation onto the samples. Once at room temperature, the sections were washed as follows: 70% ethanol, 30 sec; 100% ethanol, 30 sec; Carnoy's fluid (ethanol/chloroform/acetic acid, 6:3:1), 2 min; 100% ethanol, 30 sec; water, 30 sec; and 100% ethanol, 30 sec. After washing the plate was allowed to dry at room temperature prior to matrix coating.

Protein imaging. MALDI matrix 2,5-dihydroxyacetophenone (DHA) was spray-coated onto the

MALDI target plates via an automatic sprayer (TM Sprayer, HTX Technologies, Chapel Hill,

NC). DHA was made up as 15 mg/ml in 90% acetonitrile with 0.2% trifluoroacetic acid. Six

passes were applied in a criss-cross spray pattern with a nozzle temperature of 85°C, a flow rate

of 0.2 ml/min, 2 mm track spacing, and a stage velocity of 1100 mm/min. The sections were

rehydrated prior to analysis by warming the plate for 2 min at 37°C followed by exposure of the

plate to 1 ml 50 mM acetic acid for 3 min at 37°C.   Images were acquired with a MALDI TOF

mass spectrometer (Rapiflex Tissuetyper, Bruker, Billerica, MA) equipped with a Smartbeam 3D

10 kHz Nd:YAG laser that was frequency tripled to 355 nm wavelength. Data were collected in

the positive ion mode using 2000 laser shots per pixel with the laser operating at 10 kHz. The

pixel spacing was 25 µm (center-to-center distance) in both x and y dimensions. Data were

collected from m/z 2,200 to 20,000.

Results

Greater than 20 peaks with differential distributions were visualized following MALDI

IMS of the orbitofrontal cortex. Peaks were detected throughout the mass range. One peak (m/z

14,156.9) was localized to the forceps and anterior commissure, indicating that it was likely a

myelin-related protein (see Fig. 21). A majority of peaks detected did not provide insight into

the parcellation of the orbitofrontal cortex. However, there were two pairs of peaks that

highlighted complementary anatomical features. The first pair of ion images clearly show

laminar differences, with one peak (m/z 7554.7) predominant in the superficial cortical layers,

while another (m/z 2831.0) is largely restricted to the deep lamina (Fig. 21A-C). The ion image

for m/z 3152.9 shows a lack of signal within the region of AId_1 specifically (Fig. 21E), while the signal for m/z 8581.5 seems to be most dense within this same region.

Figure 21. Representative ion images which show differential protein distribution in the OFC. Top row: Complementary patterns showing ions present only in deep layers (**A**) and another primarily found in superficial lamina (**B**). (**C**) Merge of these two ion maps. Forceps is shown by a peak which was exclusively found in white matter (m/z 14156.9). (**D-F**) Another set of complementary ions highlighting a region of the OFC which includes AId_1. White matter is illustrated using the same ion image as top row (m/z 14156.9). Scale bar: 500 μm

Discussion

In this preliminary MALDI IMS study, we identified many ions distributed throughout the OFC. However, there were five ions that most clearly highlighted anatomical features of the OFC. Four ions could be divided into two pairs of proteins which showed complementary distributions, while the fifth ion (m/z 14,156.9) was restricted to the white matter, providing a clearer anatomical picture. However, we have not determined the identity of these proteins, as this was a preliminary study and protein identification can prove challenging (Gessel et al., 2014). Additionally, this experiment was performed in one hemisphere from one animal, thus these results are not yet generalizable.

MALDI IMS is discovery-based and does not require *a priori* knowledge of proteins to be analyzed. This a clear advantage over standard techniques used to examine protein distribution, such as immunohistochemistry, which is limited by the sensitivity and specificity of antibodies. Additionally using this technology, we are able to probe the distribution of many different proteins simultaneously. However, MALDI IMS is biased by the conditions under which the experiment is performed. The proteins detected are limited by their abundance, size, and crystallization and ionization given the matrix used (Römpp and Spengler, 2013). We did not perform any enrichment or enzymatic digestion steps, or alter the standard conditions for this experiment, though this may change the proteins that we are able to detect (Gessel et al., 2014).

The ability to perform MALDI IMS at a resolution of 25 μm is critical for the analysis of the OFC. Because the cytoarchitectonic areas within the OFC are quite discrete, particularly within the deep lamina, it is critical to examine these areas at high resolution.

APPENDIX B

EXAMINING PYRAMIDAL CELL HETEROGENEITY WITHIN THE mPFC

Schizophrenia is a debilitating mental illness that affects approximately 1% of the population worldwide. A number of anatomical features have been consistently reported in schizophrenia, including increased ventricular size, decreased cortical thickness, decreased dopamine (DA) innervation of the PFC, and a loss of dendritic spines on PFC pyramidal cells (Akil et al., 1999; Howes and Kapur, 2009). In order to investigate the relationship between cortical dopamine loss and decreased dendritic spine density in rats, we injected 6-hydroxydopamine (6-OHDA) into the ventral tegmental area (VTA), from which the mPFC dopamine innervation is derived, to ablate the prefrontal dopamine innervation. We then performed intracellular fills, using the fluorophore Lucifer yellow, of pyramidal cells and determined the density of dendritic spines.

Dopamine denervation of the mPFC resulted in decreased dendritic spine density on both the apical and basal dendrites of layer 5 pyramidal cells (PCs). It was subjectively noted, however, that only some layer 5 PCs exhibited spine loss, while others appeared resistant to this loss. We hypothesized that the vulnerability of PCs may be related to the cell's projection target. To explore this hypothesis, we retrogradely-labeled prelimbic PCs from one of five sites: the nucleus accumbens (NAS), basolateral amygdala (BLA), ventral tegmental area (VTA), mediodorsal nucleus of the thalamus (MD), or the contralateral PFC (cPFC). The retrogradely-labeled neurons were then filled with Lucifer yellow and spine density assessed. There was decreased dendritic spine density only in the layer 5 PCs projecting to the NAS or MD.

Pyramidal cells originating in other layers or projecting to other targets were not significantly affected by the dopamine denervation.

In order to understand the molecules that subserve this heterogeneity, I used both targeted and a discovery-based approaches. In both techniques, laser capture microdissection (LCM) was used to excise pyramidal cells from specific layers of cortex. Because LCM is visually guided, it is possible to excise specific cells based on a variety of characteristics, such as shape and expression of fluorescent markers or tracers. Following LCM, we determined the expression of the five dopamine receptors by qPCR in pyramidal cells projecting to specific targets. In a proof-of-concept discovery-based experiment, we performed MuDPIT proteomics on LCM-excised layer 5 pyramidal cells.

Methods

Animals and tissue preparation.

Adult Sprague-Dawley rats were used for these experiments and all experiments were performed in accordance with institutional and national guidelines. Rats underwent surgery in which red cholera toxin, subunit B (CTB) was injected into either the MD, VTA, NAS, BLA, or cPFC as outlined in Chapter 3. After a one-week survival period, which allowed CTB to efficiently retrogradely-label pyramidal cells in the mPFC, the rats were sacrificed and the frontal cortices were flash frozen in powdered dry ice. The PFC was then cryosectioned at a thickness of 10 μm and sections were mounted onto polyethylene terephthalate (PET) MembraneSlides (Carl Zeiss Microscopy), which allows for more efficient microdissection than typical microscope slides.

Dopamine receptor expression.

For each projection target and cortical layer or interest, 250 PCs were identified under fluorescent illumination, and collected directly into RNA extraction buffer (PicoPure RNA isolation kit, Life Technologies). RNA extraction, isolation, reverse transcription, and pre-amplification (14 cycles) were performed on all samples simultaneously. Quantitative PCR was performed for all samples using eight assays. Three housekeeping genes (GAPDH, beta-2-microglobulin, and cyclophilin A) were monitored as well as five assays of interest: dopamine receptor D_1 (D_1), dopamine receptor D_2 (D_2), calcium-calmodulin-dependent kinase II alpha (CaMKIIα), glutamate decarboxylase 2 (GAD2; GAD 65), and glial fibrillary acidic protein (GFAP). Taqman probes were used and obtained from Life Technologies. Values were calculated for each assay based on a standard curve of all samples pooled together. For experimental assays (D_1, D_2, CaMKIIα, GAD2, GFAP), values were normalized to the geometric mean of the three housekeeping genes (GAPDH, B2M, Ppia) to control for amount of sample.

Proteomics Proof-of-Concept Experiment.

One thousand PCs were microdissected under brightfield illumination from layer 5 of the prelimbic area of the PFC, and collected into 100mM ammonium bicarbonate. Immediately following collection, cells were lysed with 50% trifluoroethanol (*v/v*). Lysed cells were then given to the Vanderbilt Proteomics Core, who reduced, alkylated, digested with trypsin, and performed MuDPIT (multi-dimensional protein identification technology) on a hybrid quadrupole-orbitrap mass spectrometer (Orbitrap Velos, Thermo Fisher).

Enrichment analysis was performed using WebGestalt, a web-based gene set analysis toolkit (Wang et al., 2013). Gene Ontology (GO) analysis was performed using the default

multiple testing adjustment (BH: Bejamini & Hochberg) and the significance level was set to report only the 10 GO classifications with the most significant adjusted p-values (<0.01).

Results

Distribution of dopamine receptor expression.

Pyramidal cells located in the prelimbic cortex that were retrogradely labeled from various sites were visualized by fluorescence, then isolated and captured by LCM. Quantitative PCR analyses revealed that pyramidal cells expressing D_1 or D_2 mRNA were both present in layer 5, consistent with previous reports. Dopamine receptor D_1 expression was greatest in L5 pyramidal cells projecting to MD, while D_2 was expressed at the highest levels in layer 5 pyramidal cells innervating the NAS (see Table 2). The astrocytic marker, glial fibrillary acidic protein (GFAP), and the interneuron marker glutamate decarboxylase 2 (GAD2), were detected in relatively low quantities in most cell groups analyzed. A marker for pyramidal cells (Liu and Jones, 1996), calcium/calmodulin-dependent protein kinase II alpha (CaMKIIα) was detected in all cell groups.

Table 2. Dopamine receptor expression in pyramidal cells projecting to various targets.

	D1	D2	CaMKIIα	GFAP	GAD2
MD L6	+	N.D.	+ / -	+ / -	+ / -
NAS L5	++	++++	++	+	++
cPFC L5	+	+	+	+	+
MD L5	++++	++	+++	++	++
VTA L5	+ / -	+ / -	+	+ / -	+ / -
BLA L5	+ / -	+	+	+ / -	+ / -
BLA L2/3	++	+ / -	++	++	++
PC control	+	+ / -	+	+ / -	+

Key: ND = not detected   +/- : <0.3
+ : 0.3-1.0   ++: 1.0-2.0   +++: 2.0-3.0   ++++ : >3.0

Proteomics proof-of-concept.

Following selective excision of prelimbic pyramidal cells, 1179 proteins were identified in this experiment. The sodium-potassium ATPase, subunit alpha was identified at the top hit, with the most spectra assigned to it (1609 spectra), indicating that excitable cells were in fact excised. Within the top four hits was the pyramidal cell marker, CaMKIIα, with 1200 spectra assigned to it. Known non-pyramidal cell proteins, such as astrocytic (GFAP) and interneuron (GAD1) markers were detected in low abundance (see Fig. 22). GAD2, another commonly used interneuron marker was not detected.

		1179 Proteins 0.5% Prot FDR 36311 Spectra 0.0% Pept FDR	Accession Number	Molecular Weight	Protein Grouping Ambiguity	MudPIT
Identified Proteins (1179) Including 6 Decoys						
Sodium/potassium-transporting ATPase subunit al...			sp|P0668...	112 k...	★	1609
ATP synthase subunit alpha, mitochondrial OS=Ratt...			sp|P1599...	60 kDa	★	1568
Tubulin alpha-1B chain OS=Rattus norvegicus GN=...			sp|Q6P9V...	50 kDa	★	1301
Calcium/calmodulin-dependent protein kinase type...			sp|P1127...	54 kDa	★	1200
Glial fibrillary acidic protein OS=Rattus norvegicus...			sp|P4781...	50 kDa	★	44
Glutamate decarboxylase 1 OS=Rattus norvegicus G...			sp|P1808...	67 kDa		3

Figure 22. Proteomic analysis of LCM-captured cells show that markers of pyramidal cells (e.g., CaMKIIα) are abundant, while markers of glia (glial fibrillary acidic protein) and interneurons (glutamate decarboxylase 1 (GAD67)) are minimally present, consistent with the captured material being pyramidal cells.
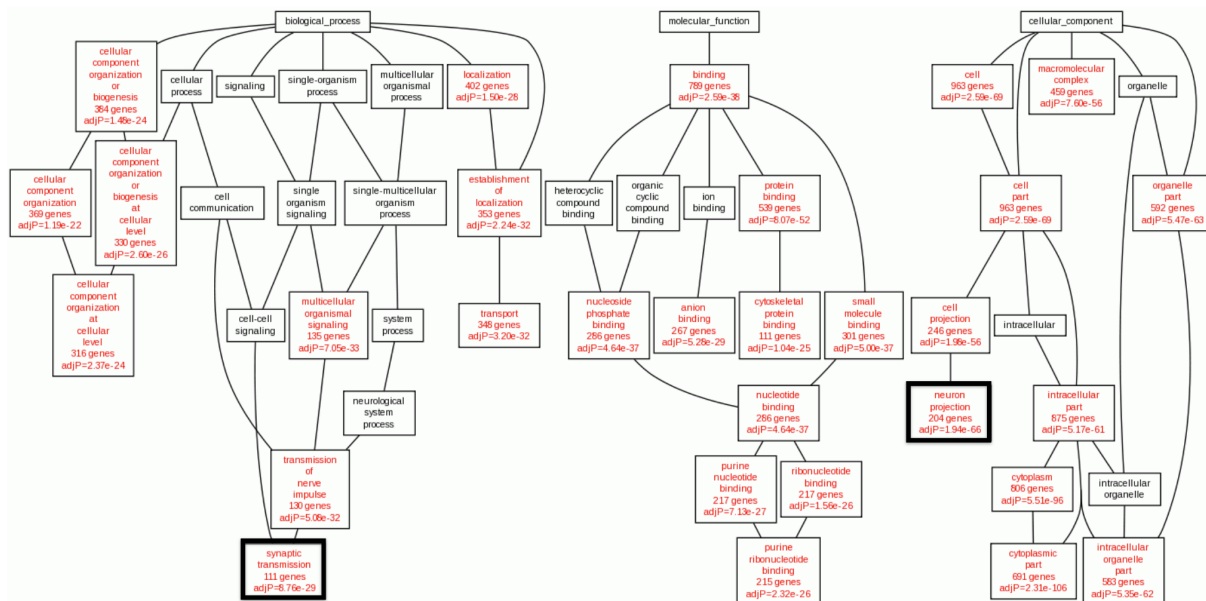
Figure 23. Results of enrichment analysis based on gene ontology (GO) classifications. Many of the GO categories that were identified as enriched were associated with neuronal function, including synaptic transmission and neuron projection. Cytosolic, pre-synaptic, and post-synaptic proteins were all identified within these classifications. This is especially interesting given that only the cell body was dissected by LCM.

Synaptic Transmission	
Gene	*Name*
Grm2	Metabotropic glutamate receptor 2 (mGluR2)
Grin2b	NMDA receptor, subunit NR2B
Gria2	AMPA receptor, subunit GluA2
Shank3	SH3 and multiple ankyrin repeat domains 3
Nedd4	E3 Ubiquitin ligase
Syt2	Synaptotagmin 2
Slc17a7	Vesicular glutamate transporter 1 (vGluT1)
Stxbp1	Syntaxin binding protein 1 (MUNC-18)
Vamp2	Synaptobrevin 2
Atp2b2	ATPase, Ca^{2+} transporting, plasma membrane 2

Neuron Projection	
Gene	*Name*
Prkca	Protein Kinase C, alpha subunit
Syngap1	Synaptic Ras GTPase activating protein 1
Ppp1ca	Protein phosphatase 1, catalytic subunit, alpha enzyme
Cask	Ca^{2+}/calmodulin-dependent serine protein kinase (MAGUK family)
Ryr2	Ryanodine receptor 2
Actb	Beta actin
Bsn	Bassoon
Actn1	Actinin, alpha 1
Ctnnd2	Catenin, delta 2
Atp1a3	ATPase, Na^+/K+ transporting, alpha 3 polypeptide

Figure 24. Representative proteins of interest uncovered in this experiment, found in enriched ontology groups.

Enrichment analysis was performed on the proteins identified in this experiment. Categories involving neuronal functions, such as synaptic transmission and neuron projection, were found to be enriched in the LCM-collected sample. Some critical neuronal proteins were

uncovered in this experiment, and those associated with the enriched groups are highlighted in Figures 23 and 24.

Discussion

Dopamine receptor expression in mPFC pyramidal cells.

We have confirmed previous reports on the localization of cells expressing dopamine receptors D_1 and D_2 in the medial prefrontal cortex, and found that pyramidal cells innervating different target areas exhibit differential dopamine receptor expression. These data, however, failed to provide a simple explanation for the projection target-dependent spine loss in response to dopamine depletion. There has not been a systemic exploration of dopamine receptor colocalization in the mPFC, although a previous report (Gaspar et al., 1995) indicated the presence of some layer 5 pyramidal cells that express both dopamine receptor D_1 and D_2 mRNAs. We have therefore begun a double fluorescent *in situ* hybridization (FISH) study to investigate co-localization of D_1 and D_2 in the mPFC in neurons which innervate different target areas. In this study, only MD- and NAS-projecting layer 5 pyramidal cells expressed both D_1 and D_2 mRNAs at relatively high levels; it is therefore possible that loss of signaling through both receptors is required to elicit spine loss following dopamine denervation. However, the two dopamine receptors canonically have opposing effects, with dopamine receptor D_1 positively coupled to adenylyl cyclase while the D_2 receptor is $G_{i/o}$-coupled. It is possible that a non-canonical signaling cascade is operating (Sesack & Bunney, 1989).

It is unlikely that other dopamine receptors are implicated in this phenomenon as neither D_3 nor D_4 were detected in any samples, and previous literature has shown that dopamine receptor D_5 is minimally expressed in the adult rodent PFC. It is possible, however, that

dopamine may signal through non-cognate receptors. For example, dopamine binds to the α_{2C} adrenergic receptor in striatal cells with high (<10nM) affinity and regulates adenylyl cyclase in these neurons. Although comparable studies have not been undertaken in the mPFC, it is possible that dopamine modulates spine number through some non-dopamine receptor.

Proteomics of mPFC pyramidal cells.

Using LCM coupled with MuDPIT proteomics, we have shown that individual cortical pyramidal cells can be collected and analyzed. This sample of pyramidal cells, captured by LCM on the basis of soma shape, expressed proteins that are restricted to pyramidal cells of the cortex in abundance (CaMKIIα). In contrast, proteins that are localized to non-pyramidal cell types, such as the astrocytic marker GFAP and the interneuron marker GAD1 were present in very low abundance.

This is, to the best of our knowledge, the first time a discovery-based proteomic study of specific pyramidal cell populations has been reported. LCM offers the unique ability of being able to dissect specific cells of interest based on a number of properties, including cell morphology, anatomical location, and presence of a fluorescent label, as shown here with subsequent qPCR analysis. Coupling LCM with a discovery-based technique like MuDPIT proteomics allows for the molecular classification of pyramidal cells. Previous approaches to classify pyramidal cell subtypes on the basis of protein expression have been limited to *a priori* defined proteins of interest; this often depends heavily on the availability and specificity of antibodies.

We have not experimentally addressed validation of the proteins that we have detected in this experiment. Because proteomics is a discovery-based method, it is critical that the presence

of all proteins of interest is confirmed using multiple methods, such as immunohistochemistry, *in situ* hybridization histochemistry, or quantitative (q) PCR analyses of captured cells. Given that specific antibodies are sometimes not available, and there are not infrequent mismatches between transcript and protein expression levels, it will likely require multiple approaches to validate the proteins detected.

This study has shown that discovery-based proteomic analysis of discretely localized types of cells can be performed. We used MuDPIT proteomics, which we know can provide good depth into the proteome (McDonald and Yates, 2002). We have not, however, undertaken comparisons of different types of proteomic methods (e.g., targeted proteomics), nor have we compared across different types of mass spectrometers.

The utility of this method is that one can explore, in an unbiased manner, the proteins expressed by different types of cells within a single animal (for example, pyramidal cells projecting to different targets from different lamina as described here), between control and experimental animals, or even between normal control subjects and those with neuropsychiatric disorders.

Technical Considerations.

We have performed laser capture microdissection on 10 μm thick sections. Thus, we are likely to predominantly, but not exclusively, collect material from pyramidal cells, as was reflected by the abundance of CaMKIIα and other proteins in our proteomics experiment. Given the close apposition of astrocytic processes and interneuron terminals to pyramidal cells, however, it is not surprising that there is contamination by transcripts and proteins that are found in these non-pyramidal cells.

We have not chosen to proceed with these methods, however, due to lack of reliable reproducibility. Though our results indicate that we were able to selectively excise pyramidal cells from appropriate lamina within the mPFC, we were unable to consistently produce similar results, particularly in the proteomics experiments. It is likely that this failure to reproduce this data is due to a combination of factors including human error, changes in the environment surrounding the laser capture microdissector leading to poor collection efficiency, and sample loss during preparation.

Despite some limitations, this technique provides a unique opportunity to dissect specific cells of interest based on a combination of properties, including cell morphology, anatomical location, and presence of a fluorescent label. LCM has allowed us to probe specific pyramidal cells of interest within a defined cortical lamina, while avoiding neighboring cells that may project to different targets. This level of cellular targeting has not been established before, and could prove invaluable if the technologies and methodologies are optimized. Once optimized, these techniques would prove invaluable in targeting the OFC, which is comprised of many distinct areas which, at points, are very small (< 350 μm in diameter) and difficult to target by standard dissection methods.

REFERENCES

Akil, M., Pierri, J. N., Whitehead, R. E., Edgar, C. L., Mohila, C., Sampson, A. R., Lewis, D. A. (1999). Lamina-specific alteration in the dopamine innervation of the prefrontal cortex in schizophrenic subjects. *American Journal of Psychiatry, 156*(10), 1580-1589.

Alcaraz, F., Marchand, A. R., Courtand, G., Coutureau, E., & Wolff, M. (2016). Parallel inputs from the mediodorsal thalamus to the prefrontal cortex in the rat. *European Journal of Neuroscience*, *44*(3), 1972–1986. http:// doi:10.1111/ejn.13316

Allard, J. S., Tizabi, Y., Shaffery, J. P., Trouth, C. O., & Manaye, K. (2004). Stereological analysis of the hypothalamic hypocretin/orexin neurons in an animal model of depression. *Neuropeptides, 38*(5), 311-5.

Allen, G. V., Saper, C. B., Hurley, K. M., Cechetto, D. F. (1991). Organization of visceral and limbic connections in the insular cortex of the rat. *Journal of Comparative Neurology*, *311*(1), 1-16.

Beckstead, R. M. (1976). Convergent thalamic and mesencephalic projections to the anterior medial cortex in the rat. *Journal of Comparative Neurology*, *166*, 403–416.

Berendse, H. W., Galis-de Graaf, Y., Groenewegen, H. J. (1992) Toporaphical organization and relationship with ventral striatal compartments of prefrontal corticostriatal projections in the rat. *Journal of Comparative Neurology*, *316*, 314-347

Berger, B., Thierry, A. M., Tassin, J. P., & Moyne, M. A. (1976). Dopaminergic innervation of the rat prefrontal cortex: a fluorescence histochemical study. *Brain Research*, *106*, 133–145.

Bradshaw, S. E., Agster, K. L., Waterhouse, B. D., & McGaughy, J. A. (2016). Age-related changes in prefrontal norepinephrine transporter density: The basis for improved cognitive. *Brain Research*, *1641*(Part B), 245–257. doi:10.1016/j.brainres.2016.01.001

Brodmann, K. (2006). *Brodmann's Localisation in the Cerebral Cotex*. (L. J. Garey, Trans.) (3rd ed.). Springer. (Original work published 1909)

Brog, J. S., Salyapongse, A., Deutch, A. Y., and Zahm, D. S. (1993) The patterns of afferent innervation of the core and shell in the "accumbens" part of the rat ventral striatum: immunohistochemical detection of retrogradely transported fluoro-gold. *Journal of Comparative Neurology, 338*(2), 255-278.

Bubser, M., & Deutch, A. Y. (1998). Thalamic paraventricular nucleus neurons collateralize to innervate the prefrontal cortex and nucleus accumbens. *Brain Research*, *787*(2), 304–310.

Buchanan, S. L., Thompson, R. H., Maxwell, B. L., & Powell, D. A. (1994). Efferent connections of the medial prefrontal cortex in the rabbit. *Experimental Brain Research*, 100, 469-483.

Chandler, D. J., Lamperski, C. S., & Waterhouse, B. D. (2013). Identification and distribution of projections from monoaminergic and cholinergic nuclei to functionally differentiated subregions of prefrontal cortex. *Brain Research*, *1522*, 38–58. http://doi.org/10.1016/j.brainres.2013.04.057

Cooch, N. K., Wied, H. M., Bali-Chaudhary, S., McDannald, M. A., Liu, T.-L., Stalnaker, T. A., & Schoenbaum, G. (2015). Orbitofrontal lesions eliminate signaling of biological significance in cue-responsive ventral striatal neurons. *Nature Communications*, *6*, 1–12. doi:10.1038/ncomms8195

Dalley, J. W., Cardinal, R. N., & Robbins, T. W. (2004). Prefrontal executive and cognitive functions in rodents: neural and neurochemical substrates. *Neuroscience and Biobehavioral Reviews*, *28*, 771–784. doi:10.1016/j.neubiorev.2004.09.006

Damasio, H., Grabowski, T., Frank, R., Galaburda, A. M., & Damasio, A. R. (1994). The return of Phineas Gage: Clues about the brain from the skull of a famous patient. *Science*, *264*(5162), 1102–1105.

Dandash, O., Pantelis, C., Fornito, A. (2017). Dopamine, fronto-striatal-thalamic circuits and risk for psychosis. *Schizophrenia Research*, *180*, 48-57.

Daubner, S. C., Le, T., & Wang, S. (2011). Tyrosine hydroxylase and regulation of dopamine synthesis. *Archives of Biochemistry and Biophysics*, *508*(1), 1–12. doi:10.1016/j.abb.2010.12.017

Descarries, L., Lemay, B., Doucet, G., & Berger, B. (1987). Regional and laminar density of the dopamine innervation in adult rat cerebral cortex. *Neuroscience*, *21*(3), 807–824.

Deutch, A. Y., & Cameron, D. S. (1992). Pharmacological characterization of dopamine systems in the nucleus accumbens core and shell. *Neuroscience*, *46*(1), 49–56.

Divac, I., Björklund, A., Lindvall, O., & Passingham, R. E. (1978a). Converging projections from the mediodorsal thalamic nucleus and mesencephalic dopaminergic neurons to the neocortex in three species. *Journal of Comparative Neurology*, *180*, 59–72.

Divac, I., Kosmal, A., Bjorklund, A., & Lindvall, O. (1978b). Subcortical projections to the prefrontal cortex in the rat as revealed by the horseradish peroxidase technique. *Neuroscience*, *3*, 785–796.

Divac, I., & Mogensen, J. (1985). The prefrontal "cortex" in the pigeon catecholamine histofluorescence. *Neuroscience*, *15*(3), 677–682.

Divac, I., Wikmark, R., & Gade, A. (1975). Spontaneous alternation in rats with lesions in the frontal lobes: an extension of the frontal lobe syndrome. *Physiological Psychology*, *3*(1), 39–42.

Fadel, J., Bubser, M., & Deutch, A. Y. (2002) Differential activation of orexin neurons by

antipsychotic drugs associated with weight gain. *Journal of Neuroscience, 22*(15), 6742-6747.

Fallon, J. H. (1981). Collateralization of monoamine neurons: mesotelencephalic dopamine projections to caudate, septum, and frontal cortex. *Journal of Neuroscience, 1*(12), 1361–1368.

Febvret, A., Berger, B., Gaspar, P., & Verney, C. (1991). Further indication that distinct dopaminergic subsets project to the rat cerebral cortex: lack of colocalization with neurotensin in the superficial dopaminergic fields of the anterior cingulate, motor, retrosplenial and visual cortices. *Brain Research, 547*(1), 37-52.

Figee, M., Pattij, T., Willuhn, I., Luijes, J., van den Brink, W., Goudriaan, A., … Denys, D. (2016). Compulsivity in obsessive-compulsive disorder and addictions. *European Neuropsychopharmacology*, *26*, 856-868.

Filley, C. M. (2010). The frontal lobes. In S. Finger, F. Boller, & K. Tyler (Eds.), *History of Neurology* (Vol. 95, pp. 557–570). Elsevier B.V. doi:10.1016/S0072-9752(08)02135-0

Fitoussi, A., Dellu-Hagedor, F., & de Deurwaerdere, P. (2013). Monoamines tissue content analysis reveals restricted and site-specific correlations in brain regions involved in cognition. *Neuroscience*, *255*, 233–245. doi:10.1016/j.neuroscience.2013.09.059

García-Molina, A. (2012). Phineas Gage and the enigma of the prefrontal cortex. *Neurología, 27*(6), 370-375.

Gaspar, P., Berger, B., Febvret, A., Vigny, A., & Henry, J. P. (1989). Catecholamine innervation of the human cerebral cortex as revealed by comparative immunohistochemistry of tyrosine hydroxylase and dopamine-beta-hydroxylase. *Journal of Comparative Neurology*, *279*(2), 249–271. doi:10.1002/cne.902790208

Gaspar, P., Bloch, B., & Le Moine, C. (1995). D1 and D2 receptor gene expression in the rat frontal cortex: cellular localization in different classes of efferent neurons. *European Journal of Neuroscience*, *7*(5), 1050–1063.

Gerfen, C. R., & Clavier, R. M. (1979). Neural inputs to the prefrontal agranular insular cortex in the rat: horseradish peroxidase study. *Brain Research Bulletin*, *4*(3), 347–353.

Gessel, M. M., Norris, J. L., Caprioli, R. M. (2014) MALDI imaging mass spectrometry: spatial molecular analysis to enable a new age of discovery. *Journal of Proteomics, 107*, 71-82. doi.org/10.1016/j.jprot.2014.03.021

Goldman-Rakic, P. S., & Porrino, L. J. (1985). The primate mediodorsal (MD) nucleus and its projection to the frontal lobe. *Journal of Comparative Neurology*, *242*, 535–560.

Goldman-Rakic, P. S., & Selemon, L. D. (1997). Functional and anatomical aspects of prefrontal pathology in schizophrenia. *Schizophrenia Bulletin*, *23*(2), 437–458.

Goldstein, R. Z., & Volkow, N. D. (2011). Dysfunction of the prefrontal cortex in addiction: neuroimaging findings and clinical implications. *Nature Reviews Neuroscience, 12*, 652–669. doi:10.1038/nrn3119

Gore, B. B., Soden, M. E., Zweifel, L. S. (2014) Manipulating gene expression in proection-specific neuronal populations using combinatorial viral approaches. *Current Protocols in Neurosicence, 4*(435), 1-20. doi:10.1002/0471142301.ns0435s65

Gremel, C. M., Chancey, J. H., Atwood, B. K., Luo, G., Neve, R., Ramakrishnan, C., et al. (2016). Endocannabinoid modulation of orbitostriatal circuits gates habit formation. *Neuron, 90*(6), 1312–1324. http://doi.org/10.1016/j.neuron.2016.04.043

Groenewegen, H. J. (1988). Organization of the afferent connections of the mediodorsal thalamic nucleus in the rat, related to the mediodorsal-prefrontal topography. *Neuroscience, 24*(2), 379–431.

Grove, E. A. (1988). Efferent connections of the substantia innominata in the rat. *Journal of Comparative Neurology, 277*(3), 347-364.

Gunaydin, L. A., Kreitzer, A. C. (2016) Cortico-basal ganglia circuit function in psychiatric disease. *Annual Review of Physiology, 78*, 327-350.

Heilbronner, S. R., Rodriguez-Romaguera, J., Quirk, G. J., Groenewegen, H. J., Haber, S. N. (2016). Circuit-based corticostriatal homologies between rat and primate. *Biological Psychiatry, 80,* 509-521. doi.org/10.1016/j.biopsych.2016.05.012

Hökfelt, T., Johansson, O., Fuxe, K., Goldstein, M., Park, D. (1977) Immunohistochemical studies on the localization and distribution of monoamine neuron systems in the rat brain II. Tyrosine hydroxylase in the telencephalon. *Medical Biology, 55*(1), 21-40.

Hökfelt, T., Martensson, T. R., Björklund, A., Kleinau, S., & Goldstein, M. (1984). Distributional maps of tyrosine-hydroxylase-immunoreactive neurons in the rat brain. In A. Bjorklund & T. Hokfelt (Eds.), *Handbook of Chemical Neuroanatomy* (Vol. 2: Classical Transmitters in the CNS, Part I, pp. 277–379). Amsterdam: Elsevier.

Hoover, W. B., & Vertes, R. P. (2007). Anatomical analysis of afferent projections to the medial prefrontal cortex in the rat. *Brain Structure and Function, 212*(2), 149–179. http://doi.org/10.1007/978-3-642-70573-1

Hoover, W. B., & Vertes, R. P. (2011). Projections of the medial orbital and ventral orbital cortex in the rat. *Journal of Comparative Neurology, 519*, 3766–3801. doi:10.1002/cne.22733

Howes, O. D., Kapur, S. (2009). The dopamine hypothesis of schizophrenia: version III – the final common pathway. *Schizophrenia Bulletin, 35*(3), 549-562. doi:10.1093/schbul/sbp006

Hwang, E., Willis, B. S., & Burwell, R. D. (2017). Prefrontal connections of the perirhinal and postrhinal cortices in the rat. *Behavioural Brain Research*. http://doi.org/10.1016/j.bbr.2017.07.032

Jones, M. W., Kilpatrick, I. C., & Phillipson, O. T. (1986). The agranular insular cortex: a site of unusually high dopamine utilisation. *Neuroscience Letters*, *72*(3), 330–334.

Kalsbeek, A., Voorn, P., Buijs, R. M., Pool, C. W., & Uylings, H. B. (1988). Development of the dopaminergic innervation in the prefrontal cortex of the rat. *Journal of Comparative Neurology*, *269*(1), 58–72. http://doi.org/10.1002/cne.902690105

Kheramin, S., Body, S., Ho, M.-Y., Velázquez-Martinez, D. N., Bradshaw, C. M., Szabadi, E., Deakin, J. F. W., et al. (2004). Effects of orbital prefrontal cortex dopamine depletion on inter-temporal choice: a quantitative analysis. *Psychopharmacology*, *175*, 206–214. doi:10.1007/s00213-004-1813-y

Kita, H. & Kitai, S. T. (1990). Amygdaloid projections to the frontal cortex and the striatum in the rat. *Journal of Comparative Neurology*, *298*(1), 40-49.

Krettek, J. E., & Price, J. L. (1974). A direct input from the amygdala to the thalamus and the cerebral cortex. *Brain Research*, *67*, 169–174.

Krettek, J. E., & Price, J. L. (1977a). Projections from the amygdaloid complex to the cerebral cortex and thalamus in the rat and cat. *Journal of Comparative Neurology*, *172*, 687–722.

Krettek, J. E., & Price, J. L. (1977b). The cortical projections of the mediodorsal nucleus and adjacent thalamic nuclei in the rat. *Journal of Comparative Neurology*, *171*, 157–192.

Kuramoto, E., Pan, S., Furuta, T., Tanaka, Y. R., Iawi, H., Yamanaka, A., …, Hioki, H. (2016). Individual mediodorsal thalamic neurons project to multiple areas of the rat prefrontal cortex: a single neuron-tracing study using virus vectors. *Journal of Comparative Neurology*, *525*, 166-185. doi: 10.1002/cne.24054

Kuroda, M., Murakami, K., Igarashi, H., & Okada, A. (1996). The convergence of axon terminals from the mediodorsal thalamic nucleus and ventral tegmental area on pyramidal cells in layer V of the rat prelimbic cortex. *European Journal of Neuroscience*, *8*(7), 1340–1349.

Leonard, C. M. (1969). The prefrontal cortex of the rat. I. Cortical projection of the mediodorsal nucleus. II. Efferent connections. *Brain Research*, *12*, 321–343.

Leonard, C. M. (2016). Finding the prefrontal cortex in the rat. *Brain Research, 1645,* 1-3. doi: 10.1016/j.brainres.2016.02.002

Lidow, M. S., Wang, F., Cao, Y., & Goldman-Rakic, P. S. (1998). Layer V neurons bear the majority of mRNAs encoding the five distinct dopamine receptor subtypes in the primate prefrontal cortex. *Synapse*, *28*, 10–20.

Lindvall, O., & Björklund, A. (1974). The organization of the ascending catecholamine neuron systems in the rat brain as revealed by the glyoxylic acid fluorescence method. *Acta Physiologica Scandinavica. Supplementum*, *412*, 1–48.

Lindvall, O., Bjorklund, A., & Divac, I. (1978). Organization of catecholamine neurons projecting to the frontal cortex in the rat. *Brain Research*, *142*, 1–24.

Liu, X. B., Jones, E. G. (1996) Localization of alpha type II calcium calmodulin-dependent protein kinase at glutamatergic but not gamma-aminobutyric acid (GABAergic) synapses in thalamus and cerebral cortex. *Proceedings of the National Academy of Sciences, 93,* 7332-7336.

Loughlin, S. E., & Fallon, J. H. (1984). Substantia nigra and ventral tegmental area projections to cortex: topography and collateralization. *Neuroscience*, *11*(2), 425–435.

Mathur, B. N., Caprioli, R. M., & Deutch, A. Y. (2009). Proteomic analysis illuminates a novel structural definition of the claustrum and insula. *Cerebral Cortex*, *19*, 2732–2379. doi:10.1093/cercor/bhn253

Mátyás, F., Lee, J., Shin, H.-S., & Acsády, L. (2014). The fear circuit of the mouse forebrain: connections between the mediodorsal thalamus, frontal cortices and basolateral amygdala. *European Journal of Neuroscience*, *39*(11), 1810–1823. http://doi.org/10.1016/j.brainres.2003.10.006

McDonald, W. H., Yates III, J. R. (2002). Shotgun proteomic and biomarker discovery. *Disease Markers, 18*, 99-105.

Meador-Woodruff, J. H., Haroutunian, V., Powchik, P., Davidson, M., Davis, K. L., & Watson, S. J. (1997). Dopamine receptor transcript expression in striatum and prefrontal and occipital cortex. *Archives of General Psychiatry*, *54*, 1089–1095.

Mesulam, M. (2006). Foreward. In D. H. Zald & S. L. Rausch (Eds.), *The Orbitofrontal Cortex* (p. vii–vi). New York: Oxford University Press.

Mishkin, M. (1964). Preservation of central sets after frontal lesions in monkeys. In J. M. Warren & K. Akert (Eds.), *The Frontal Granular Cortex and Behavior* (pp 219-241). New York: McGraw Hill.

Mogensen, J., & Divac, I. (1982). The prefrontal 'cortex' in the pigeon: Behavioral evidence. *Brain, Behavior, and Evolution*, *21*, 60–66.

Noack, H. J., & Lewis, D. A. (1989). Antibodies directed against tyrosine hydroxylase differentially recognize noradrenergic axons in monkey neocortex. *Brain Research*, *500*, 313–324.

Ongür, D., & Price, J. L. (2000). The organization of networks within the orbital and medial prefrontal cortex of rats, monkeys and humans. *Cerebral Cortex*, *10*, 206–219.

Pape, H. C., Paré, D., & Driesang, R. B. (1998). Two types of intrinsic oscillations in neurons of the lateral and basolateral nuclei of the amygdala. *Journal of Neurophysiology*, *79*, 205-216.

Paxinos, G., & Watson, C. (2007). The Rat Brain in Stereotaxic Coordinates (6 ed.). Elsevier.

Petrides, M., & Mackey, S. (2006). The orbitofrontal cortex: sulcal and gyral morphology and architecture. In D. H. Zald & S. L. Rauch (Eds.), *The Orbitofrontal Cortex* (pp. 19–37). New York: Oxford University Press.

Petrovich, G. D., Risold, P. Y., & Swanson, L. W. (1996) Organization of projections from the basomedial nucleus of the amygdala: a PHAL study in the rat. *Journal of Comparative Neurology*, *374*(3), 387-420.

Peyron, C., Tighe, D. K., van den Pol, A. N., de Lecea, L., Heller, H. C., Sutcliffe, J. G., & Kilduff, T. S. (1998) Neurons containing hypocretin (orexin) project to multiple euronal systems. *Journal of Neuroscience, 18*(23), 9996-10015.

Phillipson, O. T. (1979). The cytoarchitecture of the interfascicular nucleus and ventral tegmental area of Tsai in the rat. *Journal of Comparative Neurology*, *187*(1), 85-98.

Price, J. L. (2006a). Architectonic structure of the orbital and medial prefrontal cortex. In D. H. Zald & S. L. Rauch (Eds.), *The Orbitofrontal Cortex* (pp. 3–17). Oxford University Press.

Price, J. L. (2006b). Connections of the orbitofrontal cortex. In D. H. Zald & S. L. Rauch (Eds.), *The Orbitofrontal Cortex* (pp. 39–55). Oxford, UK: Oxford University Press.

Purves, D., Augustine, G. J., Fitzpatrick, D., Hall, W. C., LaMantia, A.-S., White, L. E. (Eds.). (2012). *Neuroscience* (5th Ed). Sunderland, MA: Sinauer Associates, Inc.

Radley, J. J., Williams, B., & Sawchenko, P. E. (2008). Noradrenergic innervation of the dorsal medial prefrontal cortex modulates hypothalamo-pituitary-adrenal responses to acute emotional stress. *Journal of Neuroscience, 28*(22), 5806–5816. doi:10.1523/jneurosci.0552-08.2008

Ray, J. P., & Price, J. L. (1992). The organization of the thalamocortical connections of the mediodorsal thalamic nucleus in the rat, related to the ventral forebrain-prefrontal cortex topography. *Journal of Comparative Neurology*, *323*(2), 167–197. http://doi.org/10.1002/cne.903230204

Reep, R. L., Corwin, J. V., & King, V. (1996). Neuronal connections of orbital cortex in rats: topography of cortical and thalamic afferents. *Experimental Brain Research*, *111*(2), 215–232.

Reep, R. L. & Winans, S. S. (1982). Efferent connections of dorsal and ventral agranular insular cortex in the hamster, *Mesocricetus auratus*. *Neuroscience, 7*(11), 2609-35.

Reppucci, C. J., & Petrovich, G. D. (2016). Organization of connections between the amygdala, medial prefrontal cortex, and lateral hypothalamus: a single and double retrograde tracing study in rats. *Brain Structure and Function*, *221*, 2937–2962. doi:10.1007/s00429-015-1081-0

Römpp, A., Spengler, B. (2013) Mass spectrometry imaging with high resolution in mass and space. *Histochemistry and Cell Biology, 139*, 759-783.

Rose, J. E., & Woolsey, C. N. (1948a). The orbitofrontal cortex and its connection with the mediodorsal nucleus in rabbit, sheep, and cat. *Research Publications-Association for Research in Nervous and Mental Disease*, *27*, 210–232.

Rose, J. E., & Woolsey, C. N. (1948b). Structure and relations of limbic cortex and anterior thalamic nuclei in rabbit and cat. *Journal of Comparative Neurology*, *89*(3), 279–347.

Santana, N., Mengod, G., & Artigas, F. (2009). Quantitative analysis of the expression of dopamine D1 and D2 receptors in pyramidal and GABAergic neurons of the rat prefrontal cortex. *Cerebral Cortex*, *19*(4), 849–860. doi: 10.1093/cercor/bhn134

Sarter, M., & Markowitsch, H. J. (1984). Collateral innervation of the medial and lateral prefrontal cortex by amygdaloid, thalamic, and brain-stem neurons. *Journal of Comparative Neurology*, *224*, 445–460.

Schiller, F. (1985) The mystique of the frontal lobes. *Gesnerus: Swiss journal of medicine and sciences*, 42(3-4), 415-424.

Schilman, E. A., Uylings, H. B. M., Galis-de Graaf, y., Joel, D., Groenewegen, H. J. (2008) The orbital cortex in rat topographically projects to central parts of the caudate-putamen complex. *Neuroscience Letters, 432,* 40-45

Sesack, S. R., Bunney, B. S. (1989). Pharmacological characterization of the receptor mediating electrophysiological responses to dopamine in the rat medial prefrontal cortex: a microiontophoretic study. *Journal of Pharmacology and Experimental Therapeutics, 248*(3), 1323-1333.

Sesack, S. R., Deutch, A. Y., Roth, R. H., & Bunney, B. S. (1989). Topographical organization of the efferent projections of the medial prefrontal cortex in the rat: an anterograde tract-tracing study with *Phaseolus vulgaris* leucoagglutinin. *Journal of Comparative Neurology, 290*(2), 213-42.

Siegel, A., Fukushima, T., Meibach, R., Burke, L., Edinger, H., & Weiner, S. (1977). The origin of the afferent supply to the mediodorsal thalamic nucleus: enhancement of HRP transport by selective lesions. *Brain Research*, *135*(1), 11–23.

Slopsema, J. S., van der Gugten, J., & de Bruin, J. P. (1982). Regional concentrations of noradrenaline and dopamine in the frontal cortex of the rat: dopaminergic innervation of the prefrontal subareas and lateralization of prefrontal dopamine. *Brain Research, 250*(1), 197-200.

Sobel, E., & Corbett, D. (1984). Axonal branching of ventral tegmental and raphe projections to the frontal cortex in the rat. *Neuroscience Letters*, *48*(2), 121–125.

Starr, M. A. (1891). *Familiar Forms of Nervous Disease* (2nd edition). New York: William Wood & Company.

Swanson, L. W. (1982). The projections of the ventral tegmental area and adjacent regions: a combined fluorescent retrograde tracer and immunofluorescence study in the rat. *Brain Research Bulletin*, *9*(1-6), 321–353.

Takahashi, Y. K., Roesch, M. R., Stalnaker, T. A., Haney, R. Z., Calu, D. J., Taylor, A. R., … Schoenbaum, G. (2009) The orbitofrontal cortex and ventral tegmental area are necessary for learning from unexpected outcomes. *Neuron*, *62,* 269-280. http://doi.org/10.1016/j.neuron.2009.03.005

Thompson, J. L., Drysdale, M., Baimel, C., Kaur, M., MacGowan, T., Pitman, K. A., & Borgland, S. L. (2017). Obesity-induced structural and neuronal plasticity in the lateral orbitofrontal cortex. *Neuropsychopharmacology*, *42*(7), 1480–1490. http://doi.org/10.1038/npp.2016.284

Thompson, J. L., Yang, J., Lau, B., Liu, S., Baimel, C., Kerr, L. E., ... & Borgland, S. L. (2016). Age-Dependent D1–D2 Receptor Coactivation in the Lateral Orbitofrontal Cortex Potentiates NMDA Receptors and Facilitates Cognitive Flexibility. *Cerebral Cortex*, *26*(12), 4524-4539.

Triarhou, L. C. (2007). The Economo-Koskinas atlas revisited: Cytoarchitectonics and functional context. *Stereotactic and functional neurosurgery*, *85*, 195–203. doi:10.1159/000103258

van de Werd, H. J. J. M., Rajkowska, G., Evers, P., & Uylings, H. B. M. (2010). Cytoarchitectonic and chemoarchitectonic characterization of the prefrontal cortical areas in the mouse. *Brain Structure and Function*, *214*(4), 339–353. http://doi.org/10.1007/978-3-642-70573-1

van de Werd, H. J. J. M., & Uylings, H. B. M. (2008). The rat orbital and agranular insular prefrontal cortical areas: a cytoarchitectonic and chemoarchitectonic study. *Brain Structure and Function*, *212*(5), 387–401. doi:10.1016/B978-012547638-6/50025-0

van Eden, C. G., Hoorneman, E. M., Buijs, R. M., Matthijssen, M. A., Geffard, M., & Uylings, H. B. (1987). Immunocytochemical localization of dopamine in the prefrontal cortex of the rat at the light and electron microscopical level. *Neuroscience*, *22*(3), 849–862.

Venator, D. K., Lewis, D. A., & Finlay, J. M. (1999). Effects of partial dopamine loss in the medial prefrontal cortex on local baseline and stress-evoked extracellular dopamine concentrations. *Neuroscience*, *93*(2), 497–505.

von Economo, C., Koskinas, G. N. (2008). Atlas of cytoarchitectonics of the adult human cerebral cortex. (L.C. Triarhou Trans.). New York, NY: Karger. (Original work published 1925)

van Eden, C. G., Hoorneman, E. M., Buijs, R. M., Matthijssen, M. A., Geffard, M., & Uylings, H. B. (1987). Immunocytochemical localization of dopamine in the prefrontal cortex of the rat at the light and electron microscopical level. *Neuroscience*, *22*(3), 849–862.

Verwer, R. W., Meijer, R. J., Van Uum, H. F., & Witter, M. P. (1997). Collateral projections from the rat hippocampal formation to the lateral and medial prefrontal cortex. *Hippocampus*, *7*(4), 397–402.

Walker, A. E. (1940). A cytoarchitectural study of the prefrontal area of the macaque monkey. *Journal of Comparative Neurology*, *73*(1), 59–86.

Wallis, J. D. (2012). Cross-species studies of orbitofrontal cortex and value-based decision making. *Nature Neuroscience, 15*(1), 13-19. doi:10.1038/nn.2956

Wang, J., Duncan, D., Shi, Z., Xhang, B. (2013) WEB-based GEne SeT AnaLysis Toolkit (WebGestalt): update 2013. *Nucleic Acids Research, 41,*W77-83.

Wei, X., Ma, T., Cheng, Y., Huang, C. C. Y., Wang, X., Lu, J., & Wang, J. (2017). Dopamine D1 or D2 receptor-expressing neurons in the central nervous system. *Addiction Biology*, *6*, 7062. http://doi.org/10.1016/j.neuroscience.2015.06.033

Weinberger, D. R., Berman, K. F., Zec, R. F. (1986). Physiologic dysfunction of dorsolateral prefrontal cortex in schizophrenia. I. Regional cerebral blood flow evidence. *Archives of General Psychiatry, 43*, 114-124.

Weiner, D. M., Levey, A. I., Sunahara, R. K., Niznik, H. B., Dowd, B. F. O., Seeman, P., & Brann, M. R. (1991). D1 and D2 dopamine receptor mRNA in rat brain. *Proceedings of the National Academy of Sciences*, *88*, 1859–1863.

Williams, S. M. & Goldman-Rakic, P. S. (1998) Widespread origin of the primate mesofrontal dopamine system. *Cerebral Cortex*, *8*, 321-45.

Winkowski, D. E., Nagode, D. A., Donaldson, K. J., Yin, P., Shamma, S. A., Fritz, J. B., & Kanold, P. O. (2017). Orbitofrontal cortex neurons respond to sound and activate primary auditory cortex neurons. *Cerebral Cortex*. 2017, 1-12. doi: 10.1093/cercor/bhw409.

Yang, Y. & Wang, J. Z. (2017). From structure to behavior in basolateral amygdala-hippocampus circuits. *Frontiers in Neural Circuits*, *11*, 86. doi: 10.3389/fncir.2017.00086. eCollection 2017.

Yoshida, A., Dostrovsky, J. O., Chiang, C. Y. (1992) The afferent and efferent connections of the nucleus submedius in the rat. *Journal of comparative neurology, 324*, 115-133.

Yoshida, M. Shirouzu, M., Tanaka, M., Semba, K., Fibiger, H. C. (1989). Dopaminergic neurons in the nucleus raphe dorsalis innervate the prefrontal cortex in the rat: a combined retrograde tracing and immunohistochemical study using anti-dopamine serum. *Brain Research, 496*(1-2), 373-376.

Zald, D. H., & Rauch, S. L. (Eds.). (2006) *The Orbitofrontal Cortex*. Oxford, UK: Oxford University Press.

Zilles, K., & Amunts, K. (2010). Centenary of Brodmann's map - conception and fate. *Nature Reviews Neuroscience*, *11*, 139–145. doi:10.1038/nrn2776
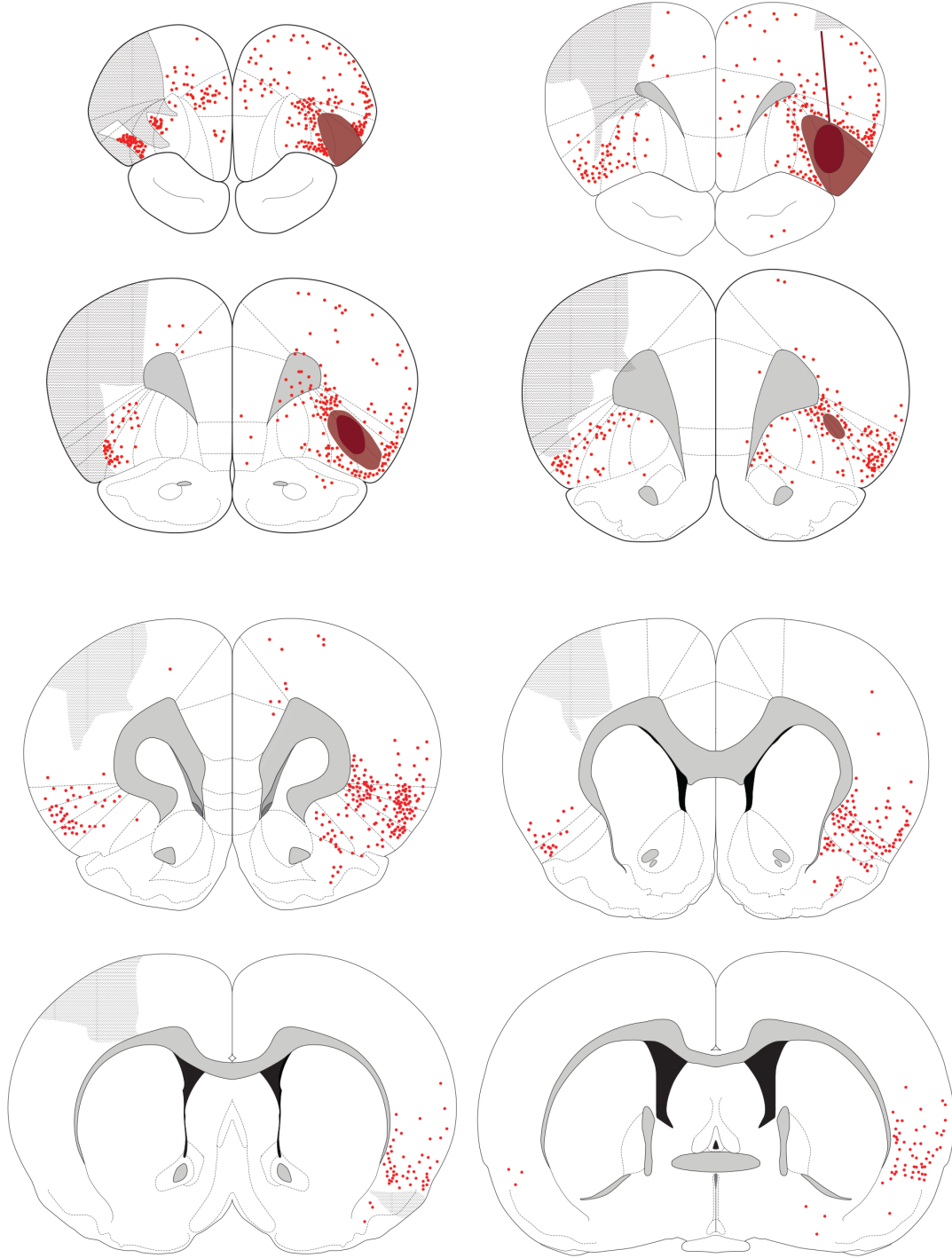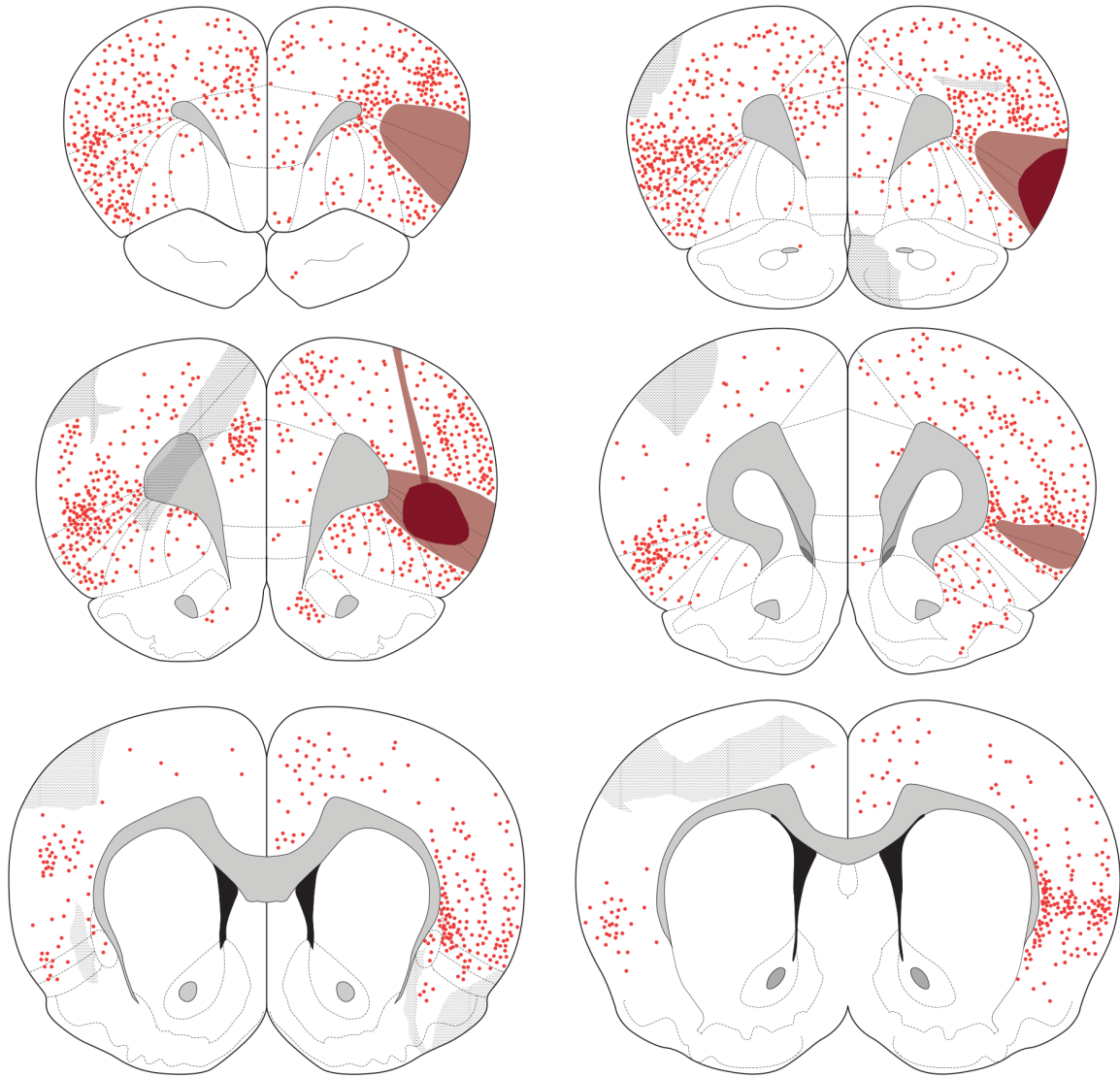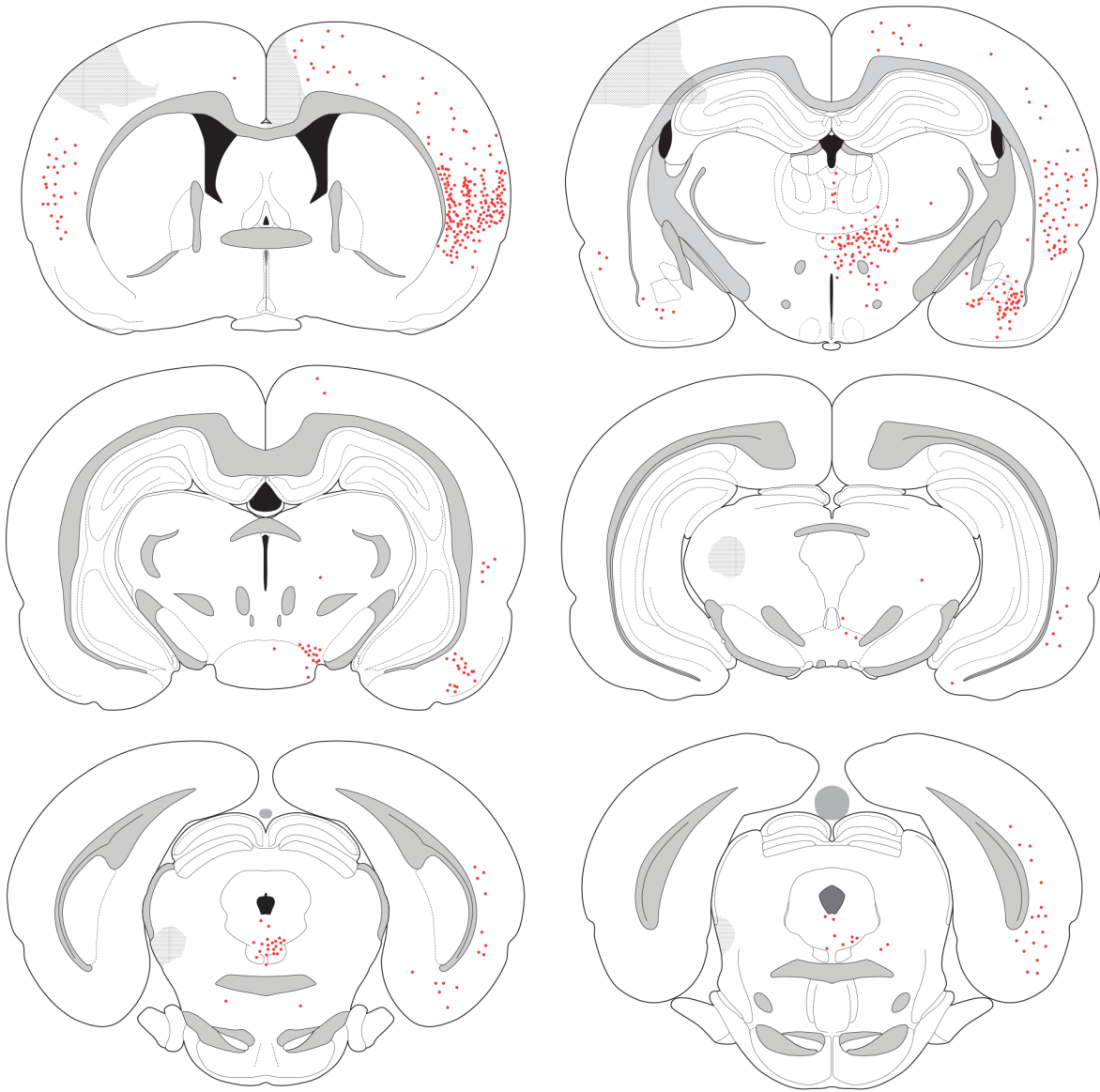
Case A1013
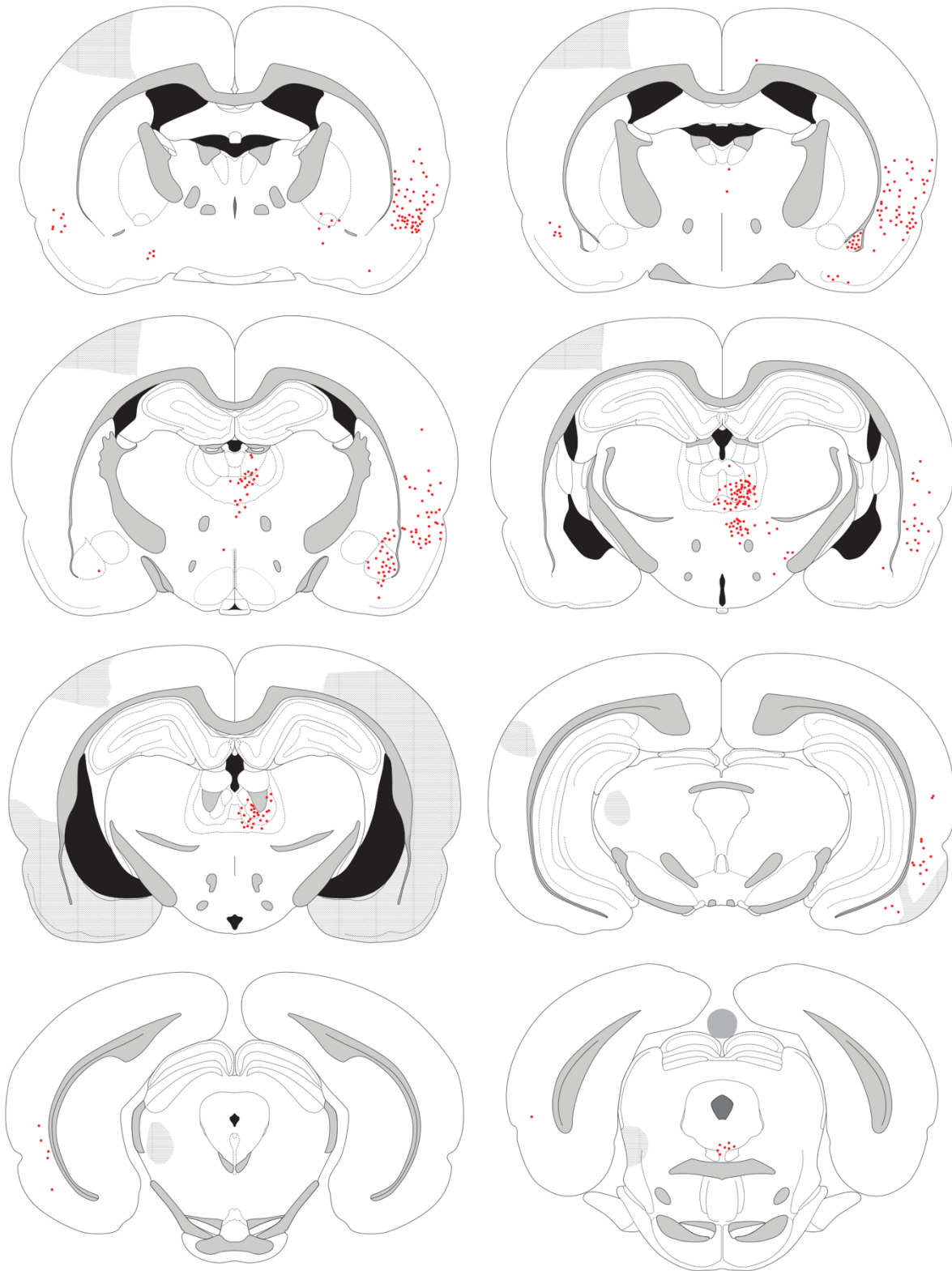
Case A1013
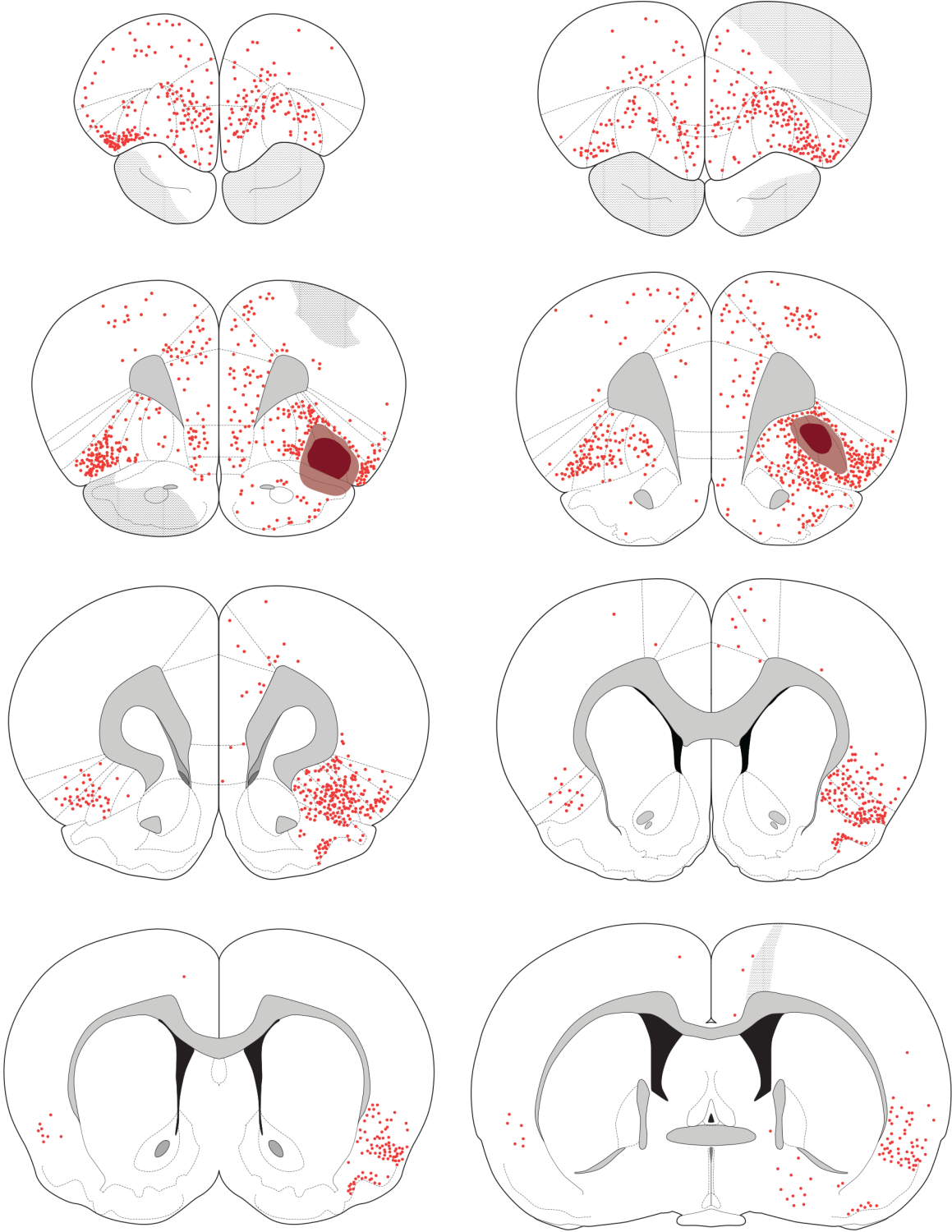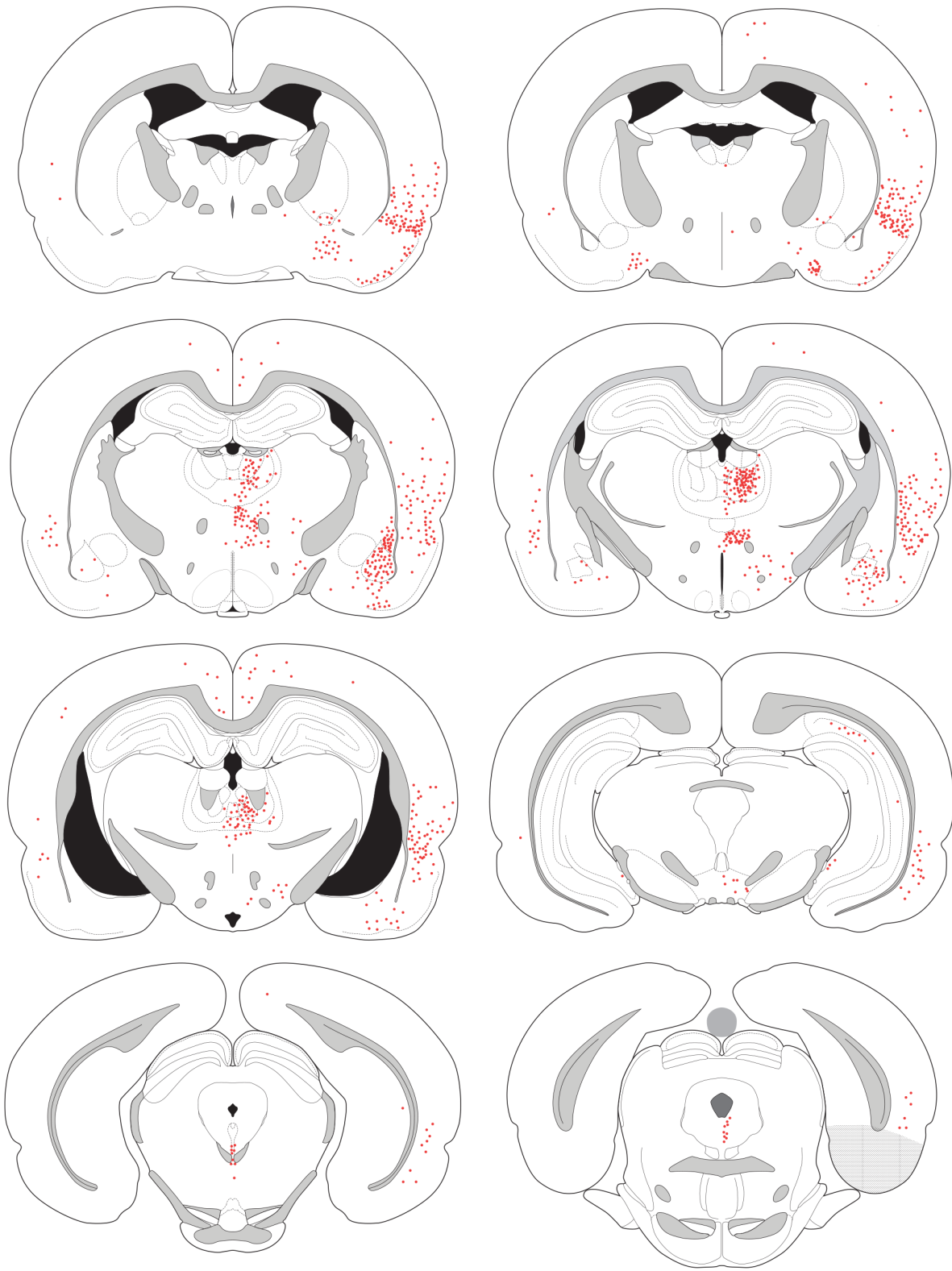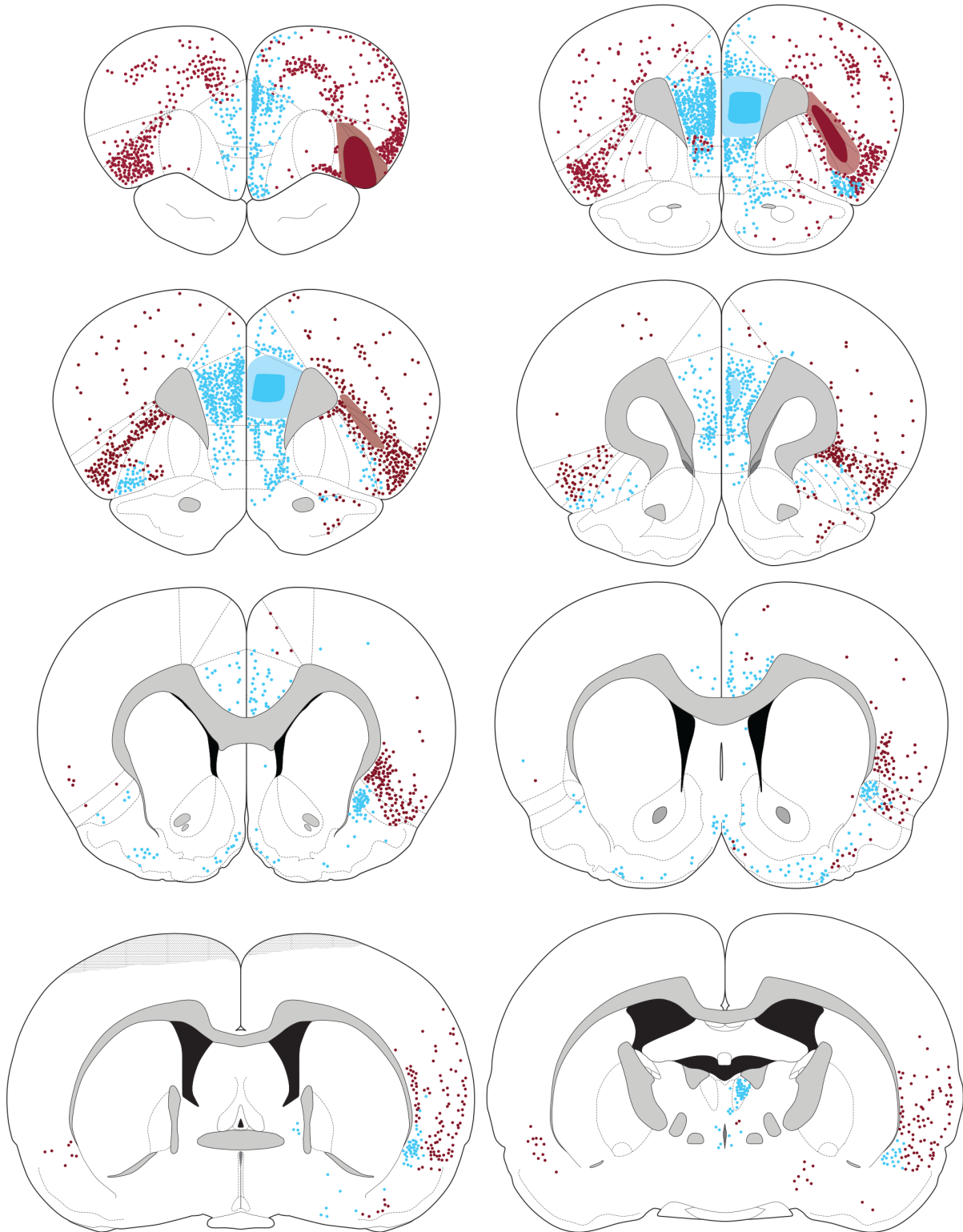
Case A1016
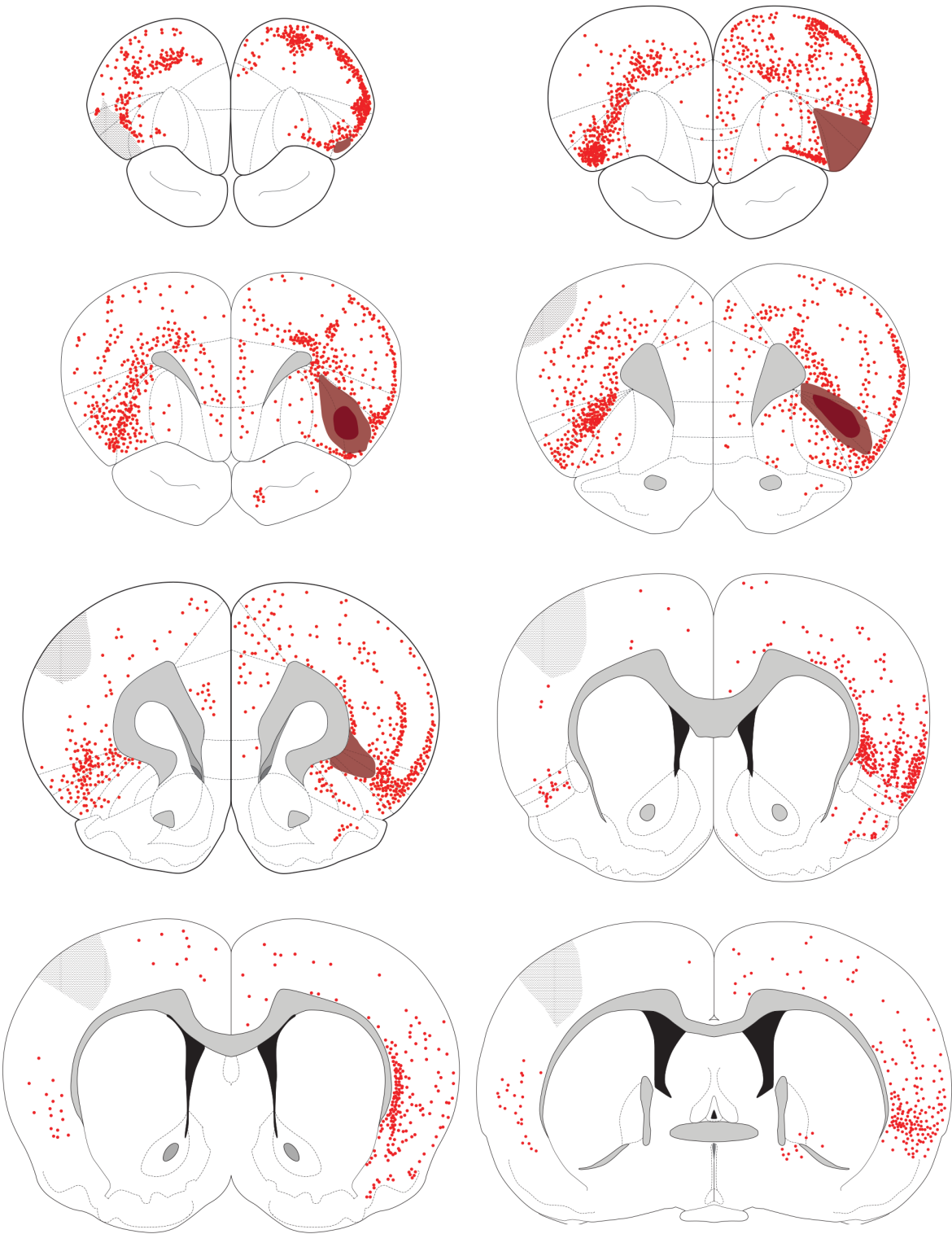
Case A1016
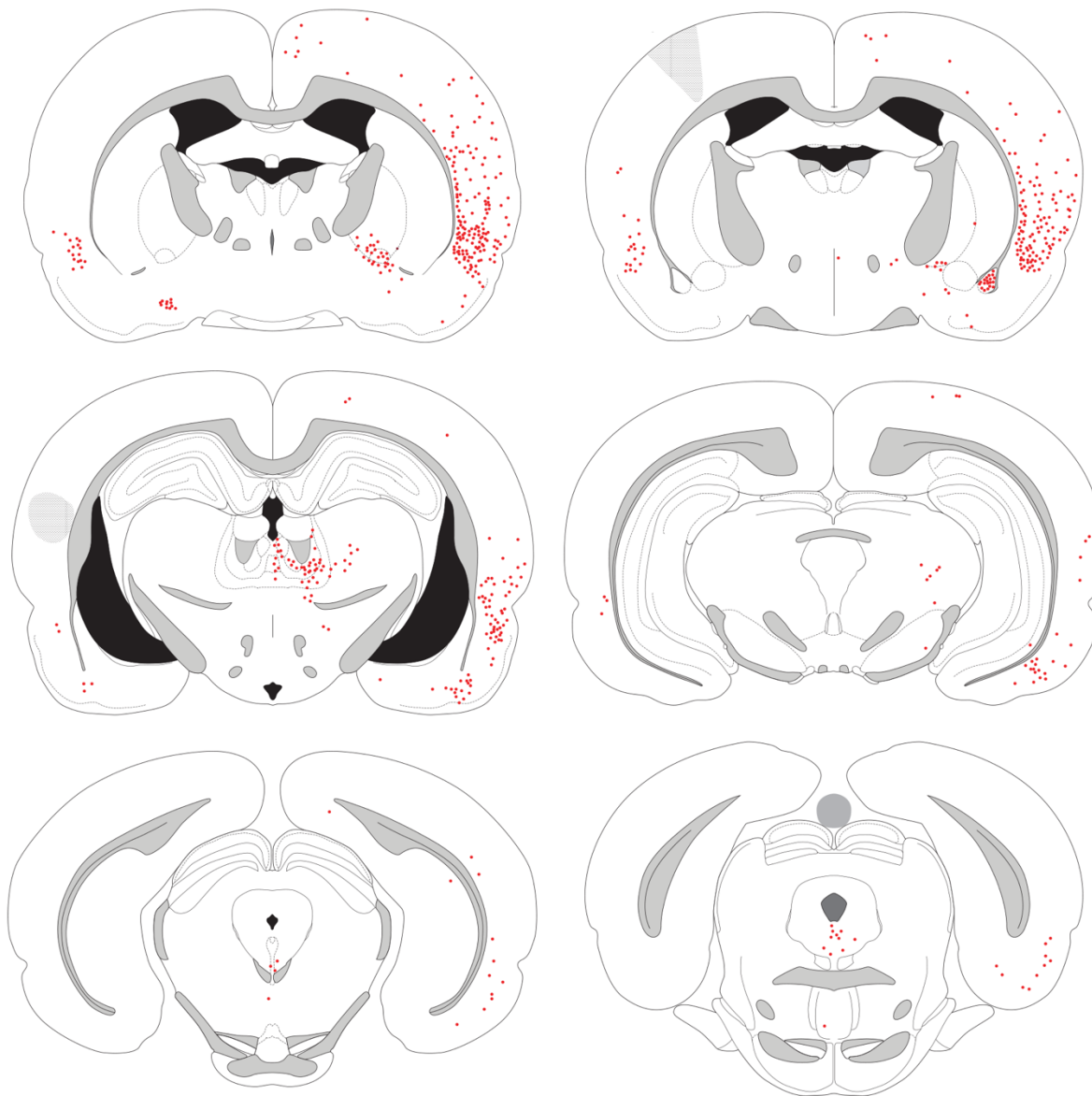
Case A1051
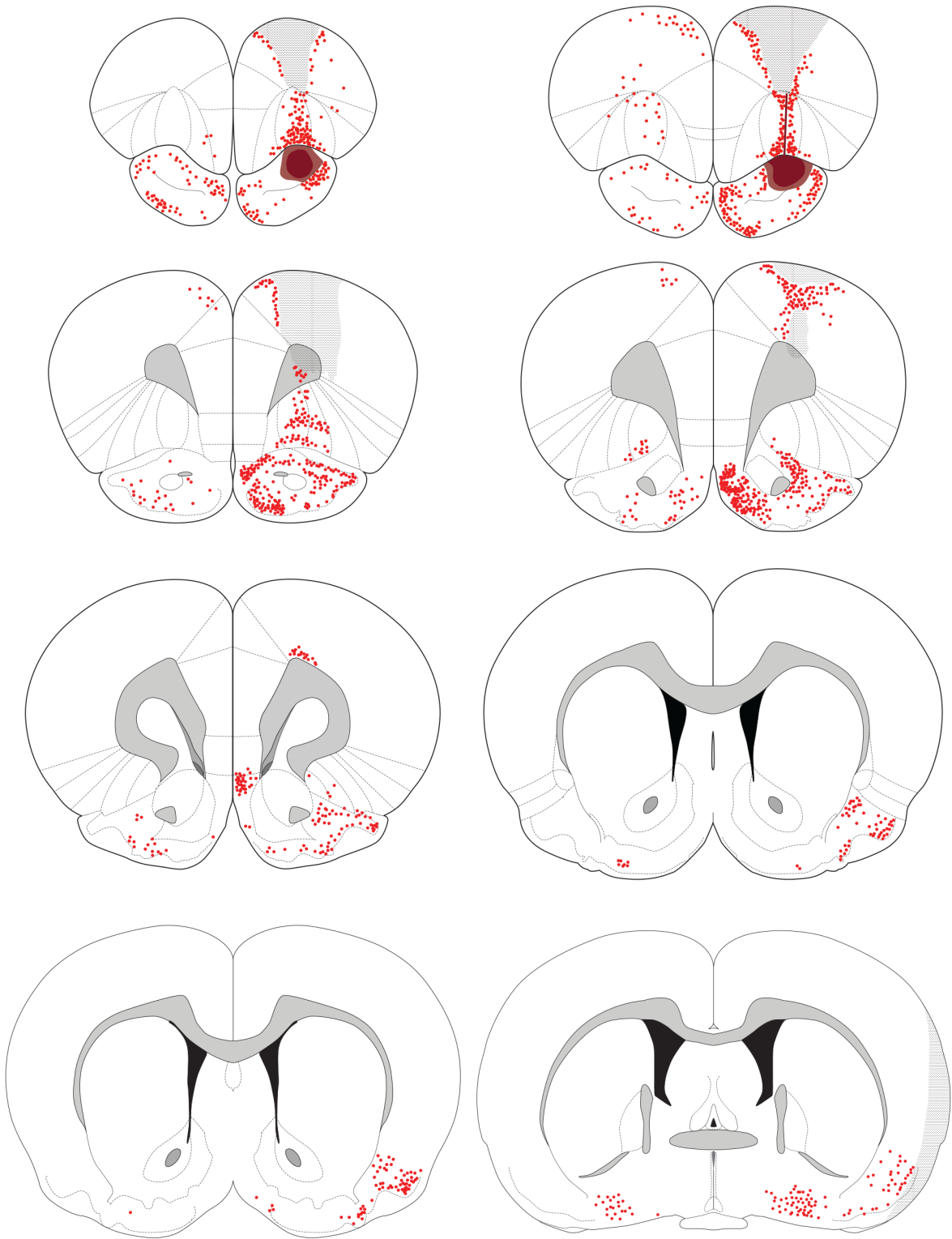
Case A1051
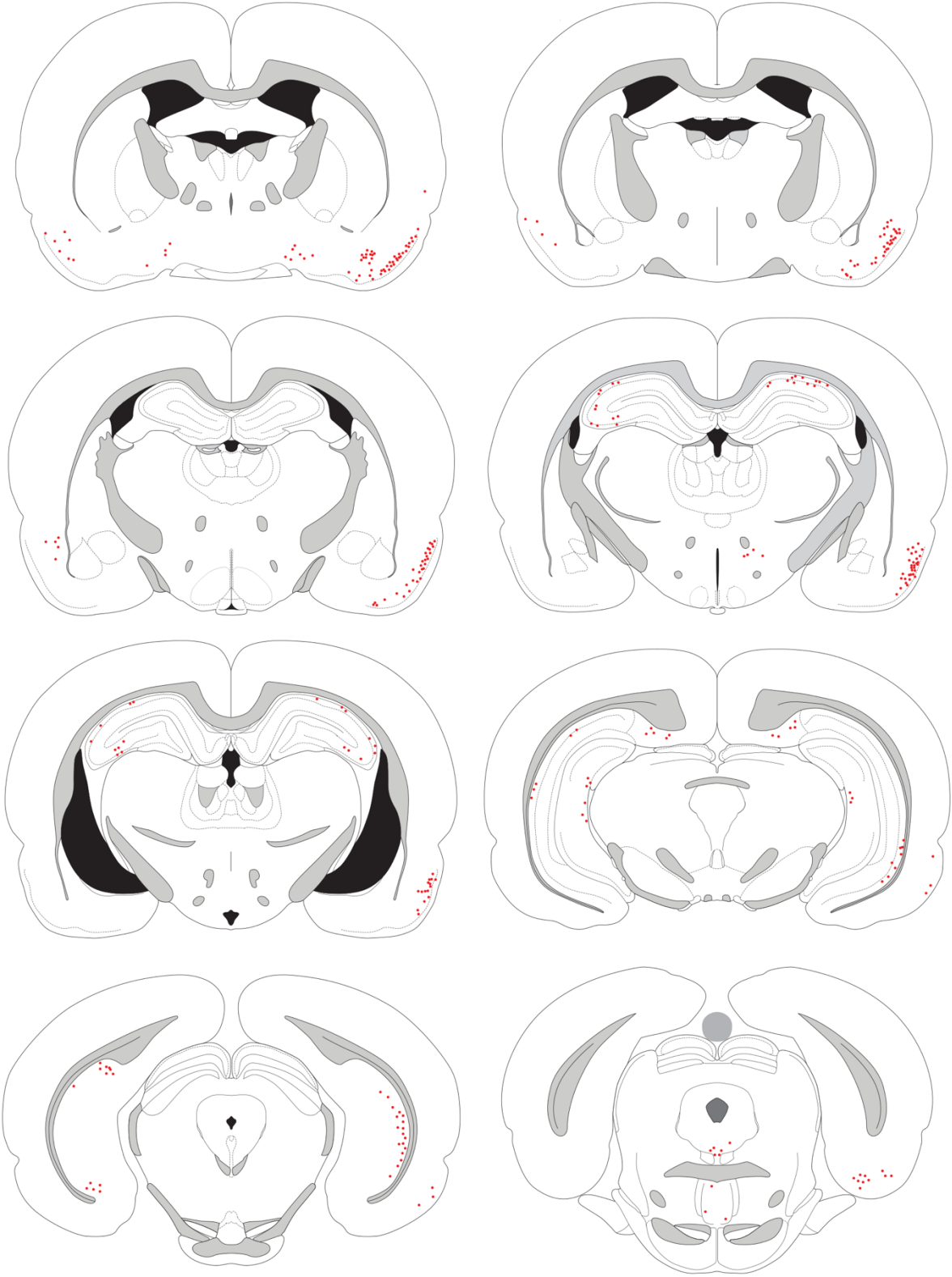
Case A1015

Case A1015

Case A1064

Case A1064

Case A1059

Case A1059